Helsinki University of Technology Publications in Materials Science and Metallurgy
Teknillisen korkeakoulun materiaalitekniikan ja metallurgian julkaisuja
Espoo 2001 TKK-MK-97

The effect of dissolved ozone on the corrosion behaviour of some stainless steels

Antero Pehkonen

Dissertation for the degree of Doctor of Science in Technology to be presented with due permission of the Department of Materials Science and Rock Engineering for public examination and debate in Auditorium V4 at Helsinki University of Technology (Espoo, Finland) on the 14th of December, 2001, at 12 noon.

Helsinki University of Technology
Department of Materials Science and Rock Engineering
Laboratory of Corrosion and Material Chemistry

Teknillinen Korkeakoulu
Materiaali- ja kalliotekniikan osasto
Korroosion ja materiaalikemian laboratorio

ISBN 951-22-5084-5
ISSN 1455-2329

Otamedia Oy, Espoo

HELSINKI UNIVERSITY OF TECHNOLOGY
P.O. BOX 1000, FIN-02015 HUT
http://www.hut.fi

ABSTRACT OF DOCTORAL DISSERTATION

Author Antero Pehkonen

Name of the dissertation
The effect of dissolved ozone on the corrosion behaviour of some stainless steels

Date of manuscript 13.11.2001 | Date of the dissertation 14.12.2001

☒ Monograph | Article dissertation (summary + original articles)

Department	Department of Materials Science and Rock Engineering
Laboratory	Laboratory of Corrosion and Material Chemistry
Field of research	Corrosion
Opponent(s)	Professor Tero Hakkarainen, professor Sannakaisa Virtanen
Supervisor (Instructor)	Professor Olof Forsén

Abstract
The corrosion behaviour of some stainless steels and pure metals has been investigated in solutions with dissolved ozone. The pH of the test solution was 1, 2, 3 and neutral (adjusted by H2SO4). 2.3 and 23 g/l Na2SO4 was added to increase the conductivity in anodic and cathodic polarisation measurements. The temperature of the test solution was 20, 50 and 75 °C. Test materials were four different stainless steels: ferritic stainless steel Polarit 815 and austenitic stainless steels Polarit 720, Polarit 752 and Ralloy 654MO. Also Armco iron, pure Mo, Ni and Cr were tested. The general electrochemical behaviour of stainless steels and pure metals was studied with potentiodynamic cyclic polarisation experiments at scanning rates 1, 10 and 100 mV/min and pitting behaviour at 10 mV/min. Potentiostatic experiments were also used. Immersion tests were also carried out mainly to produce test samples for surface examination but also to measure the weight losses. The structure and thickness of the oxidized surfaces were examined and analysed using optical microscope, SEM, GDOS, ESCA and X-ray diffractometer methods. Dissolved ozone increases the redox-potential of test solutions to about +1200 mV vs. SCE and the corrosion potential of stainless steel to the transpassive region, below the oxygen evolution potential. The current densities of stainless steels in this region increase as the amount of alloying elements increases. On the other hand, dissolved ozone increases current densities only slightly compared to oxygen bubbled solution. Higher ozone concentration obtained under high pressure has no effect on the corrosion behaviour of stainless steels. The corrosion of stainless steels is general but peeling of oxide layers was also observed. Shallow corrosion damages are formed in immersion. In cyclic polarisation experiments pits are formed in Ralloy 654MO. The pits formed are similar to those formed by chloride induced pitting. As the pH of the solution is decreased, the current density of higher alloyed steels increases at higher pH than lower alloyed steels. Dissolved ozone increases the thickness of the oxide layers greatly. In oxygen bubbled solution at pH 3 the thickness of the layers is a few nanometers and in ozonated solution 60 - 260 nm. The compositions of these oxide layers has been found to vary greatly. Cr concentration is negligible in the oxide layers especially for Ralloy 654MO and P752. Molybdenum concentrates in the outer layer, even more so with lower alloyed steels. Iron and alloying elements have oxidised to their highest valencies. The main components in the oxide layers are iron oxides and on the surfaces also MoO6 occurs.

Keywords stainless steel, ozone, tranpassive corrosion, passive layer

UDC 620.193:669.14:546.214 109 | Number of pages 109

ISBN (printed)951-22-5084-5 | ISBN (pdf)951-22-5763-7

ISBN (others) | ISSN 1455-2329

Publisher Helsinki University of Technology, Laboratory of Corrosion and Material Chemistry

Print distribution Helsinki University of Technology, Laboratory of Corrosion and Material Chemistry

The dissertation can be read at http://lib.hut.fi/Diss/

PREFACE

The experiments were carried out during the years 1994 - 2001 in the Laboratory of Corrosion and Material Chemistry, Helsinki University of Technology.

To my first supervisor Professor Emeritus Seppo Yläsaari, who unfortunately passed away before this thesis was completed, I wish to express my great gratitude for the possibility to return to academic circumstances and his support during these years. Professor Olof Forsén, my second supervisor, I wish to thank for his patience and his many kinds of support.

Dr. Sc. Jari Aromaa had an essential role on the thesis. Without his help and profound knowledge in corrosion science the process would have taken even longer.

M. Sc. Jorma Virtanen and M. Sc. Desiree Luhulima I want to thank for participating in the experimental work.

Many thanks are due to the whole staff in the Laboratory of Corrosion and Material Chemistry in keeping the atmosphere lively and inspiring.

I would also thank Mr. Janne Lumme for correcting the English text of the manuscript.

My loving family Siv, Senja, Sinna and especially Arttu has also affected very positively on this thesis. They have prevented me from plunging too deep into the subject by reminding me what are still the main values in my life.

Espoo, September 2001 Antero Pehkonen

CONTENTS

ORIGINAL FEATURES

The following features of this thesis are believed to be original:

1 In ozonated solutions, the corrosion rate of stainless steels is the higher the higher the amount of alloying elements.

2 The critical pH, below which the corrosion rate of austenitic stainless steels begins to increase in ozonated solution, is the higher the more alloyed steel. For P720 the critical pH is about 1, for P752 between 1 and 2 and for Ralloy 654MO between 2 and 3.

3 Oxide layers formed in ozonated solutions decrease the corrosion resistance of stainless steels. Layers are less protective in ozonated solutions than passive layers normally.

4 Dissolved ozone increases the thickness of the oxide layers on stainless steels P853, P720, P752 and Ralloy 654MO immersed in a solution of pH=3, T=50 °C from 4 - 5 nm in samples immersed 3 days in oxygen bubbled solution to 60 - 260 nm in samples immersed 16 days in ozonated solution. Both the thickness and the growth rate of the oxide layer increases as the alloying in stainless steels increases.

5 The chemical composition of the oxide layers on stainless steels is altered greatly in ozonated solution compared to oxides from a corresponding solution bubbled only by oxygen. Chromium is not able to form protective oxides and the main component in oxide layers are the oxides of iron. Molybdenum enriches on the surface of the layers as hexavalent oxide.

6 General corrosion occurs in stainless steels in ozonated solutions, but also peeling of the oxide layer was observed. The peeling mechanism is the following: 1) increase in the thickness of the oxide layer, 2) local corrosion initiation, 3) increased corrosion damages resulting in weakened adhesion of the oxide layer, 4) peeling of the oxide from the surface, 5) further oxidation of the exposed steel with corrosion damage.

1 INTRODUCTION

The background to this study is a larger research project carried out in HUT during the years 1994 - 1998 together with Technical Research Centre of Finland years 1996 - 1998. In this research the corrosion behaviour of both metallic and polymeric materials in ozone and peracetic acid bleaching were studied. The investigation was funded by the National Technology Agency (Tekes) and Finnish industry. The most essential part of this research was the corrosion behaviour of metallic materials and especially stainless steels in ozone bleaching. This was due to the very limited knowledge on the effect of dissolved ozone on the corrosion behaviour of materials, although ozone bleaching was already in use already at the beginning of 90`s. The material selection to the first ozone bleaching process was done without any detailed corrosion investigations.

During the early stages of this research it was found that not even the basis of the effects of dissolved ozone on the corrosion behaviour of stainless steels had been investigated. Some investigations concerning the effect of ozone were found, but the investigations were carried out either in strong acids or at low dissolved ozone concentrations in poorly defined environments, e.g. cooling waters and sea waters.

Thus the investigation was started from the effect of dissolved ozone in pure laboratory solutions without pulp and other impurities in order to understand the highly oxidising conditions of ozonated solutions. Also the validity of conventional electrochemical research methods in highly oxidizing ozone solutions needed to be evaluated. It is known that electrochemical test methods have certain limitations in very oxidising environments and the interpretation of results from electrochemical tests may cause problems. The basic problem is that in the transpassive region in addition to the dissolution of metal, secondary anodic reactions, e.g. oxygen evolution may occur. Thus the separation of the currents from these reactions may cause difficulties.

This study concerns experiments carried out in pure laboratory solutions without impurities such as salts and chlorides that exist in the ozone bleaching process. The basic test environment, distilled water at 50 °C adjusted to pH 3 with H_2SO_4, was chosen on the average environments in ozone bleaching.

The aim of this thesis is to study the corrosion behaviour of different stainless steels in pure water base solutions, where ozone is dissolved. The utilisation and possible limitations of different electrochemical corrosion research methods in very oxidizing conditions has also been estimated. Special attention is paid to the oxide layers formed on stainless steels in ozonated solutions due to the fact that great differences between passive layers formed in non ozone containing and ozonated solutions were found. The aim has been to give a wide overview on the effect of dissolved ozone on the corrosion behaviour of stainless steels.

1.1 Transpassivity

The term transpassive used to mean earlier only metal dissolution into solution by oxidation of an insoluble passive film. Today this term indicates more a potential region more noble than that corresponding to passivity where an increase of current with increasing potential is observed. Anodic dissolution in transpassive conditions may result in etching, pitting or brightening of the metal. In addition intergranular corrosion may occur [1].

The corrosion behaviour of stainless steels in the transpassive region, especially in solutions containing no chlorides, is not well understood and the number of published investigations carried out in this area is limited. This is due to the complexity of transpassivity and also due to the fact that stainless steels were originally developed for chloride and acidic solutions with lower redox potentials than in ozonated solutions. The other reason is that highly oxidising environments without chlorides so seldom occur in industry. In the pulp and paper industry, however, the utilisation of highly oxidising solutions for bleaching is common. Typical oxidants are chlorine and chlorine compounds, hydrogen peroxide and more recently also ozone and peracetic acid. The effect of chlorine and chlorine dioxide on the corrosion resistance of stainless steels has been studied intensively, but in environments without chlorides or at low chloride concentrations, such as in ozone bleaching, the basis for material selection differs clearly. Stainless steels in these solutions may in principle either be corrosion resistant, remaining in the passive state, or corrode transpassively.

Transpassive corrosion comprises a variety of phenomena and the study of transpassivity is also complicated by several factors. Electrode reactions are usually complex: they involve a variety of parallel and/or consecutive steps coupled with mass transfer processes which may lead to solid, dissolved or gaseous reaction products. Furthermore, in the case of high rate dissolution processes, a number of experimental difficulties arise which complicate measurements and interpretation of electrochemical data. In some cases, e.g. chromium and nickel in dilute sulfuric acid, transpassive dissolution may take place without visible pitting at potentials less noble than for oxygen evolution. This leads to uniform etching of metals [1].

In the transpassive region corrosion may occur in many forms. The most usual form of intergranular corrosion (IGC) is due to sensitisation. Intergranular corrosion can sometimes occur as a result of segregation of certain solute elements at the grain boundaries. However, this is known to occur only in highly oxidising corrodents containing cations in high valence states, such as the hexavalent chromium ion, and it is generally regarded as a somewhat unusual form of intergranular corrosion [2]. Intergranular corrosion of stainless steels may occur in the transpassive region at least in some oxidising solutions which contain e.g. CrO_4^{2-}, MnO_4^-, Fe^{3+} in nitric acid. High-purity alloys seem to be immune to IGC, but general corrosion may occur in the transpassive region. This suggests that IGC is not caused by Cr depletion, but the precipitation of phosphides or other compounds, which controls the attack [3, 4]. It has been found that at P-concentrations > 100 ppm or Si-levels 1000 - 10000 ppm IGC attack would occur in materials that had been annealed and water-quenched (e.g. 14Cr-14Ni, 16Cr-14Ni-0.02C and 19Cr-14Ni-0.07C steels). Similar alloys with N, C and O levels in the order of 1000 ppm were not subject to attack. However, it is evident that the mere presence of increased P or Si does not explain the increased dissolution in highly oxidising media. It is obvious that the oxidation of Cr^{3+} is more important [4, 5].

The effect of alloying elements and impurities of stainless steels on the corrosion behaviour of stainless steels is complex, not only in the transpassive region, but to some extent also in the passive region. One possible way to describe the effect of alloying is to show the effect of alloying elements and impurities on the anodic polarization curve, as in Fig. 1. In the passive region Cr, Ni and Cu have a marked decreasing effect on the current density and Mo a minor increasing effect. According to Hersbleb [5] the potential of the

transpassivation potential (E_{tr}) is affected only by Ni, which decreases this potential slightly. Si at concentrations below 0.1 % and over 2%, and P below 0.02% decrease the current density in the transpassive region. Manganese also slightly decreases the current, while Cr, Ni, Ti and Si at concentration range 0.1 - 2 % and P above concentration 0.02% have a minor increasing effect.

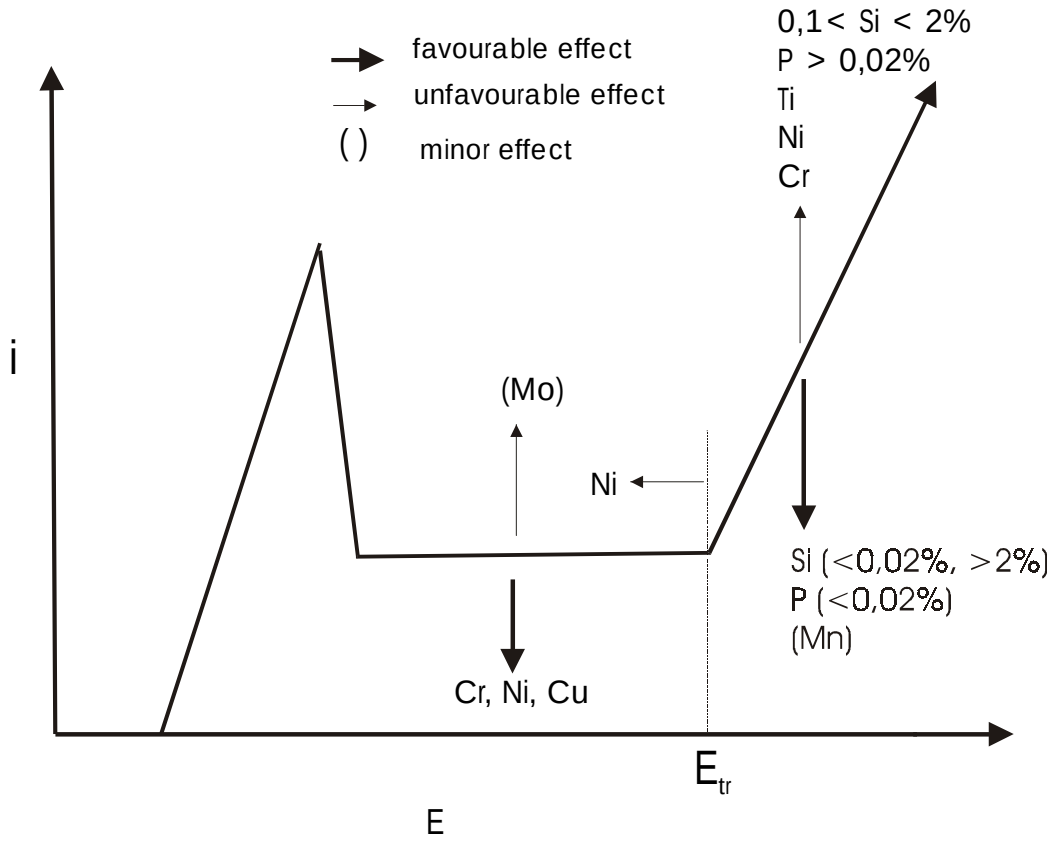

Fig. 1. The effect of alloying elements and impurities on the anodic polarisation curve of passivating stainless steels in acidic environments [5].

In acidic chloride solutions the situation is different. Chloride decreases the pitting potential of stainless steels and on the other hand at least chromium, molybdenum, nitrogen, silicon and nickel increase this potential [6].

Chromium is the main alloying element in increasing the corrosion resistance of stainless steels by forming a protective oxide layer already in slightly oxidising solutions such as water. Chromium in iron decreases the current density in the active and passive regions, and decreases also the Flade potential. In the transpassive region Cr, however, increases the current density and corrosion rate of stainless steels as in Fig. 2 [5], where the effect of chromium on the anodic behaviour of Fe-Cr alloys in 10 w-% H_2SO_4 is illustrated. The increase of Cr concentration from 12 w-% to 18 w-% increases the current density at potential 1.5 V vs. SHE (= 1.27 V vs. SCE) significantly. In the passive region and the beginning of the transpassive region current densities of lower alloyed stainless steels are higher. This means that a certain critical potential exists in the beginning of transpassive region, above which the current density of lower alloyed stainless steels are lower than that of higher alloyed steels. Thus in oxidising environments the potential of stainless steels has an essential role.

The reason for the increased current density in the transpassive region is the oxidation of chromium to hexavalent chromate or bichromate ions already at potentials below that of oxygen evolution [1]. At potential about +955 mV vs. SCE chromium, both as a pure metal and as an alloying element, starts to dissolve as CrO_4^{2-} [7].

Cr_2O_3 is a p-type semiconductor, which oxidises to higher valencies during anodic polarisation. According to literature [8] Cr_2O_3 oxidises to CrO_2, which is a n-type semiconductor. CrO_2 oxidises to soluble CrO_3. This oxidation causes the transformation of chromium from passive state to transpassive.

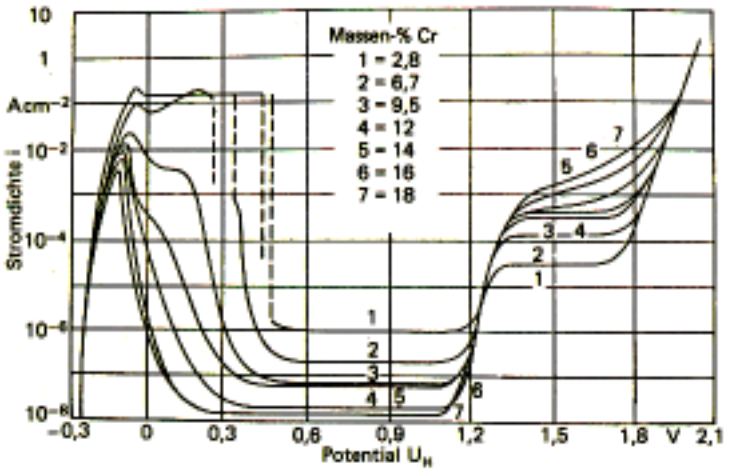

Fig. 2. The effect of Cr on the anodic polarization behaviour of Fe-Cr -alloys in 10 wt-% H_2SO_4 [5].

Nickel lowers the corrosion rate in the active region by decreasing the current density of the active peak [5]. Nickel decreases also the passive region corrosion rate of stainless steels in acids (e.g. in 80% H_2SO_4 at 80 °C) but on the other hand increases the Flade potential and decreases the transpassivation potential and increases the current density in transpassive region, when stainless steels with different Ni concentrations are compared [5].

The beneficial effect of Mo on the corrosion resistance of stainless steels is still a subject open to discussion. Mo is the essential alloying element in Cr- and CrNi - stainless steels, increasing the local corrosion resistance [5]. There is still no agreement on the mechanism of its action. It is obviously due to several factors: an enrichment of Mo in the oxide layer, thickening of the passive film and stabilising the Cr oxides by the presence of Mo^{6+}. It has also been suggested that Mo retards the corrosion process by adsorption, by formation of Mo compounds or by synergistic interaction of Mo ions with other oxides or oxihydroxides [9]. The two main mechanisms are the bipolar passive film model and the solute-vacancy interaction model [10]. Molybdenum decreases, as does nickel, the current density of the active peak in the anodic polarisation curve. The Flade potential and the current density in the passive region are slightly increased by Mo. The effect of molybdenum on the current density of stainless steels in the transpassive region is obviously not known, because no investigations concerning this was found. The effect of molybdenum may be estimated according to Pourbaix diagrams, which show that also Mo oxidizes to hexavalent and it is obvious that this oxide dissolves at least partly in acidic solutions.

1.2 Corrosion behaviour of metals in ozonated solutions

There has been considerable confusion in literature concerning the effects of ozone on the corrosion behaviour of metals and alloys. This is true in investigations, where low dissolved ozone concentrations have been investigated. Some investigations show increased corrosion of eg. carbon steels, brasses, nickel-alloys and stainless steels in ozonated waters, but others indicate either decreased or neutral effects. Most often these investigations concern environments in water purification of fresh water or in cooling waters (with and without chlorides), where the ozone concentrations are low and the service conditions have sometimes been poorly defined. In these studies the behaviour of ozone as a biocide has often been the essential task rather than the corrosion behaviour of metals [11-21]. Furthermore the number of publications where higher ozone concentrations were studied is smaller. In these investigations test solutions have mainly been far from those used in this thesis: pure water solution of pH from 1 to neutral [22-30].

Ozone is a strong oxidising agent with a standard electrode potential of 2.07 V vs. SHE. The decomposition mechanism of ozone in aqueous solutions is a matter of uncertainty. Views on the mechanism differ widely, because of the variety of the ways in which decomposition can take place under different conditions [31]. Most often the overall stoichiometry can be explained by equation (1) [17, 32, 33]. Depending on the pH of the solution in which it is dissolved, molecular ozone will either react directly with components in solutions or decompose into hydroxyl radical, oxygen and hydroxide. At pH values above 7.5, the decomposition of ozone to hydroxyl radicals increases. Below this pH value molecular ozone is stabilized and only a small fraction converts to radicals.

$$2O_3 + H_2O + e^- \rightarrow OH^{\bullet} + 5/2O_2 + OH^- \quad (1)$$

The hydroxyl free radical ($OH^{\bullet}$) is a more powerful oxidizer than ozone, with a potential of 2.80 V (vs. SHE). It is, however, obvious that the lifetime of this radical or its formation is very restricted, because it reacts rapidly with water contaminants [17, 32, 33].

When metals oxidise in solution with dissolved ozone, reaction (1) is the cathodic reaction. Dissolved ozone may increase the cathodic reaction both by reaction (1) and by increasing the dissolved oxygen concentration if oxygen reduction also occurs. If no anodic reaction occurs the reaction mechanism of ozone decomposition follows according of Horváth [31] equations (2) - (5):

$$O_3 + H_2O \rightarrow HO_3^+ + OH^- \quad (2)$$

$$HO_3^+ + OH^- \leftrightarrow 2HO_2 \quad (3)$$

$$O_3 + HO_2 \rightarrow HO + 2O_2 \quad (4)$$

$$HO + HO_2 \rightarrow H_2O + O_2 \quad (5)$$

The decomposition rate of dissolved ozone rises strongly with increasing temperature and pH. This has been estimated by Stumm with a formula (6) in distilled water at temperature 287.7 K [31].

$$\log\frac{[O_3]_0}{[O_3]_\tau} = k[OH^-]^{0.75}\tau \quad (6)$$

Where $[O_3]_0$ is the initial ozone concentration and $[O_3]_\tau$ the same concentration at time τ. The dependence on temperature is exponential. This decomposition occurs in neutral solutions at higher rates than in acidic solutions. The rate of decomposition is controlled by the relatively slow reactions (2) and (4), whereas reaction (3) leads to equilibrium. It can be seen that pH greatly affects the decomposition rate.

Horváth suggests that the decomposition rate can be written (7):

$$\frac{d[O_3]}{d\tau} = -3k^{1/2}[HO_3^+]^{1/2}[OH^-]^{1/2}[O_3] \quad (7)$$

In acidic ozonated solutions the reduction of ozone and the reduction of oxygen either formed by the ozone reduction reaction (reaction 5) or dissolved (reaction 8) are possible cathodic corrosion reactions.

$$O_2 + 4H^+ + 4e^- \leftrightarrow 2H_2O \quad (8)$$

At lower pH the amount of oxygen formed in ozone reduction will decrease, but because ozonated solutions bubbled by O_2/O_3 gas mixture contain dissolved oxygen in large amounts, the cathodic reaction of oxygen is not affected. In addition hydrogen evolution will also be evident in acidic solution. It has been suggested that the cathodic reduction of ozone controls the mixed potential in corrosion reactions (reaction 1) [14, 26].

In dissolved ozone solution dissolved metal ions oxidise to higher oxidation state. Strong dissolved complexes containing Fe^{3+} as FeO^{2+} and $FeOH^{2+}$ may occur in ozonated 10% sulphuric acid [27].

As an extremely oxidising agent, dissolved ozone affects the corrosion behaviour of metals by increasing the corrosion potential. In principle, corrosion potentials of stainless steels may rise into the transpassive region in ozonated solution, although in literature such results have not found. The corrosion potential of carbon steel has been reported to increase with increasing ozone concentration to about 435 mV vs. SCE in 10% H_2SO_4 [27] and in distilled water dissolved ozone increases the corrosion potential from -650 mV to about 0 mV vs. SCE. Dissolved ozone increases the corrosion potential of stainless steels significantly when the concentration exceeds a certain limit concentration. Dissolved ozone (2.1 mg/l) increases the corrosion potentials of stainless steels AISI 304, 430 and 403 to 750 - 860 mV vs. SCE in deionized water at room temperature [23, 26]. The highest corrosion potential is for AISI 430, where chromium concentration is highest. In 10-% NaCl solution (pH 10 - 12) the corrosion potential of austenitic (type 316L) and duplex (Cr 12-23, Ni 5.3-6.3, Ti 5xC-0.8) steels have been reported to be as much as 300 mV higher than their pitting potentials [30].

Dissolved ozone increases corrosion rates for carbon steels and low alloyed steels in aqueous solutions. In deionized water where the corrosion rate (in stagnant and slow flow rates) is about 2 or 3 times higher in the presence of 2.1 mg/l ozone than in the absence of

ozone [26]. According to Matsudaira [26] and Sato [23] dissolved ozone concentrations 0 - 7 mg/l have no effect on the corrosion rate of stainless steels AISI 304, 430 and 403 in deionized water and corrosion rates in immersion tests are low.

The effect of ozone in cathodic polarization is clearly noticeable. Cathodic current densities increase with increasing ozone concentrations, suggesting ozone is reduced at the carbon steel surface [23, 26].

Because ozone, as a strong oxidant even at very small concentrations (about 1 mg/l) raises the corrosion potential and decreases the repassivation potential, it is obvious that higher concentrations and flow rates lead to the destruction of the passive films and thus causes pitting and crevice corrosion [14].

The effect of ozone on the oxide layers formed on carbon steel SS41 in ozonated deionized water have been studied [23, 26]. X-ray analysis data for the corrosion products of carbon steel SS41 both in the presence of ozone and in the absence of ozone are shown in table 1. Ozone oxidises all the oxides to trivalent state.

Table 1. Structure of the corrosion products analysed by X-ray diffraction [23].

structure/ condition	γ-$Fe_2O_3 \cdot H_2O$ lepidocrocite	½$Fe_2O_3 \cdot H_2O$ goethite	α-Fe_2O_3 hematite	γ-Fe_3O_4 magnetite
O_2 8,5 mg/l	+++	+	-	++
O_2 8,5 mg/l + O_3 2,1 mg/l	++	+++	+	-

Note +++ > ++ > + relative amounts

Ozone obviously oxidises iron to ferrous ions (9), which are immediately oxidised further for example to ferric hydroxide (eq. 10).

$$Fe \rightarrow Fe^{2+} + 2e^{-} \tag{9}$$

$$2Fe^{2+} + 4OH^{-} + O_3 + H_2O \rightarrow 2Fe(OH)_3 + O_2 \tag{10}$$

1.3 Structure of passive layers

The effect of ozone on the composition of oxide layers on stainless steels has not been investigated earlier. The structure of passive layers on stainless steels is briefly discussed here as a basis for the discussion of the surface analysis results so that the changes caused by ozone in oxide layers are easier to understand.

The structure and chemical composition of oxide layers on stainless steels is a matter of complexity and because the thickness of the oxide layer is only some atomic layers, its examination is a rather difficult task. The passive films formed at least on austenitic stainless steels is often reported to be duplex, consisting of an inner barrier oxide layer and outer deposit hydroxide or salt film. The inner oxide barrier film is considerably less hydrated than the often thin outer deposit layer and consists mainly of Cr_2O_3 . The outer film often contains salts or hydroxides of the alloy metals.

The inner oxide layer is the primary diffusion barrier against cations dissolving from the base metal and against aggressive anions such as Cl^- penetrating from the solution [34]. However, it is still uncertain if the passive layer on stainless steels consists of stoichiometric oxide with a form M_2O_3 or M_3O_4, or layer of adsorbed oxygen [5]. The thicknesses of passive layers on stainless steels are typically only a few nanometers.

The oxidising power of the solution is one of the main parameters, which determine the oxidation state of an element in a passive film. This means that the composition of passive films alters if the potential of steel changes, eg. in ozonated solution the oxide layer is different from that in less oxidizing solutions, even if the potential is still in the passive region. The potential also affects the thickness of the passive film; at higher potentials the layer has been found to thicker. Other parameters are pH of the solution, local pH within highly hydrated passive films, the age of the passive film and the location of the metal ion relative to the external surface [34]. The potential affects also water bound in the passive film. At higher potentials the water content is lower.

Chromium and molybdenum are more likely to contribute to passivity, especially in the barrier layer, than iron or nickel. Mo will contribute only in a narrow range of potential before it undergoes transpassive dissolution. It is clear that chromium is the main passivating species in stainless steels [34]. Passive layers are regarded mostly as amorphous, but in the transpassive region Cr_2O_3 in the inner barrier layer may be crystalline [34].

The role of Mo in improving the corrosion resistance of stainless steels in chloride containing solutions is well known, but again there exists a variety of opinions on the nature of the passivity of molybdenum and the existence of Mo in oxide layers of stainless steels. This is because Mo may exist in a number of oxidation states. Molybdenum may also enrich just below the passive film [35, 36]. Most studies agree that Mo^{4+} is incorporated into the inner region of the passive film, whereas Mo^{6+} is present in the outer layer [34]. There is also a consensus on enrichment of Mo in the film produced during active-passive transition in acidic solution, but according to Ürgen [36] the findings on the presence and enrichment of Mo in the films formed in the passive region are controversial. It has also been reported [34] that at higher potential in 0.1 M HCl + 0.4 M NaCl the outer hydrated passive film contains more Mo^{6+} than Mo^{4+}. Hexavalent Mo has been observed in both cationic and anionic complexes as Mo trioxide and ferrous molybdate. It has been most commonly reported to exist in the quadrivalent state as Mo dioxide and oxyhydroxide.

The number of investigations concerning the corrosion behaviour of pure Mo in very oxidizing environment is limited. Suggestions based on electrochemical data say that MoO_3 is formed in the transpassive region [35]. A relatively thick oxide layer is formed in the transpassive region on pure molybdenum consisting of a mixture of Mo_2O_3, MoO_2, $MoO(OH)_2$, Mo_2O_5 and MoO_3. On pure Mo no MoO_4^{2-} exists at least in HCl solutions [37].

The passive films on stainless steels act as n-type semiconductors for anodic potentials and p-type for cathodic potentials respectively. Cr_2O_3, which is the main compound of the inner oxide layer, is a p-type semiconductor. Nevertheless passive films are n-type semiconductors for anodic potentials. This is due to the hydroxide outer layer [38].

1.4 The utilisation of Pourbaix-diagrams in very oxidising solutions

Pourbaix-diagrams can be used in the estimation of the basic corrosion behaviour of stainless steels in very oxidising environments but with a certain caution. These diagrams give the stability areas of the possible compounds, that can form only for pure metals. Because passive layers on stainless steels consist usually of chromium and molybdenum oxides or hydroxides, the most essential task is to evaluate the behaviour of these metals. Thus it may be assumed that Pourbaix-diagrams can be utilized to give some basic comprehension for the corrosion of stainless steels in solutions with high redox-potential [39].

The corrosion potentials of stainless steels in solutions containing dissolved ozone are found to lie over +700 mV vs. SCE (+945 mV vs. SHE). Potentials above the oxygen evolution line are in the transpassive region [39], but in solutions with dissolved ozone corrosion potentials are lower than the oxygen evolution potential at pH value below about 5.5, as is mainly the case in this study.

Here the behaviour of stainless steels are studied in acidic ozonated solutions, mainly at pH 3 and at temperature 50 °C. Pourbaix diagrams are valid at temperature 25 °C, but it is obvious that this difference in temperature has only a negligible effect on the diagrams.

Iron oxidises at pH 3 in oxidising environment to trivalent and forms solid Fe_2O_3, if solid substances are metallic iron and iron oxides (Fig. 3). Fe_2O_3 dissolves depending on the potential to Fe^{2+} and at higher potentials to $FeOH^{2+}$ [40].

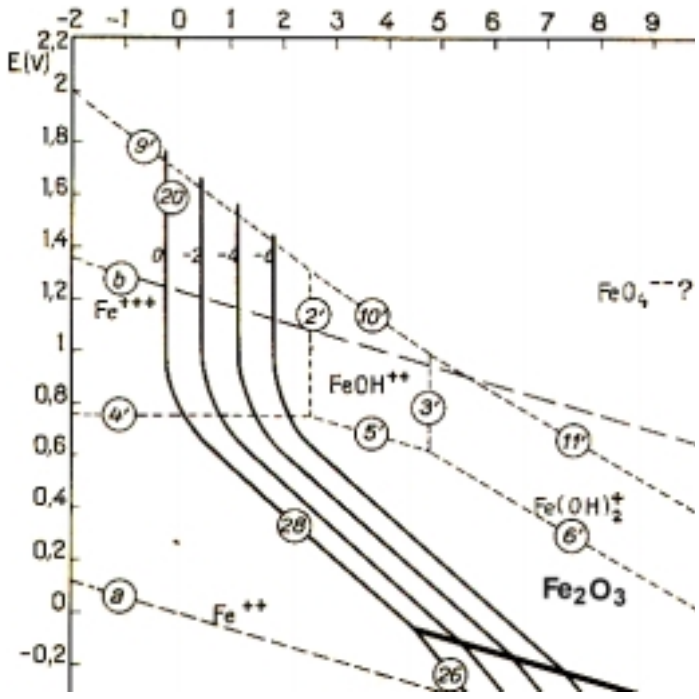

Fig. 3. Potential-pH equilibrium diagram for the system iron-water, at 25 °C [40].

The situation for chromium is more complicated; chromium may form anhydrous or hydrous oxides and hydroxides. Trivalent chromium can form complexes with sulphate. In solutions not containing chlorides and considering anhydrous Cr_2O_3, at pH 3 and T 25

°C solid Cr_2O_3 exists and chromium dissolves as Cr^{3+} up to potential about 880 mV vs. SHE (Fig. 4). Above this potential and under about 950 mV vs. SHE, $Cr(OH)_4$ may form. At higher potentials hexavalent chromium is as $HCrO_4^-$ or $Cr_2O_7^{2-}$. At pH region below 2.80 chromium oxide dissolves as trivalent ion. Trivalent chromium ion forms complexes at potentials higher than the oxygen evolution potential.

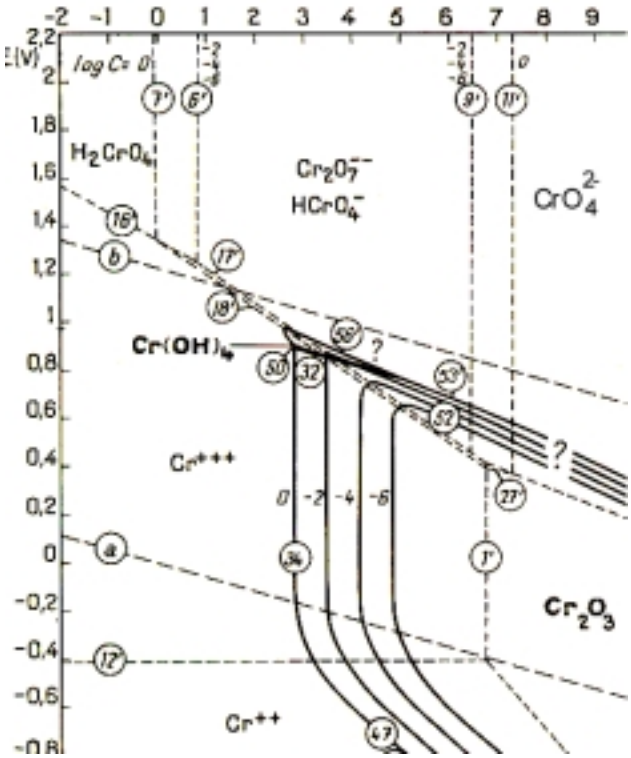

Fig. 4. Potential-pH equilibrium diagram for the system chromium-water, at 25 °C [40].

According to the Pourbaix-diagram for pure molybdenum (Fig. 5.), at pH 3 hexavalent Mo-oxide MoO_3 is formed, when potential is above about 140 mV vs. SHE. MoO_3 dissolves as $HMoO_4^-$. When pH decreases, also the stable region of MoO_3 decreases.

The solubility product of MoO_3 depends on pH. Pourbaix has symbolized these compounds by the ion $HMoO_4^-$ in diagram (Fig. 5), but the nature of the ions varies with the pH. These ions are shown in table 2.

Table 2. The nature of molybdenum complexes [40].

pH	Compound
about 0.9	$Mo_{24}O_{78}^{12-}$
0.9 - 1.5	$Mo_{12}O_{41}^{10-}$
1.5 - 4.5	$Mo_6O_{21}^{6-}$
4.5 - 6	$Mo_3O_{11}^{4-}$
6 - 14	MoO_4^{2-}

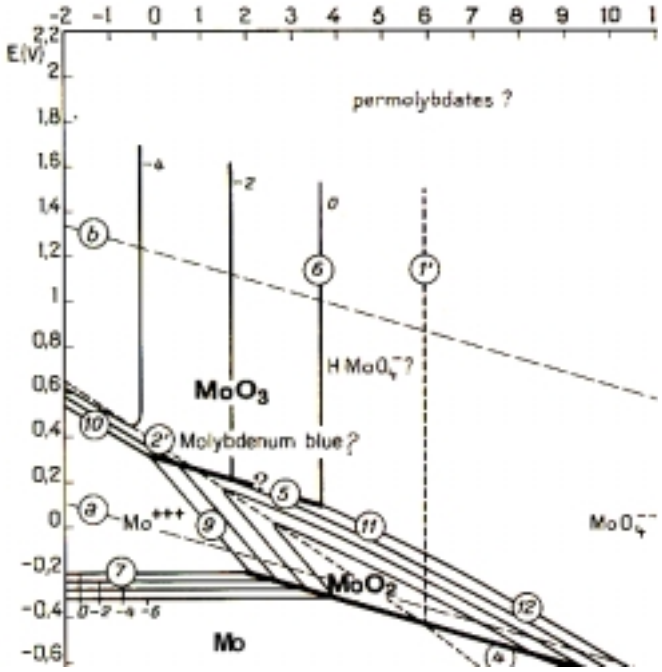

Fig. 5. Potential-pH equilibrium diagram for the system molybdenum-water, at 25 °C [40].

MoO_3 does not combine directly with water to form hydrates. These are obtained only from molybdates, there exist two hydrates $MoO_3 \cdot H_2O$ and $MoO_3 \cdot 2H_2O$. The solubility values of these hydrates and MoO_3 are fairly close. The dissolution of MoO_3 is therefore considered as in Fig. 5 and in equation (11) [40].

$$MoO_3 + H_2O \rightarrow HMoO_4^- + H^+ \qquad (11)$$

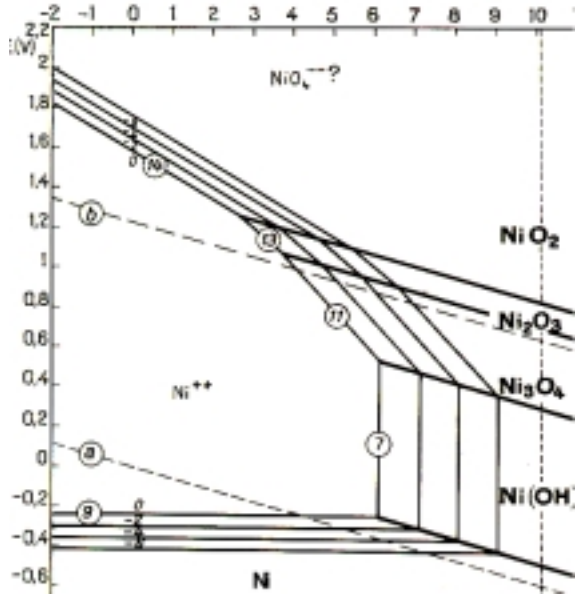

Fig. 6. Potential-pH equilibrium diagram for the system nickel-water, at 25 °C.

Pure nickel dissolves as Ni^{2+} at pH 3 between potentials about -440 and 1220 mV vs. SHE(Fig. 6).

Some intermetallic oxides, as spinels, may also form in the passive layers of stainless steels. Some calculations for ternary systems of Fe-Cr-Ni at higher temperature have been made [41]. According to these diagrams for nickel species at temperature of 100 °C, no differences in acidic solutions (< pH 7) exist. In the diagram for iron species at temperature 100 °C , an area of $FeOH^{2+}$ complex is found between Fe^{3+} and $FeOH^{2+}$ shown earlier in Fig. 3. If the Pourbaix diagram for pure chromium and chromium species in ternary Fe-Cr-Ni system at 100 °C are compared, only minor changes in dissolved complexes can be seen. In solid species no $Cr(OH)_4$ exists as in Pourbaix diagram for pure chromium. It is obvious that at higher temperatures, but below 75 °C as in this investigation, no essential changes in ternary Fe-Cr-Ni systems occur.

1.5 Conclusion of the literature survey

The corrosion behaviour of metals and alloys in ozonated solution has not been investigated in depth. Most corrosion investigations concern only immersion tests in solutions where the ozone concentration is low. In some references authors have presented the possibility of crevice corrosion or pitting, but no experimental data was found. The passive layers formed on pure metals and stainless steels has not been investigated. The common opinion is that the corrosion resistance of stainless steels is good in all ozonated aqueous solution without chlorides and in neutral or near neutral region.

It is presumed in this study that dissolved ozone increases greatly the corrosion potentials of metals and alloys so that these may reach the transpassive region, where local corrosion is possible. It is also assumed that the radical formed in the decomposition of dissolved ozone has no effect on the corrosion behaviour of stainless steel. Ozone decomposes to oxygen and the main cathodic reaction is oxygen reduction.

In the passive range the structure of the oxide layer on stainless steels is duplex. The inner layer is mainly Cr_2O_3 and outer deposit hydrated film. It is assumed that the composition of the oxide layer is affected by dissolved ozone, because iron and the alloying elements of stainless steels all oxidise in theory to their highest oxidation states (Fe^{3+}, Cr^{6+}, Mo^{6+}, Ni^{2+}) and the amount of bound water in the oxide layer decreases. The amorphous character of the passive layer may change.

2 EXPERIMENTAL MATERIALS AND PROCEDURES

In this investigation several electrochemical methods were used. In very oxidising environments the utilisation of electrochemical corrosion research methods and especially the correct interpretation of results may be difficult. Immersion tests were carried out both in order to estimate the corrosion rate of stainless steels in ozonated solutions but mainly to produce oxide layers for further surface examinations.

The electrochemical behaviour of stainless steels was studied by corrosion potential measurements, potentiodynamic anodic and cathodic polarisation curves, determination of the corrosion current densities by the Tafel method and potentiostatic method. Results of corrosion potential measurements show the potential range, where stainless steels lie; is it in the passive or transpassive region and the difference between the corrosion potential the oxygen evolution potential, which is essential in the interpretation of data measured in electrochemical experiments. If the corrosion potential is lower than the oxygen evolution potential, the results from polarisation measurements can be interpreted using basic principles. The anodic and cathodic polarisation experiments were done with and without stabilisation of the corrosion potential. In experiments without stabilisation the effect of alloying elements on the corrosion behaviour of the stainless steels was studied. In experiments after the stabilisation the overall corrosion behaviour of the stainless steels with an oxide layer formed in ozonated solution was investigated. The tendency of stainless steels to pitting corrosion was investigated by cyclic polarisation measurements at a low scanning rate. It is assumed that the main corrosion form of stainless steels in ozonated solutions is uniform corrosion, but because in literature [14] the possibility of pitting in ozonated solution was mentioned, electrochemical pitting corrosion experiments were also done.

The oxide layers formed during immersion tests in ozonated solutions were examined by optical microscope and SEM. The chemical composition of oxide layers was analysed by GDOS, ESCA and X-ray diffractometer methods in order to estimate the effect of dissolved ozone as an extremely strong oxidiser, which may considerably alter the composition, structure and the thickness of oxide layers on stainless steels. In some immersion tests the dissolved metals were analysed by AAS method in order to estimate the kinetics of the dissolution and the proportions of dissolved alloying elements.

Test materials used in this investigation were ferritic stainless steel Polarit 853 (P853) and three austenitic stainless steels: Polarit 720 (P720), Polarit 752 (P752) and Ralloy 654MO (UNS S42654). The Polarit steels are from AvestaPolarit and the P853 corresponds to AISI 409, P720 to AISI 304L type and P752 to AISI 316L type stainless steels. All Polarit steel samples are from cold rolled, cold annealed and pickled production sheets. The structure of steels is checked in every batch. Ralloy 654MO is an austenitic stainless steel produced by hot isostatic pressing (HIP) by Rauma Materials Technology and the sample was from Helsinki University of Technology, Laboratory of Engineering Materials, were the structure of the sample was examined. The structure of all the steel samples was normal. The chemical compositions of these steels are shown in Table 3. Analyses are from corresponding batches made by producers. Pure metals Cr, Ni and Mo and Armco iron as pure iron were also investigated. Pure chromium (99.7+%) and molybdenum (99.9%) were supplied by Goodfellow and pure cathode Ni (99.97%) by Outokumpu Harjavalta Metals. Armco iron was produced by American Rolling Mill Co. Analyses of these metals are also from the producers (Table 3).

Table 3. The chemical compositions of stainless steels and Armco iron.

Steel	C	Cr	Ni	Mo	Mn	P	S	Si	Cu	others
Polarit 853	0.018	11.6	0.2	0.03	0.44	0.04	0.003	0.2	0.21	Ti 0.2
Polarit 720	0.020	18.2	9.1	0.2	1.4	0.02	0.002	0.2	0.19	
Polarit 752	0.030	17.6	11.5	2.5	2.51	0.029	0.002	0.5	0.28	
Ralloy 654MO	0.020	24.6	20.9	7.2	3.65	0.03	0.005	0.2	0.41	N 0.49
Armco iron	0.009	0.010	0.016						0.008	

The primary test solution consisted of distilled water with reagent grade 95 - 97 wt-% sulphuric acid (Merck 731) to adjust the pH to a value of 3. Experiments were also carried out at pH 1 and 2 (adjusted with H_2SO_4) and in neutral region. The basic temperature studied was 50 °C but experiments were also done at temperatures 20 and 75 °C. Temperature was measured in an Avesta-cell so that the thermometer was in contact to the sample surface inside the cell. This temperature was 2 - 5 °C lower than the solution temperature. Temperatures referred to in these experiments are the sample surface temperatures. Sodium sulfate (Riedel-de Häen 36482) was added to the solution in order to increase the conductivity in electrochemical experiments. In a solution of pH 3 without any supporting electrolyte the conductivity is too low to carry out polarisation experiments. In potentiodynamic polarisation experiments a dosage of 23 g/l Na_2SO_4 was used. In pitting experiments a Na_2SO_4 concentration of 2.3 g/l was used in order to minimise the possible inhibiting effect of sodium sulfate on local corrosion. When sodium sulfate was used, it was added after pH adjustment. The lower Na_2SO_4 concentration has no other effect in anodic polarisation experiments but a certain fluctuation in current density at a potential region slightly higher than the corrosion potential. Corrosion potential measurements were done both with sodium sulfate dosage (23 g/l) and without. Immersion tests were carried out in solutions without sodium sulfate. In ozone production 99,5 % O_2 (Aga) was utilized. Nitrogen and air used in purging were 99.5 % N_2 and bottled air (Aga).

2.1 Electrochemical experiments

Cyclic potentiodynamic polarisation experiments at a scanning rate of 100 mV/min were used in order to estimate the general corrosion behaviour of stainless steels and pure metals. The effect of scanning rate was studied on samples immersed 22 h in ozonated solution; scan rates were from 1 mV/min to 100 mV/min. Also the effects of solution parameters such as pH, temperature and dissolved gases (ozone, oxygen and nitrogen) were investigated using cyclic polarisation measurements. Cyclic polarisation measurements at a low scanning rate of 10 mV/min were also carried out to study pitting, which is possible in transpassive corrosion. Long term corrosion potential measurements were carried out, because in polarisation experiments it was found, that the stabilisation of the corrosion potential (open circuit potential) lasted a long time and the corrosion potential measured in anodic polarisation measurements varied greatly. Potentiostatic experiments were carried out to confirm the results of polarisation measurements and in order to estimate the dissolution mechanism in the transpassive range. The main goal of the electrochemical experiments was to compare the corrosion behaviour of different stainless steels and to estimate the effect of certain factors in the solution rather than to define the exact corrosion rate of stainless steels. The corrosion rate of stainless steels were, however, determined with the Tafel method at sweep rates of 50 and 100 mV/min.

Polarisation measurements were done using ACM Instruments Auto Tafel Potentiostat. Potentiostatic measurements were done with EG&E Princeton Potentiostat/Galvanostat Model 273. In corrosion potential measurements data was collected with a Grant 1200 data logger. Test materials were wet-ground to 800 grit, rinsed in distilled water and ethanol and dried immediately before the experiments. Cathodic cleaning was done at a potential of -1.5 V vs. SCE for 5 min. Cleaning at potential -1.0 V was found to be insufficient in the test solution with dissolved ozone to remove the oxidized layer. Polarisation measurements and Tafel experiments were also done without cathodic cleaning in experiments, where samples were immersed for 22 h before the electrochemical experiments.

After cathodic cleaning the surfaces of the specimens were left unpolarised for 1 min in polarisation experiments, after which polarisation was started usually from potential -800 mV vs. SCE in the anodic direction. The specimen was polarized in cyclic measurements up to a current density of 5 mA/cm^2. Potentiodynamic polarisation experiments for stainless steels and platinum were carried out at a scanning rate of 1, 10 and 100 mV/min and 10 mV/min for pure chromium, nickel and molybdenum. Corrosion potential measurements were started immediately after cathodic cleaning.

Cathodic polarisation experiments for stainless steels were done both after cathodic cleaning and after 22 h immersion in ozonated solution to a potential of -1000 mV vs. SCE at scanning rate 100 mV/min. The cathodic polarisation curves for platinum presented here are from the cathodic phase of cyclic polarisation experiments

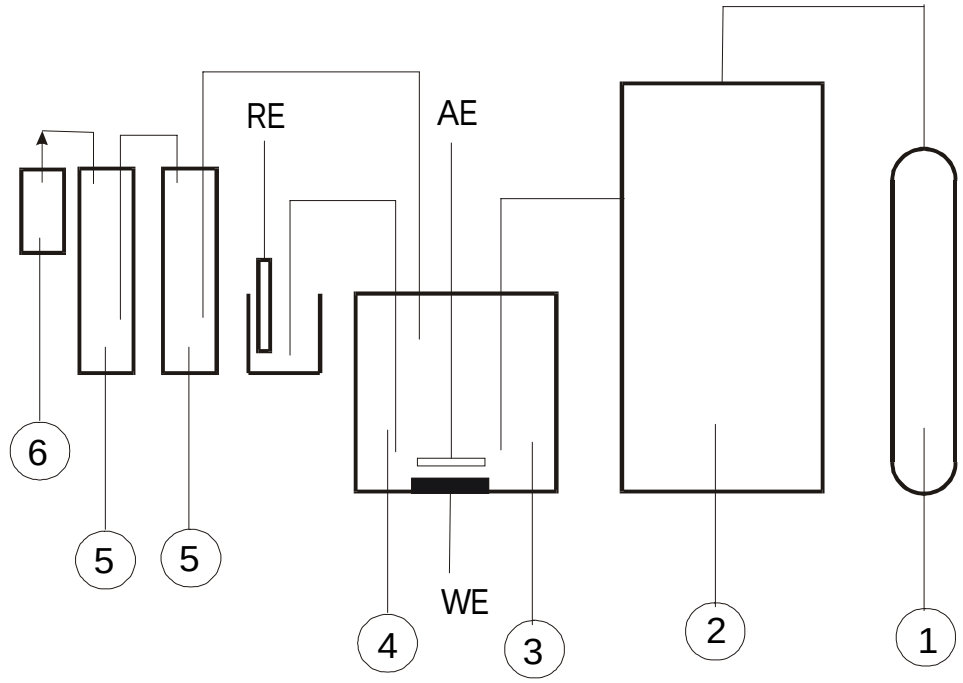

Fig. 7. Schematic figure of the test equipment. 1) oxygen gas, 2) ozonator, 3) Avesta-cell, 4) Luggin capillary, 5) KI-solution, 6) ejector.

.

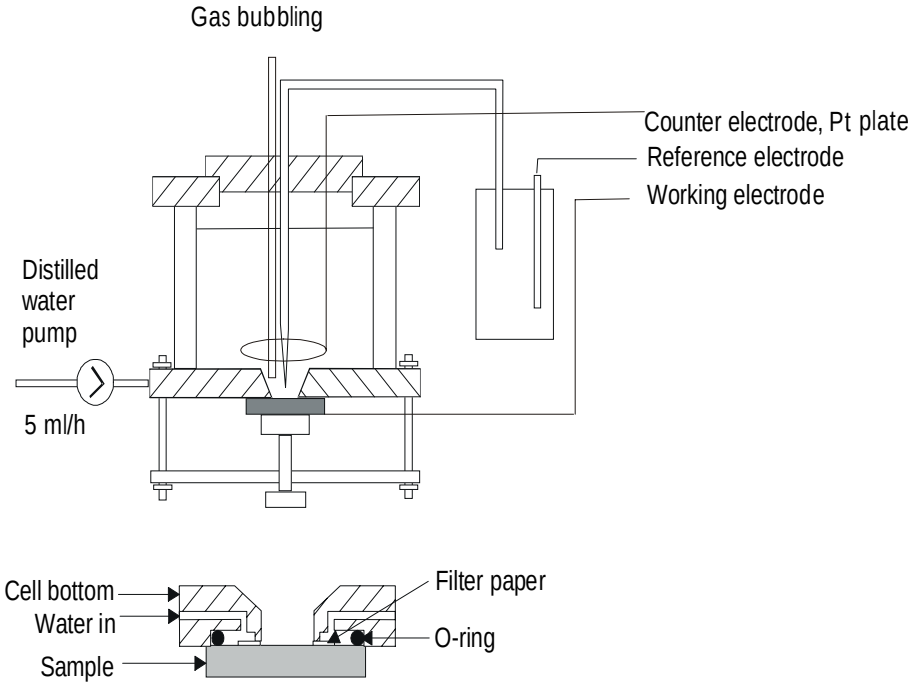

Fig. 8. Schematic picture of the Avesta-cell.

Electrochemical tests were carried out with the laboratory equipment shown in Fig. 7. Gaseous ozone was produced by a corona discharge GEV 5 laboratory ozonator type L220 - 2.5/5.0, which produces about 5 g/h ozone from oxygen and 2.5 g /h ozone from air. The ozone concentration of the gas mixture was about 20 g/m^3. The ozone concentration was adjusted by the voltage of the ozonator where necessary. The gas mixture was bubbled continuously into the cell, where ozone and oxygen dissolves into the solution while the outlet gas was removed by an ejector trough KI-solution, (BP/USP no. 2821114) which decomposes the ozone. Platinum was used as the counter electrode material.

An Avesta-cell was used in the experiments [42]. The cell was constructed at the Helsinki University of Technology, Laboratory of Corrosion and Material Chemistry. The principle of this cell is illustrated in Fig. 8. Distilled water was pumped through a filter paper between the specimen and the body of sample holder at a speed of about 5 ml/h. This prevents crevice corrosion that often occurs in conventional sample holders. Distilled water was used only in pitting corrosion tests. The stirring of the solution was done by gas bubbling: the sinter or tube for bubbling was installed just above the sample so that the gas flow did not reach the sample surface but still stirred the solution sufficiently. The Avesta-cell was heated by a water mantle. A plate working electrode was used in the cell and the Pt counter electrode was above the sample. The saturated calomel reference electrode (Radiometer type 401) was placed in a separate vessel at temperature T=25 °C connected to the measurement cell by Luggin capillary. Experimental potential values in this study are given vs. SCE at temperature T=25 °C, unless otherwise stated.

The dissolved ozone content in test solutions was 15 - 20 ppm at temperature 50 °C, 24 - 28 ppm at 20 °C and about 2 - 6 ppm at temperature 75 °C. The higher Na_2SO_4 concentration slightly decreases the ozone content. In pressure vessel experiments it was not possible to measure the

dissolved ozone concentration, but it is estimated to be about 250 ppm at 10 bar and at room temperature.

Ozone concentration was measured using a spectrophotometer (Hach DR/2000) and a colorimetric test kit (Chemetrics K-7402). Both use a methyl-substituted form of DPD (N,N-diethyl-p-phenylenediamine) reagent and the test kit potassium iodide as an activator. When using the test kit ozone reacts with the iodide to liberate iodine. The iodine then reacts with the reagent to give a blue-violet colour which is proportional to the amount of ozone in the sample. Results were quantified by visual comparison with standards using a high-range comparator. In spectrophotometric analyses ozone reacts with DPD to form a red colour which is again proportional to the amount of dissolved ozone.

In the analysis using the colormetric test kit a sample of 25 ml was taken with a pipette from the Avesta-cell. Two droplets of potassium iodide activator (A-7400) was added in the solution. A ozone ampoule (Chemets R-7402) was immersed in the sample and the tip was snapped off. Sample and reagent are mixed by tilting the ampoule so the bubble travels from end to end. After 2 minutes the resulting colour was compared to the comparator (Chemets C-7402) to quantify the result. The ozone concentration range in comparators used were from 0.6 to 2.0 mg/l. In order to analyse higher ozone concentrations, the solution needed to be diluted before the measurement.

The analysis of ozone by spectrophotometer was done according to Hach method 8177. After 3 min one DPD total chlorine powder pillow was added to a sample of 25 ml and ozone was analysed.

2.2 Pressure cell experiments

To study the corrosion behaviour of stainless steels in solutions with higher ozone concentration electrochemical experiments were carried out also using pressure vessel equipment (Fig. 9) constructed in at the Helsinki University of Technology, Laboratory of Corrosion and Material Chemistry. At the starting point both vessels were half full of distilled water. The ozone/oxygen gas mixture of was lead to the upper part of one of the pressure vessels (3). The vessels were connected together by a tube. The ozone/oxygen gas mixture fills the vessel on the right side and a corresponding amount of water is run out (6). The ozonator is switched off and the inlet valve of the gas mixture and outlet valve for water are closed and nitrogen is fed to the left hand side vessel in order to increase the pressure of the ozone gas in the other vessel (7). The equipment includes also a pressure meter (4) and a blow-off valve (5). The pressurized gas is lead to another pressure vessel (8), which is used as a test cell. The solution is bubbled continuously and the excess gas is lead trough a to a KI solution, where the ozone is decomposed.

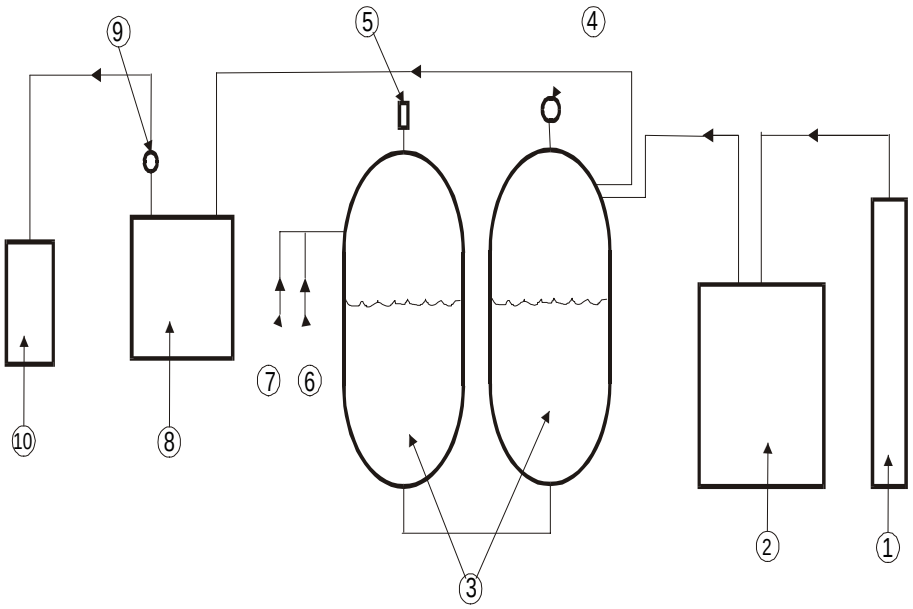

Fig. 9. Schematic figure of the pressure equipment. 1) oxygen gas, 2) ozonator, 3) pressure vessels, 4) pressure meter, 5) blow-off valve, 6) water inlet, 7) nitrogen inlet, 8) cell, 9) pressure valve, 10) KI-solution.

2.3 Immersion tests

Immersion tests were carried out in solutions of pH 3 and temperature 50 °C with and without Na_2SO_4. Stainless steels P720, P752 and Ralloy 654MO were investigated in 60 day experiments both in solutions containing no sodium sulfate and 23 g/l sodium sulfates. Sample size was about 20 x 40 x 2 mm. One side of the samples were as delivered by Outokumpu Polarit (pickled and prepassivated for P720, P720 and P752) and the other sides were ground to 800 grid. Stainless steel Ralloy 654MO was in every experiment ground to 800 grid. Specimens were placed to hang by a teflon tape in a glass cell, which was heated in a thermostated water bath. Immersion experiments were done periodically between Friday afternoons and Monday mornings because during working days other experiments of this investigation were done and no simultaneous tests were able to carry out. Between weekends samples were hold in air. All samples were in the same cell and they were weighted after 3, 12, 20, 23, 29, 32, 36, 42, 45, 48, 53, 57 and 60 days. The solution was also changed after each weight loss measurement.

The corrosion rate of steels P720 and Ralloy 654MO were studied more closely. Samples were ground to 800 grid on both sides. The duration of experiments was 1, 2, 4, 8 and 16 days so that each test material was in its own cell and each test period was a separate test. After each experiment, samples were washed, dried and weighed. After immersion test the solutions were analysed by AAS (Fe, Cr, Ni and Mo) and sample surfaces by GDOS method. In this test series the growth rate and mechanism of the oxide layers on stainless steels was investigated but also the weight losses of the materials were examined.

2.4 Surface analyses

The surfaces of the samples exposed in immersion tests were analysed by GDOS, ESCA and X-ray diffractometer methods. GDOS analyses were carried out in Rautaruukki Steel, Laboratory Service Department, Raahe and ESCA analyses at the Center of Chemical Analysis at Helsinki University of Technology. The appearance of surface was examined by an optical microscope and SEM.

GDOS analyses were carried out using Leco SDP-750 GDOS Spectrometer. Glow discharge optical spectroscopy (GDOS) is an atomic emission technique used for bulk and depth profile analysis of metals. The Grimm-type glow discharge lamp provides a low pressure argon environment over the sample surface. A high negative potential (typically -800 - to -1200V) is applied to the sample. Spontaneously produced Ar^+ ions cause plasma formation and further production of Ar^+ ions. This plasma is called a glow discharge. Some of these high velocity Ar^+ ions reach the sample surface where they uniformly sputter (or mill out) material from the sample. Sputtered material diffuse into the glow discharge plasma where it dissociates into atomic particles and reaches higher energy levels. The light emitted from excited state species, as they return back to their lower energy levels, is characteristic of the elements composing the sample. The wave lengths and intensity of the light emissions are used to identify and quantify the composition of the sample. The layer-by-layer removal of sample material presents the signal in such a manner that temporal information is also related to depth into the sample. This allows for the presentation of both qualitative and quantitative depth profile analysis [43]. Experiences have shown that 0.01% is a practical detection limit for common steel elements [44]. It has been found out in practice by Rautaruukki that GDOS results on stainless steels under about 10 nm are semiquantitative and the accuracy is low. GDOS-analysis were made for stainless steels P720 and Ralloy 654MO immersed in ozonated solution for 1, 2, 4, 8, and 16 days and in oxygen bubbled solution for 3 days. No sodium sulfate was introduced. The analysed area was about 12 mm^2.

ESCA-analysis were carried out in the Chemical Analysis Centre of Helsinki University of Technology using AXIS 165 (KRATOS Analytical) equipment. Stainless steels Polarit 720 and Ralloy 654MO were investigated. Samples were cleaned by ultrasonic cleaner in methanol for 5 min, dried in air and attached to sample holder with a carbon tape. Surface measurements were made at three different points of each sample. Measurements were wide-spectrum of the wide energy range (0 - 1100eV) and high resolution HiRes spectrum for metals (Fe, Cr, Ni, Mo, Mn) and for O and C. ESCA profiling was made in two positions. The analysis area of each measurements was about 1 mm^2. The analysis depth in surface analyses varied depending on the element from 2 nm to 10 nm. The charging of the sample surface was compensated by neutralizing the surface during measurement by slow electrons. The running parameters in wide spectrums measurements were: initiation emission: monochromatized Al Kα (13 kV, 8 mA), measurement range: general spectrum 0 - 1100 eV and resolution adjustment: analyser pass energy: 80 eV, step 1 eV; lens: hybrid, aperture: slot. During narrow range spectrums running parameters were: initiation emission: monochromatized Al Kα (13 kV, 8 mA) and resolution adjustment; analyser pass energy: 20 eV, step 1 eV; lens: hybrid, aperture: slot. The analysed ranges were: C 1s (280-300 eV), O 1s (524 - 544 eV), P2p-Si2s-S2s (125-175 eV), Fe 2p (690-750 eV), Cr 2p (560-600 eV), Ni 2p (840-890 eV), Mn 2p (630-660 eV), Mo 3d (220-240 eV) and Ca 2p (330-380) eV.

Surface examinations were carried out by JEOL JXA 840A scanning electron microscopy. X-ray diffractometer experiments were done using IBM PS/2 m-50 diffractometer with Philips PW 1710 control unit. In analysis, APD program was utilized. Current in surface analysis was 30 mA and voltage 40 kV. Both the SEM and X-ray diffractometer were located at the department of Materials Science and Rock Engineering.

3 EXPERIMENTAL RESULTS AND DISCUSSION

The redox potential of the test solution is strongly dependent on the O_3 concentration of the solution (Fig. 10). As the O_3 concentration increases to a value of about 0.5 ppm the redox potential increases to about 1000 mV (pH=3, T=20 °C, no Na_2SO_4). The further increases in ozone concentration increase the redox potential only slightly: at O_3 concentration of 28 ppm the redox potential is about 1190mV. The exact ozone concentration at which the abrupt increase in redox potential occurs cannot be accurately determined, because of the analysis method of ozone. Also a certain exact ozone concentration in solution was difficult to obtain in the experimental equipment and it was adjusted by changing the ozonator voltage. The redox-potential in nitrogen (99.5 % N_2) bubbled solution was about +380 mV and in oxygen (99.5 % O_2) bubbled about +550 mV respectively.

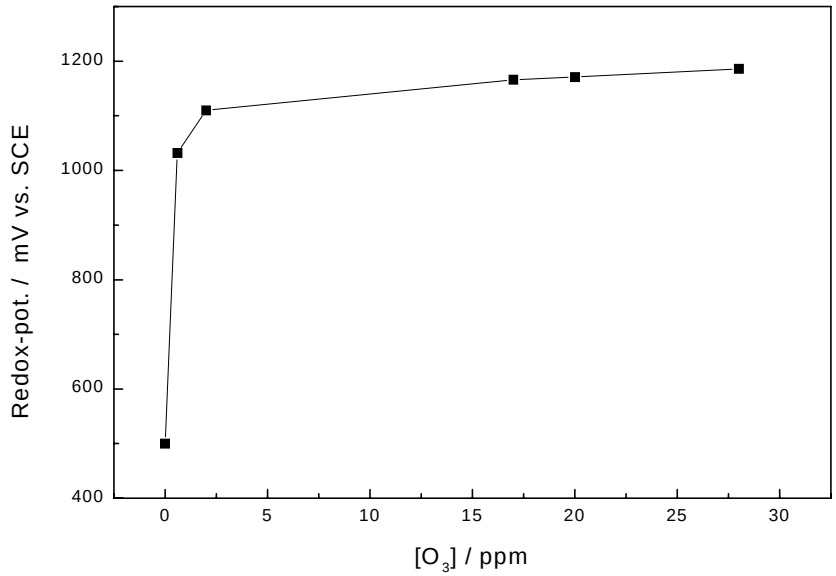

Fig. 10. The redox potential of the ozone solution, pH=3, T=20 °C.

The redox-potentials measured in the nitrogen and oxygen bubbled solutions differ from the corrosion potential of platinum in anodic polarisation (Fig. 11). The reason for this is that platinum surface is not stabilized after cathodic cleaning. The platinum surface - through contact with air and oxygen-rich water - will adopt an oxygen layer or coating and this layer will influence the voltage. The thicker the oxygen coating the higher the voltage readings. If the electrode is cleaned, the layer is removed and test results will be lower.

The anodic polarisation behaviour of pure platinum in nitrogen and oxygen bubbled solution and in ozonated solution shows (Fig. 11), that the same chemical reactions occur in ozonated solutions on the platinum electrode as in oxygen and nitrogen bubbled solutions. The current density of platinum electrode in transpassive region is only slightly
higher in ozonated solution than in oxygen and nitrogen bubbled solution. The main effect in these solutions is the change of the corrosion potential from -60 mV in nitrogen bubbled solution to +340 mV in oxygen bubbled solution and further to about +1035 mV in ozonated solution. Nitrogen used in this investigation contains 0.5 % oxygen.

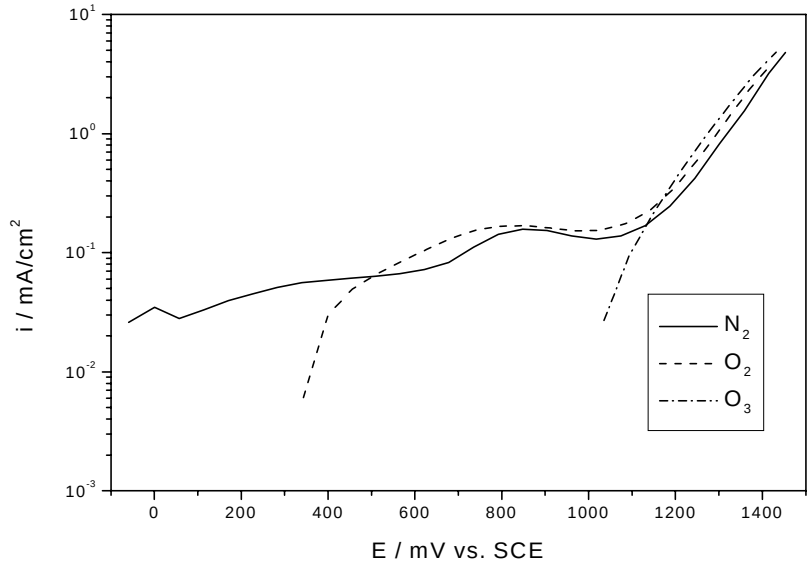

Fig. 11. The effect of dissolved N_2, O_2 and O_3 on the anodic polarisation behaviour of platinum in 23 g/l Na_2SO_4, pH=3, T=50 °C.

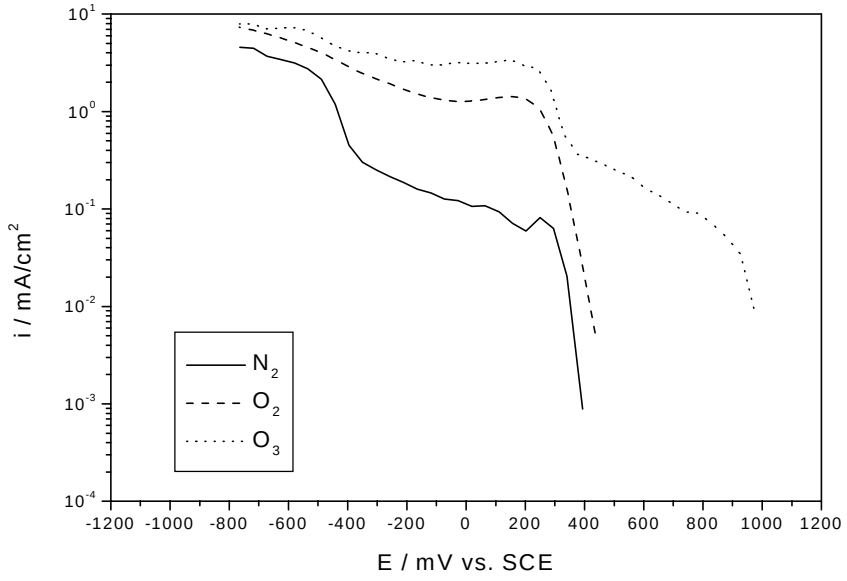

Fig. 12. The effect of dissolved N_2, O_2 and O_3 on the cathodic polarisation behaviour of platinum in 23 g/l Na_2SO_4, pH=3, T=50 °C.

The effect of dissolved nitrogen, oxygen and ozone on the cathodic polarisation of platinum indicates (Fig. 12) that the main cathodic reactions in the ozonated solution are the reduction of ozone and oxygen. In ozonated solution the cathodic reaction rate is about two times higher than in oxygen bubbled solution at lower potential region below 300 mV, where reduction of dissolved oxygen begins.

3.1 Corrosion potentials

In corrosion potential measurements the changes of open circuit potentials of test materials were followed without any interference by external current. The potential was measured with a reference electrode (SCE). The condition of stainless steel, i.e. if a steel lies in passive or in transpassive region, was examined. Corrosion potential measurements were carried out for pure chromium, nickel and molybdenum, Armco iron and for stainless steels P852, P720, P752 and Ralloy 654MO.

The differences in the corrosion potentials of pure Cr, Ni and Mo in ozonated solution at pH 3, with 2.3 g/l Na_2SO_4 at temperature 50 °C are large (Fig. 13). The corrosion potential of pure chromium increases rapidly to a value of about +790 mV, after which it decreases slightly to a value of about +740 mV. The corrosion potentials of molybdenum and especially nickel lie clearly at a lower range: Ni at about -190 mV and Mo at +20 mV respectively. Corrosion potential of Armco iron was about -720 mV in ozonated solution without any changes during the measurement.

At potential +740 mV vs. SCE (about +985 mV vs. SHE) at pH 3, chromium is, according to Pourbaix [40] (Fig. 4), in active region and forms first $Cr(OH)_4$ (considering anhydrous Cr_2O_3), which dissolves and forms hexavalent $HCrO_4^-$ or $Cr_3O_7^{2-}$ ions. Molybdenum oxidizes at potential +20 mV (+265 mV vs. SHE) through MoO_2 to MoO_3, which obviously dissolves partly to MoO_4^- ions. Nickel dissolves as Ni^{2+}-ions at potential -190 (+55 mV vs. SHE) and this ion is stable also at higher potential to about +950 mV) [40, 41]. Iron dissolves at -720 mV (-475 mV vs. SHE) at pH 3 as Fe^{2+}, which may oxidise and forms apparently $FeOH^{2+}$-complex [40].

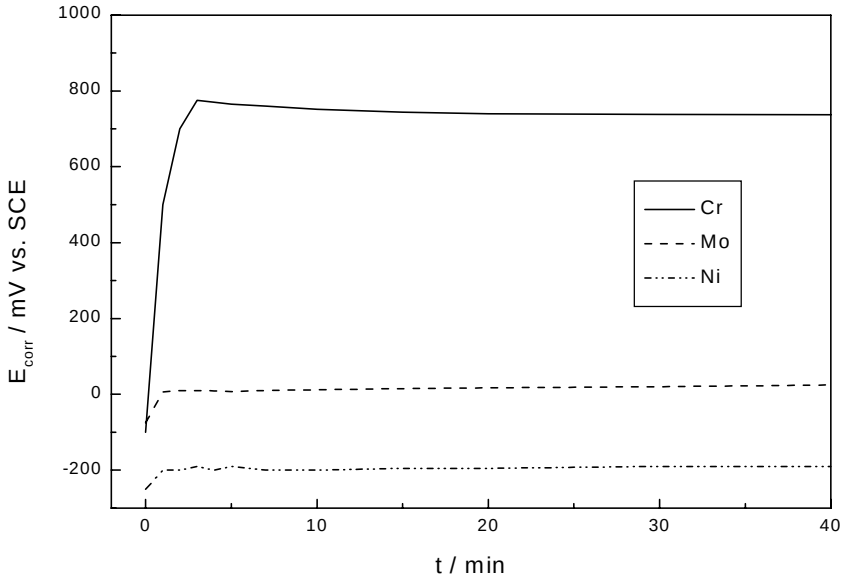

Fig. 13. Corrosion potential of Cr, Mo and Ni in ozonated solution, 23 g/l Na_2SO_4, pH= 3, T= 50 °C.

Corrosion potential measurements for stainless steels were carried out at a Na_2SO_4 concentration of 23 g/l. The duration of corrosion potential experiments for stainless steels was up to 24 h, because the stabilisation of the potentials occurs slowly. The corrosion potentials of the studied stainless steels are all at the same level, about +660 - +750 mV, but the corrosion potential of the highly alloyed stainless steel Ralloy 654MO is slightly lower (about +660 mV) than that of other stainless steels (Fig. 14). However, clear differences in the potential increase rate can be noticed. The higher the chromium content or the total amount of alloying elements the higher is the increase rate of corrosion potential. The corrosion potential of ferritic steel P853 increases clearly at a lower rate than that of the other stainless steels. The corrosion potential of highly alloyed Ralloy 654MO reaches its steady state value after about 2.5 h, but the corrosion potential of ferritic stainless steel stabilizes not until after about 17 h.

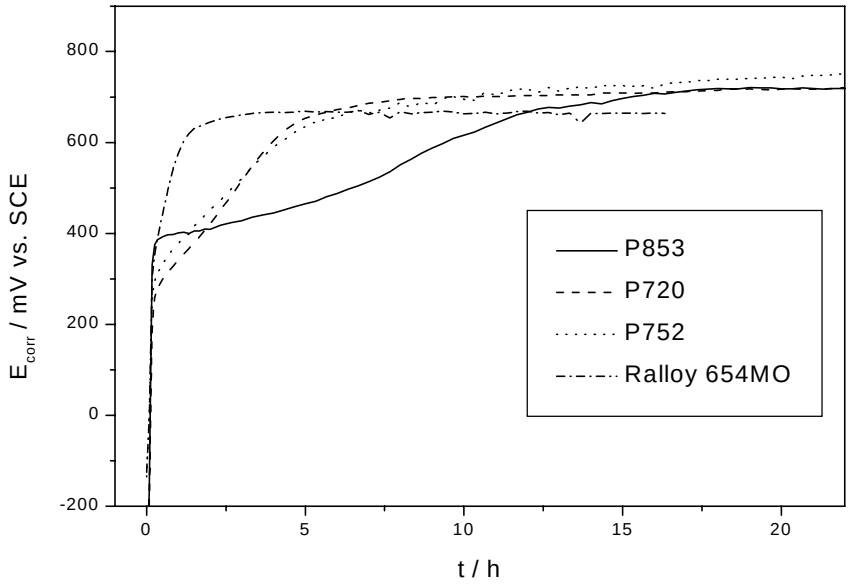

Fig. 14. Corrosion potential of stainless steels P853, P720, P752 and Ralloy 654MO in ozonated solution, 23 g/l $NaSO_4$, pH=3, T=50 °C.

The stability of alloying elements Fe, Cr, Ni and Mo in stainless steels may also be studied using corrosion potential measurements of stainless steels and Pourbaix-diagrams. Here the amount of dissolved metal is kept negligible and temperature 25 °C. At potential region +660 - +750 mV vs. SCE (+905 - +995 mV vs. SHE), iron oxidises, according to Pourbaix, to Fe^{3+} (Fe_2O_3 or $Fe(OH)_3$. The formation of oxides is more probable in ozonated solutions than hydroxides. Fe_2O_3 dissolves as $FeOH^{2+}$ [40, 41]. According to Pourbaix chromium dissolves as $HCrO_4^-$ or $Cr_2O_7^{2-}$ above potentials of about +960 mV vs. SHE; solid $Cr(OH)_4$ or $Cr(OH)_3$ is formed below this potential. According to Beverskog [41], who has studied ternary Pourbaix diagrams for the Fe-Cr-Ni system, chromium dissolves as $HCrO_4^-$ above potential +960 mV vs. SHE and below this as Cr^{3+}. Nickel dissolves as Ni^{2+} and molybdenum forms MoO_3 [40]. This oxide dissolves obviously at least partly in test solution of pH 3. Solubility of MoO_3 is in cold water 1,066 g/l and in hot water 20,55 g/l) [45].

Pourbaix diagrams give only a rough estimate of the thermodynamical behaviour of stainless steels and they give actually no information about the kinetics of chemical reactions. If the diagrams for pure metals and ternary Fe-Cr-Ni are compared, no essential differences can noticed. Ternary diagrams consider also the spinels $NiFe_2O_4$, $FeCr_2O_4$ and $NiCr_2O_4$ which are likely to occur on the oxide layers of stainless steels. Molybdenum is not present in these ternary diagrams. This complicates the interpretation of the diagrams. However, differences between diagrams for pure metals and ternary Fe-Cr-Ni diagram at temperature T=25 °C and at pH 3 are minor.

3.2 Anodic polarisation experiments

Potentiodynamic anodic polarisation measurements in ozonated solution were done both for samples immersed 22 h and for samples cathodically cleaned before experiments.

3.2.1 Anodic polarisation after cathodic cleaning

The effect of dissolved ozone on the corrosion behaviour of stainless steels after cathodic cleaning compared with nitrogen and oxygen bubbled solutions is illustrated in Fig 15. Ozone increases strongly the corrosion potential of the steel P752. Stainless steel P752 is active in nitrogen bubbled solution at sweeping rate 100 mV/min and passive in oxygen bubbled solutions. In ozonated solution the corrosion potential is within or close to the secondary active region. The corrosion potential in anodic polarisation measurements is not a steady state corrosion potential, which according to corrosion potential measurements is about 740 mV and in anodic polarisation measurement 650 mV. Ozone increases also the current density of stainless steel P752 in the secondary active, secondary passive and transpassive regions.

The slope of the anodic polarisation curve in ozonated solution from potential +750 mV to the maximum potential of the secondary active peak is about 64 mV/decade, 134 mV/decade in oxygen and 169 mV/decade in nitrogen bubbled solutions and in the transpassive region above potential +1330 mV respectively about 136 mV/decade in each solution. This means that the current density of the secondary active area and the transpassive region is not only because of the water decomposition but also oxidation of metals occur. Because of the changes in the slopes the oxidation reactions in ozonated solutions differ from those in oxygen and nitrogen bubbled solutions. The rate determinating reaction in secondary active area in oxygen and nitrogen bubbled solutions is oxidation of Cr_2O_3 to $Cr(OH)_4$ [40], where one electron is consumed. At temperature 50°C in one electron reaction the slope is theoretically 128.2 mV/decade. This agrees with the slope of the curve in oxygen bubbled solutions. In two electron reaction the theoretical slope is 64.1 mV/decade. The rate determinating anodic reaction in ozonated solutions is obviously oxidation of $Cr(OH)_4$ to hexavalent chromium ion. According to the results it is possible that in ozonated solution chromium forms hydroxide already in the passive region.

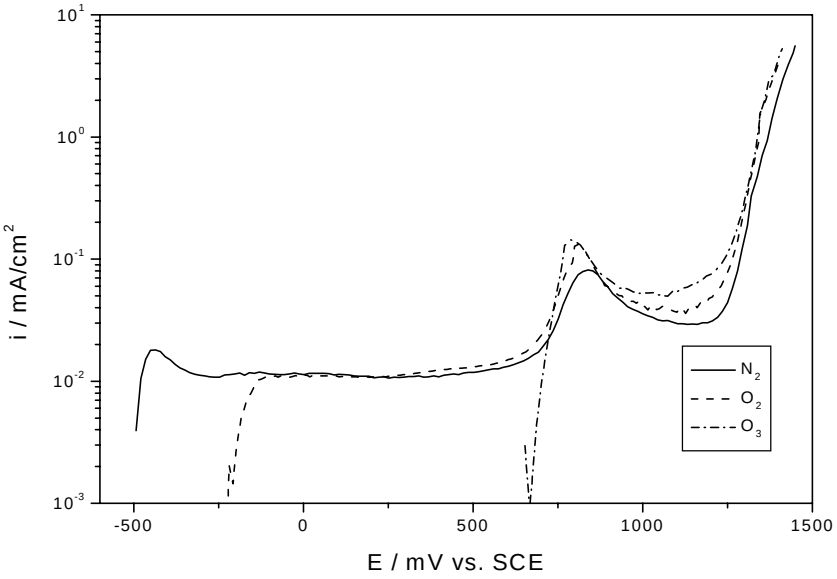

Fig. 15. The effect of dissolved N_2, O_2 and O_3 on the polarisation behaviour of stainless steel P752 in solution, 23 g/l Na_2SO_4, pH=3, T=50 °C.

The reproducibility of the experiments is rather good. The only exception is the corrosion potential, which varies in anodic polarisation tests from test to test (Fig. 16).

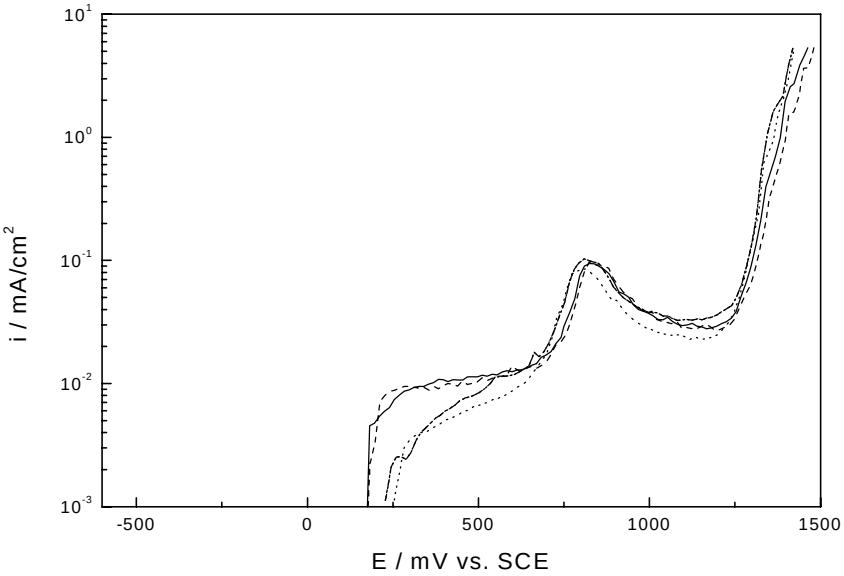

Fig. 16. Reproducibility of anodic polarisation curves of stainless steel P752 in ozonated solution, 23 g/l Na_2SO_4, pH 3, T=50 °C.

In order to estimate the effect of the alloying elements of stainless steels, polarisation behaviour of Armco Iron, chromium, nickel and molybdenum were also examined. Anodic polarisation measurements were carried out both in oxygen bubbled and ozonated solutions.

The effect of dissolved ozone on the corrosion potential of Armco iron in anodic polarisation is negligible (Fig. 17). Ozone has no essential effect on the shape of the polarisation potential curve or on the open circuit potential. The current density in ozonated solution is higher by about one order of magnitude. Armco Iron corrodes rapidly in both solutions.

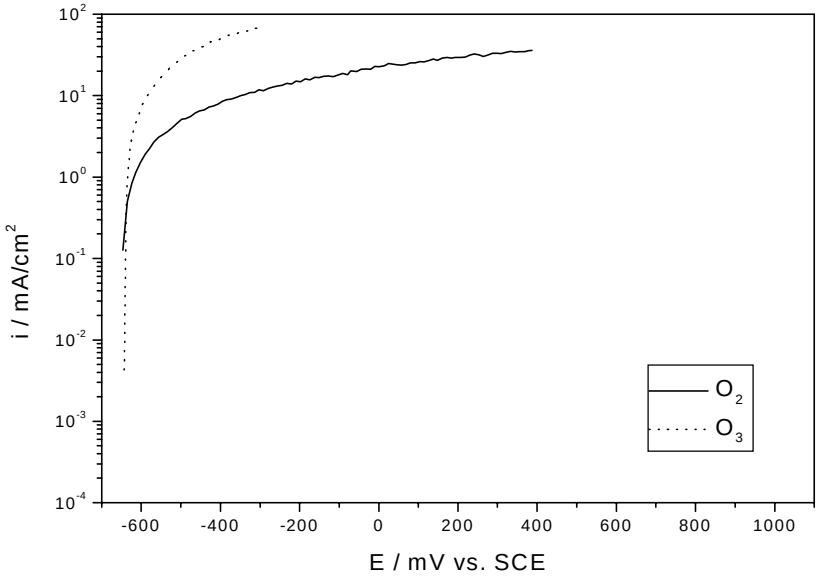

Fig. 17. The effect of dissolved O_2 and O_3 on the polarisation behaviour of Armco iron in solution, 23 g/l Na_2SO_4, pH=3, T=50 °C.

The corrosion potential of pure chromium is increased by ozone (Fig. 18) from about -250 mV to about +260 mV. The current density increases in oxygen bubbled and ozonated solutions after the transpassivation potential, about +700 mV. In transpassive region the current densities are equal in both solutions. The effect of ozone on the corrosion behaviour of pure chromium is only to increase the corrosion potential. In both solutions trivalent chromium oxide oxidises to hexavalent form at potentials above +700 mV.

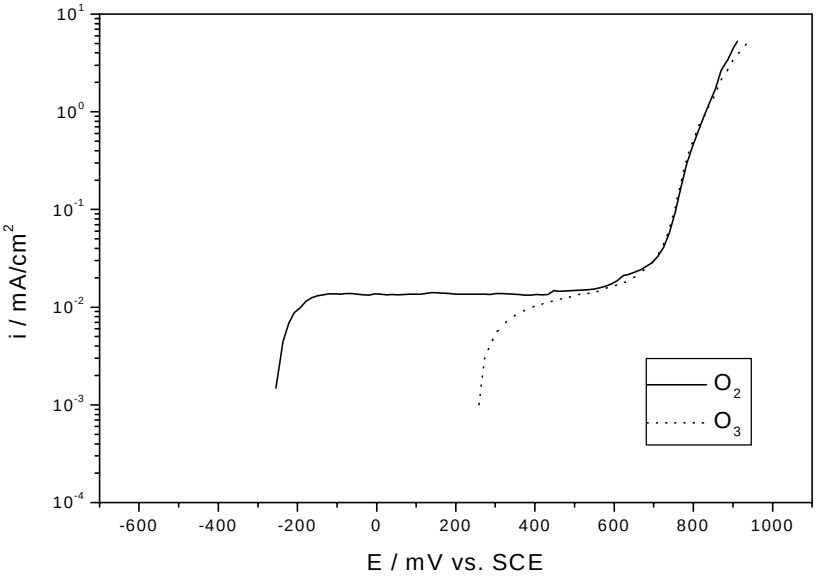

Fig. 18. The effect of dissolved O_2 and O_3 on the polarisation behaviour of pure chromium in solution, 23 g/l Na_2SO_4, pH=3, T=50 °C.

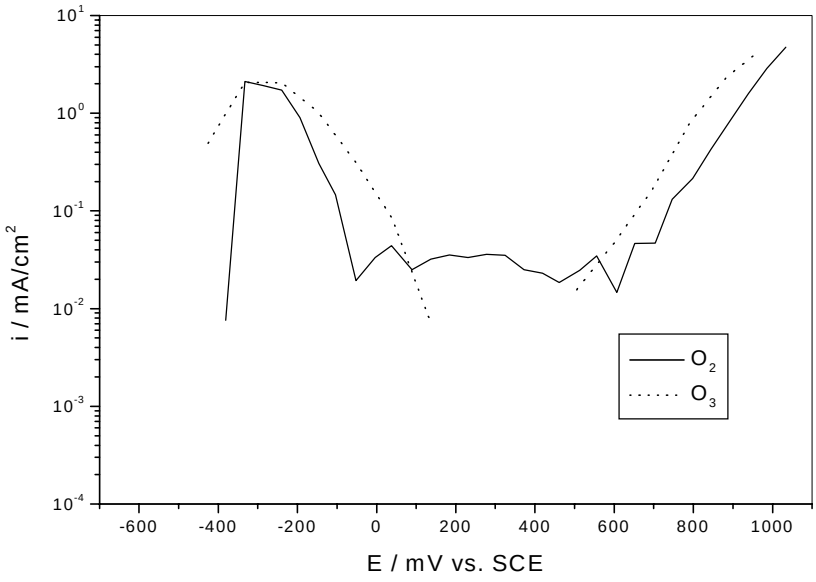

Fig. 19. The effect of dissolved O_2 and O_3 on the polarisation behaviour of nickel in solution, 23g/l Na_2SO_4, pH=3, T=50 °C.

The effect of dissolved ozone on the polarisation behaviour of pure nickel is minor. The corrosion potential is -320 mV in ozonated and -380 mV in oxygen bubbled solutions (Fig. 19). In oxygen bubbled solutions nickel is in the active state at sweep rate 100 mV/min. In ozonated solutions Ni may be either active or passive, because negative current is observed between potentials +140 and +500 mV.

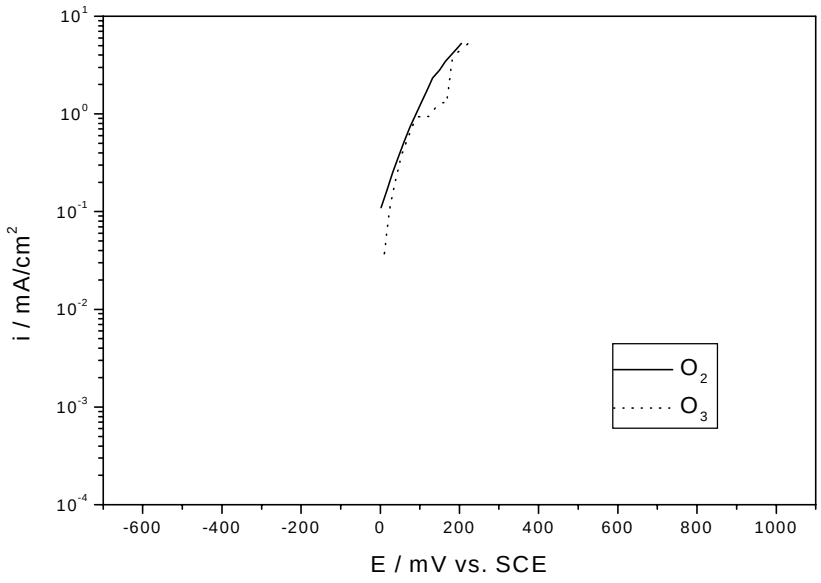

Fig. 20. The effect of dissolved O_2 and O_3 on the polarisation behaviour of molybdenum in solution, 23 g/l Na_2SO_4, pH=3, T=50 °C.

The effect of dissolved ozone on the anodic polarisation behaviour of molybdenum is also minor (Fig. 20). The corrosion potential is +2 mV in oxygen solution and +10 mV in ozonated solution. Molybdenum dissolves in oxygen bubbled and ozonated solutions at the same rate.

The corrosion potential in polarisation curves is not a steady state corrosion potential and it is clearly lower than in corrosion potential measurements. Also variations of the apparent corrosion potential are large in several parallel experiments. This means that in ozonated solutions polarisation curves alone give only a very limited view of the corrosion behaviour of metals and alloys. The current densities of materials in ozonated solution may be estimated by taking the value measured in long term corrosion potential measurements and by fitting this potential to the polarisation curves shown in figures 18 - 20. The corresponding current densities of pure chromium, nickel and molybdenum are shown in Table 4. The current density of pure nickel is the largest. On the other hand current density in the transpassive region of nickel (Fig. 19) begins to increase at about the same potential region than for chromium. This means that also nickel is oxidised at the secondary active peak, but its effect is obviously lower than the effect of chromium, because passive layers are mainly chromium oxide. A factor of uncertainty, however, must be considered when using this method, because a steady state and a transient situation are compared. Despite this the method seems to be a good tool for comparing the electrochemical corrosion behaviour of different stainless steels in ozonated solutions.

Table 4. The current densities of Cr, Ni and Mo at corrosion potential in ozonated solution, 23 g/l Na_2SO_4, pH=3, T=50 °C.

metal	E_{corr} / mV	i / mA/cm^2
Cr	740	0.3
Ni	-190	1
Mo	20	0.1

The anodic polarisation behaviour of stainless steels P853, P720, P752 and Ralloy 654MO in ozonated solution are illustrated in Fig. 21. The corrosion potential of Ralloy 654MO is the highest (about +600 mV) and those of less alloyed steels, Polarit 853, 720 and 752, are lower, from about 70 mV to 230 mV.

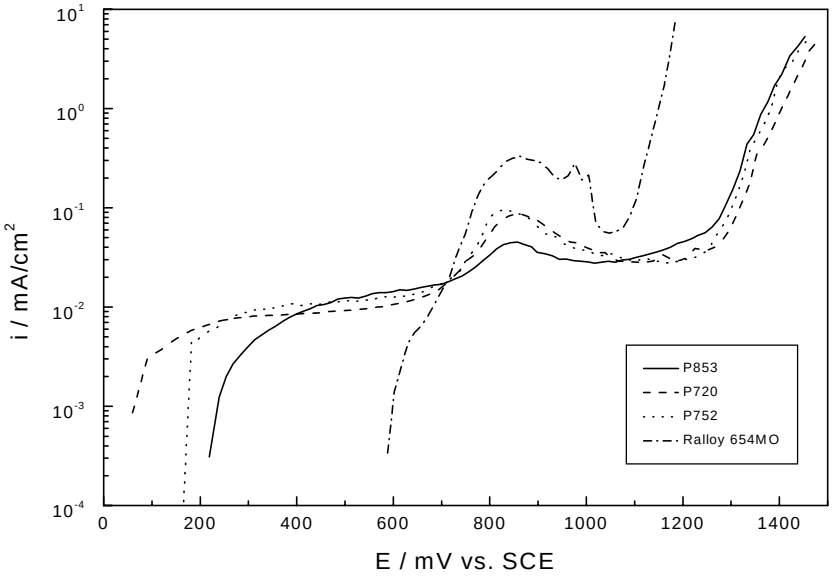

Fig. 21. Anodic polarisation behaviour of stainless steels Polarit 853, Polarit 720, Polarit 752 and Ralloy 654MO in ozonated solution: 23 g/l Na_2SO_4, pH=3, T=50 °C.

The secondary active peak at about +850 mV is, according to literature, due to oxidation of Cr^{3+} to hexavalent chromium ion [40]. The Cr concentration of stainless steel Ralloy 654MO is higher than that of the other steels studied here and the current density of the secondary active peak of Ralloy 654MO is also the highest. The current density of ferritic stainless steel Polarit 853 is almost an order of magnitude lower than that of Ralloy 654MO at the secondary active peak. Also the potential region of the secondary active peak widens as the Cr concentration increases. The secondary passive region is clearly wider and the current densities lower for the less alloyed stainless steels Polarit 853, 720 and 752 than for Ralloy 654MO. This passive region is for Ralloy 654MO only about 50 mV, while it is 300 - 400 mV for other steels. After secondary passive region the current density of Ralloy 654MO begins to increase at lower potential (+1100 mV) than of other steels (+1250 mV).

The current densities from the polarisation curves at steady state corrosion potential are shown in Table 5. The current density of Ralloy 654MO is the highest and the current density of ferritic steel P853 is lower than that of austenitic steels P720 and P752. Thus it seems again that the corrosion rates of more alloyed stainless steels in solutions containing dissolved ozone are higher than those of less alloyed steels.

Table 5. The current densities of stainless steels P852, P720, P752 and Ralloy 654MO at corrosion potential in ozonated solution, 23 g/l Na_2SO_4, pH=3, T=50 °C.

metal	E_{corr} / mV	i / mA/cm^2
P853	719	0.02
P720	720	0.02
P752	750	0.03
Ralloy 654MO	665	0.08

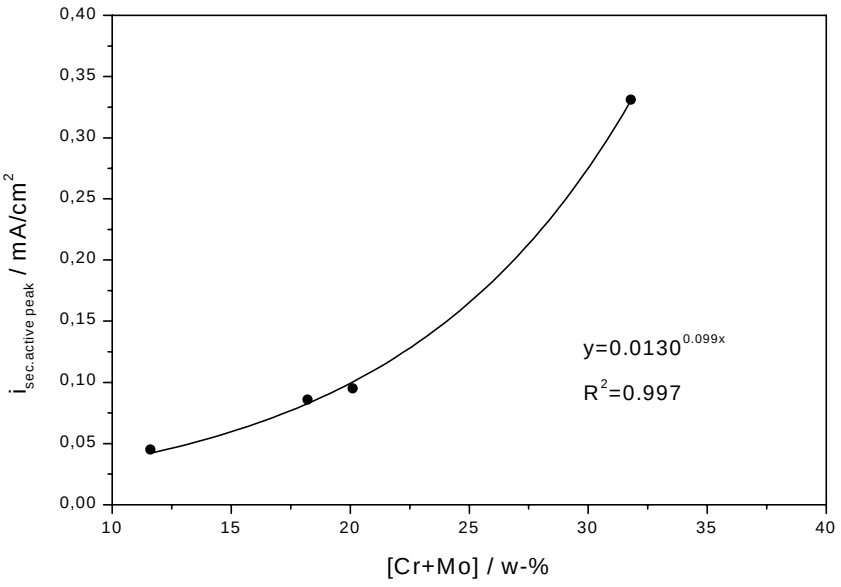

Fig. 22. The effect of (Cr+Mo) concentration on the current density at the secondary active peak of stainless steels P853, P720, P752 and Ralloy 654MO.

The current densities at the secondary active peak of stainless steels (Fig.21) as a function of (Cr + Mo) concentration follow an exponential equation ($y = 0.0130\ e^{0.099x}$), where y = i/(mA/cm^2) and x = [Cr+Mo] / wt-%, (Fig. 22). The slopes of the linear equations in form $\log(i) = a + b \cdot C$, where C = [Cr], [Ni], [Mo], [Cr+Ni+Mo], [Cr+Ni] or [Ni+Mo] concentration, log (i) the current density of the active peaks and a and b constants, are shown in table 6. The low concentrations of Ni and Mo for P853 and Mo for P720 have been ignored in these calculations.

Table 6. The slopes for current densities at the secondary active peaks for stainless steels P853, P720, P752 and Ralloy 654MO in ozonated solution. pH=3, T=50 °C.

elements	b
Cr	0.0349
Ni	0.0289
Mo	0.0344
Cr+Ni+Mo	0.0133
Cr+Ni	0.0143
Ni+Mo	0.0149
Cr+Mo	0.0232

Chromium and molybdenum have the largest effect on the current density of the active peak and nickel affects less than the other elements. The effect of element combinations is lower than pure metals.

The reactions in the beginning of the transpassive region can not be explained with the help of polarisation curves. It is obvious that these reactions are due both to the dissolution of certain alloying elements and to chemical oxidation reactions in the oxide layers or in the solution. This is why both corrosion potential and anodic polarisation measurements were made also for pure alloying elements (Cr, Ni, Mo) and for platinum.

3.2.2 The effect of sweep rate

The effect of sweep rates 1, 10 and 100 mV/min on the anodic polarisation behaviour of stainless steel was investigated for samples immersed 22 h in ozonated solution (pH=3, T=50 °C, 23 g/l Na_2SO_4).

Increasing the scanning rate from 1 to 10 mV/min has only a negligible effect on the polarisation curve of stainless steel P853 (Fig. 23). At scanning rate 100 mV/min the current density below potential 830 mV is lower than for 1 and 10 mV/min. The secondary active peak is higher at sweep rate 100 mV/min and the current density in the secondary passive region is higher than at lower scanning rates.

In the polarisation curve of stainless steel P720 at scanning rate 1 mV/min the current density at potentials below 830 mV is higher than at scanning rates 10 and 100 mV/min (Fig. 24). This is caused by the lower corrosion potential. At scanning rates 10 and 100 mV/min the current density is higher in the secondary passive region than for 1 mV/min. At the scanning rate of 100 mV/min the current density of the secondary active peak is clearly higher.

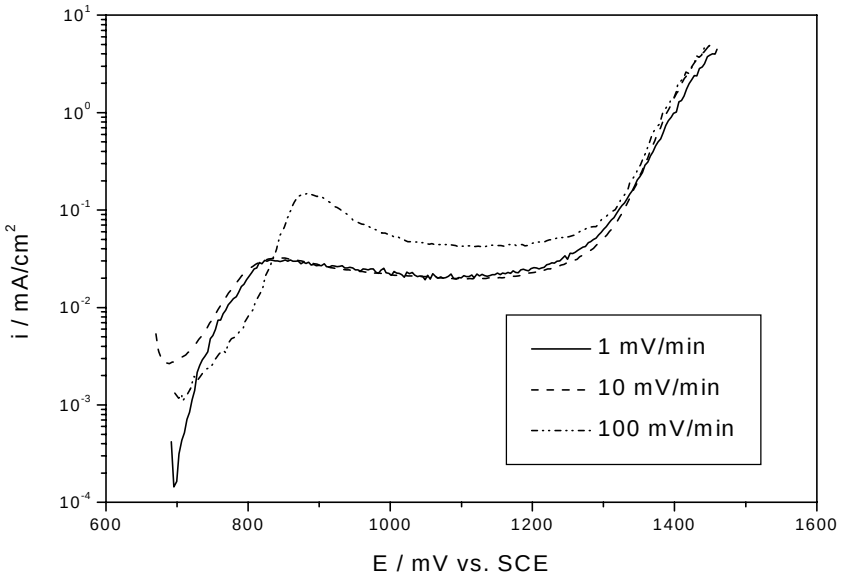

Fig. 23. The effect of scanning rate on the anodic polarisation behaviour of stainless steel P853 immersed 22 h before experiment in ozonated solution, pH=3, 23 g/l Na_2SO_4, T=50 °C.

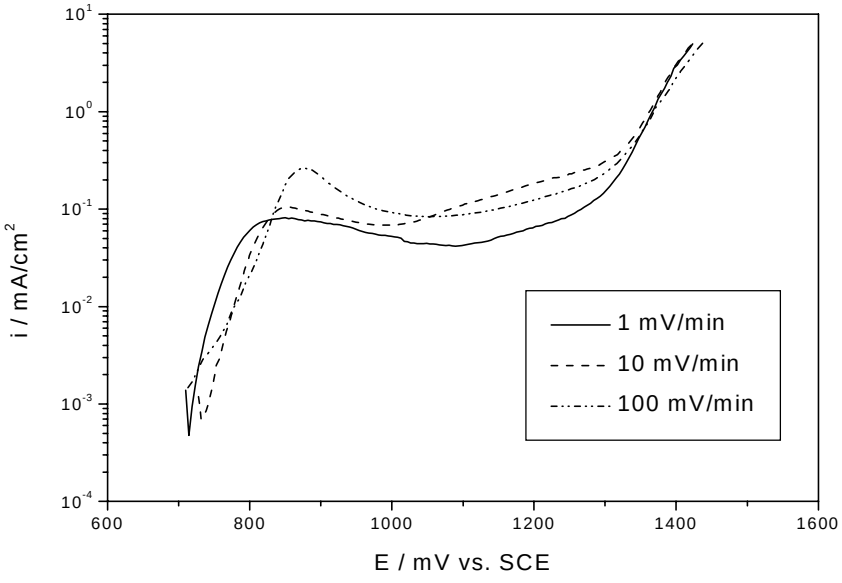

Fig. 24. The effect of scanning rate on the anodic polarisation behaviour of stainless steel P720 immersed 22 h before experiment in ozonated solution in ozonated solution, pH=3, 23 g/l Na_2SO_4, T=50 °C.

The differences in the polarisation curves of P752 at scanning rates 1, 10 and 100 mV/min are shown in Fig. 25. Again at the scanning rate 100 mV/min the current density is lower below potential about 820 mV than at 10 mV/min. At scanning rate of 100 mV/min again a higher secondary active peak can be seen. Current density is lowest at the sweep rate 1 mV/min.

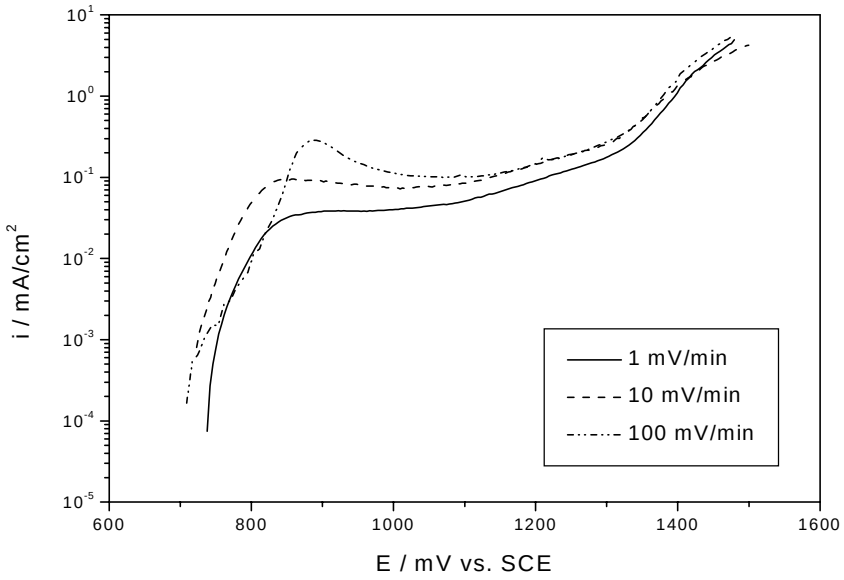

Fig. 25. The effect of scanning rate on the anodic polarisation behaviour of stainless steel P752 immersed 22 h before experiment in ozonated solution in ozonated solution, pH=3, 23 g/l Na_2SO_4, T=50 °C.

The polarisation behaviour of Ralloy 654MO differs from the other steels. No secondary active peak or secondary passive region can be seen. Also the effect of the scanning rate is not so evident (Fig. 26). The current density for scanning rate 100 mV/min is lower than for 10 mV/min at potentials below +850 mV.

The current densities in the polarisation curves decrease below potential 820 - 840 mV as the scanning rate increases from 10 to 100 mV/min in all stainless steels. This unusual situation is caused either by changes in the oxide layers formed on stainless steels in ozonated solution or by the changes in corrosion potential in separate experiments. The oxide layers are thicker than in solutions without dissolved ozone and also the chemical composition of the oxide layers differ from the "normal" passive layers. Ar potentials between 850 mV and 900 mV, the current densities generally increase with higher scanning rates. In Ralloy 654MO no secondary active peak or secondary passive region can be seen, but in lower alloyed steels an active peak occurs. At scanning rate 100 mV/min the current density of the active peak in the polarisation curves of P853, P720 and P752 is higher than at lower sweep rates.

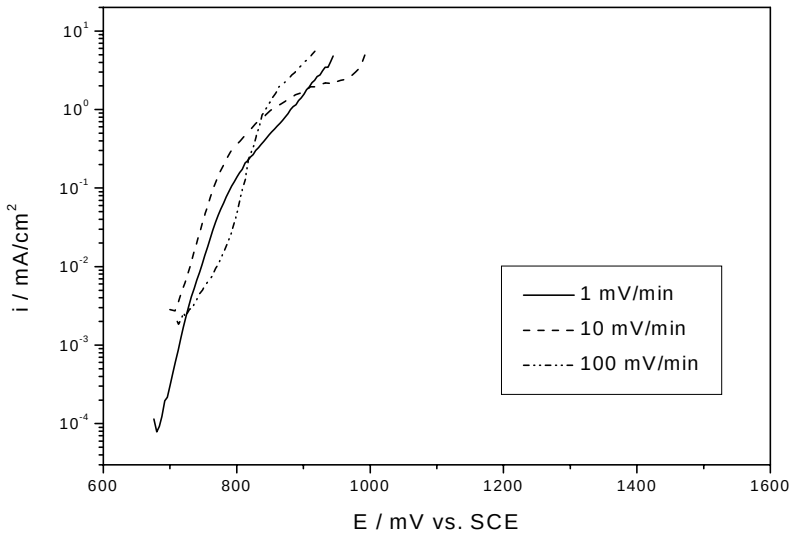

Fig. 26. The effect of scanning rate on the anodic polarisation behaviour of stainless steel Ralloy 654MO immersed 22 h before experiment in ozonated solution in ozonated solution, pH=3, 23 g/l Na_2SO_4, T=50 °C.

3.2.3 The effect of stabilisation

The effect of 22 h immersion in ozonated solution on the anodic polarisation behaviour of stainless steels compared with cathodically cleaned (5 min -1.5 V) steels are shown in Fig. 27 - 30. The sweep rate was 100 mV/min.

After 22 h immersion in ozonated solution the thickness of the oxide layers on the alloys differ greatly. On P720 the thickness measured by GDOS is about 4 nm and on Ralloy 654MO 52 nm. Oxide layers are more or less uneven with faults and some porosity. Thus the effective surface area after 22 h immersion is not the same as in experiments immediately after cathodic cleaning. Also the effective surface area is not the same on every steel. It is larger in Ralloy 654MO and P752 than on other steels. All this affects not only the cathodic polarisation behaviour of the stainless steels, but and also the interpretation of the results.

Polarisation curves after 22 h immersion in ozonated solution differ from the curves in the experiments where polarisation was started from potential -800 mV immediately after cathodic cleaning (5 min at -1.5 V). After 22 h immersion corrosion potentials of all studied steels are higher. The current densities of the secondary active peak and the secondary passive region are higher for P853, P720 and P752 after 22 h immersion. This increase is greatest for P752 and lowest for P853. The polarisation behaviour of Ralloy 654MO differ from the others. After 22 h immersion neither a secondary active peak nor a secondary passive region is observed.

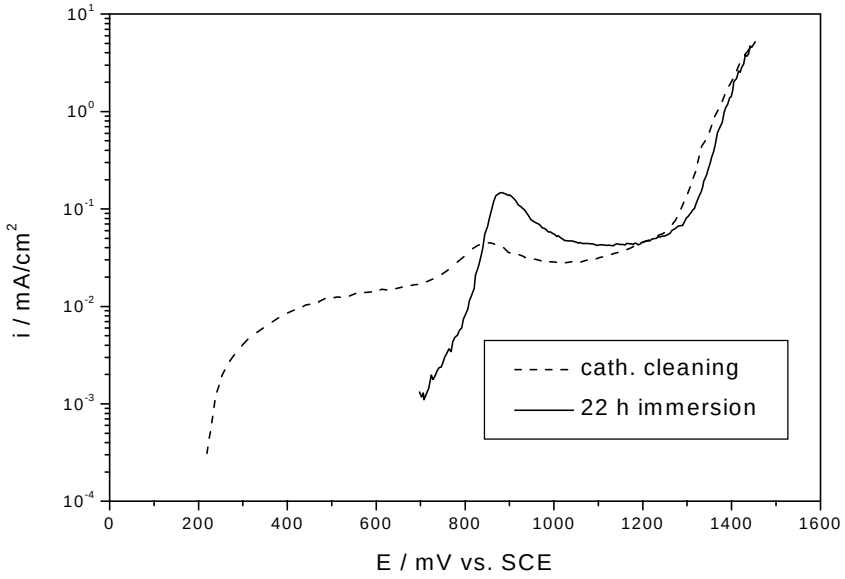

Fig. 27. The effect of 22 h immersion in ozonated solution (pH=3, 23 g/l Na_2SO_4, T=50 °C) on the anodic polarisation behaviour of stainless steel P853.

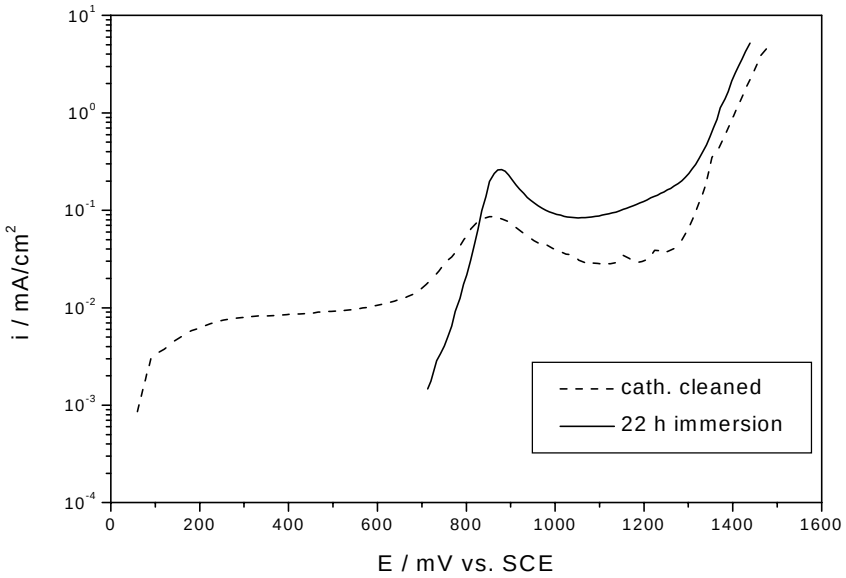

Fig. 28. The effect of 22 h immersion in ozonated solution (pH=3, 23 g/l Na_2SO_4, T=50 °C) on the anodic polarisation behaviour of stainless steel P720.

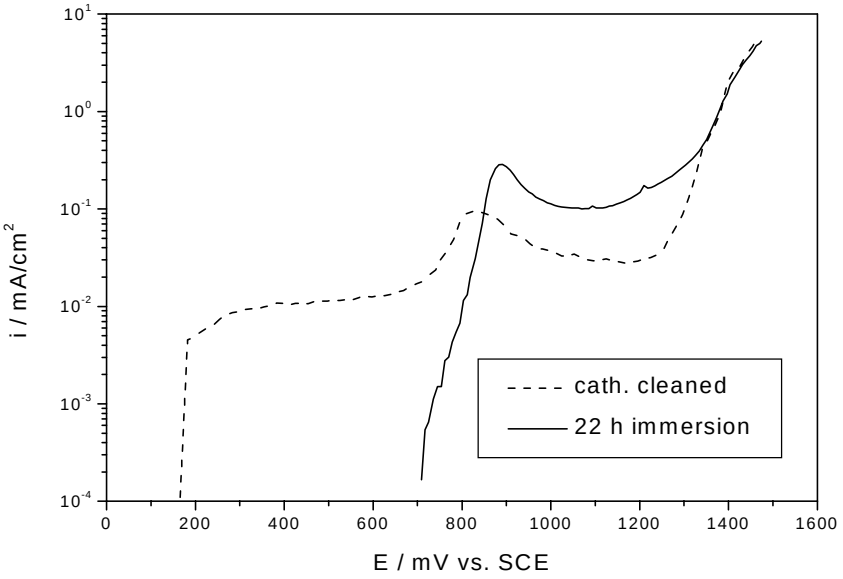

Fig. 29. The effect of 22 h immersion in ozonated solution (pH=3, 23 g/l Na_2SO_4, T=50 °C) on the anodic polarisation behaviour of stainless steel P752.

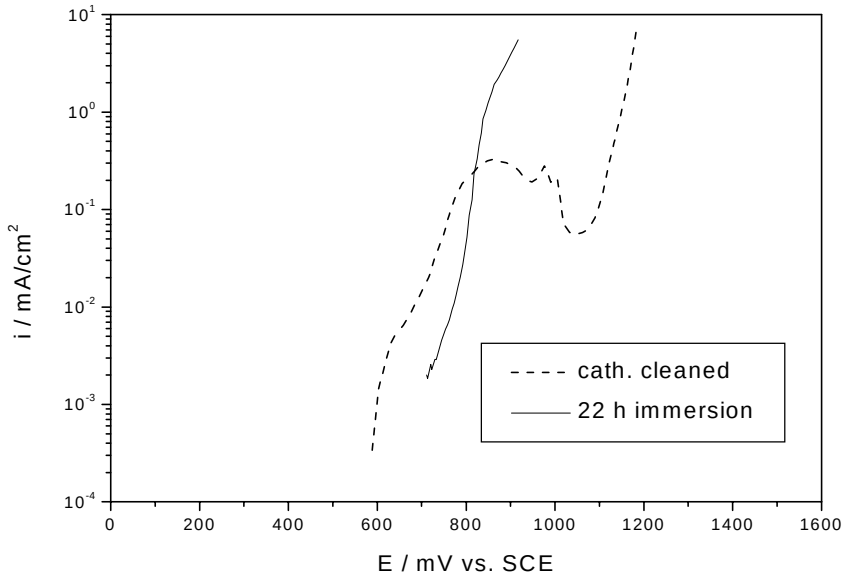

Fig. 30. The effect of 22 h immersion in ozonated solution (pH=3, 23 g/l Na_2SO_4, T=50 °C) on the anodic polarisation behaviour of stainless steel Ralloy 654MO.

Both the larger effective surface area and the chemical changes in the oxide layers after 22 h immersion affects the shape of the polarisation curves. However, the strong influence

on the polarisation behaviour of Ralloy 654MO is due to the chemical changes in the oxide rather than the effect of increased effective surface area which is minor. In GDOS analyses it has been found (hereafter in this thesis) that the chromium concentration in the outer oxide layer of Ralloy 654MO is strongly decreased and the iron and molybdenum concentrations are increased. For steels P853, P720 and P752 changes in the oxide after 1 day are minor. The slopes of the polarisation curves are about 60 mV/decade for all studied steels after 22 h immersion. It can again be assumed that the rate determinating reaction is the oxidation of $Cr(OH)_4$ to hexavalent chromium ion. Oxide layers on P853, P720 and P752 are thinner after 22 h immersion and they have a higher protective nature compared to the oxide layer of Ralloy 654MO.

3.2.4 The effect of pH

The effect of pH has been studied at pH values 1, 2, 3 and near neutral. The purpose of these tests was to evaluate for each material the critical pH value at which the corrosion rate starts to increase in ozonated solution. The Na_2SO_4 concentration of the solution was 23 g/l.

The anodic polarisation behaviour of ferritic stainless steel P853 at pH 1, 2, 3 and 7.7 is illustrated in Fig. 31. In the solutions of pH 1 and 2, the corrosion potential is between -520 - -560 mV, which means that steel may be in an either active or passive state in these solutions. A clear secondary active peak occurs at each pH. As the pH decreases the potential and the current density of the secondary active peak increases (table 7). At pH 7.7 the peak is negligible.

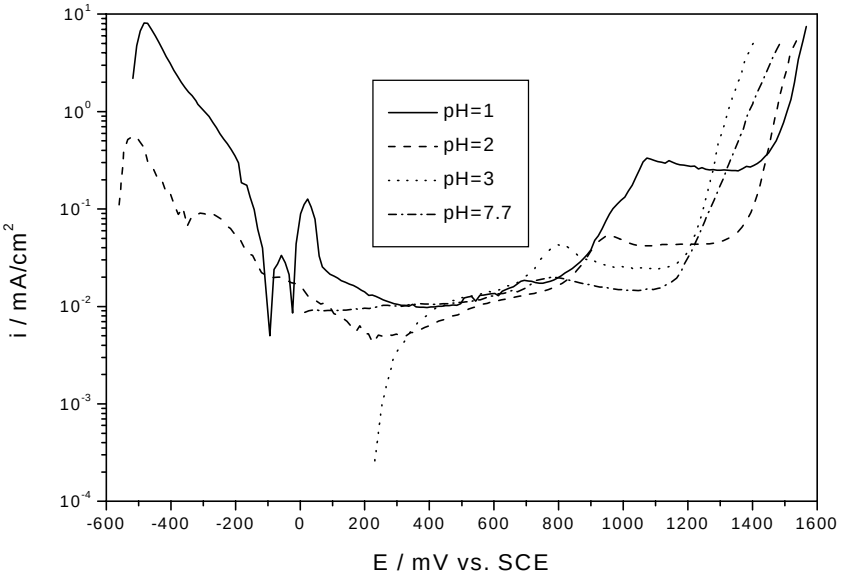

Fig. 31. Anodic polarisation behaviour of stainless steel P853 in ozonated solution at pH 1, 2, 3 and 7.7, 23 g/l Na_2SO_4, T=50 °C.

Table 7. Current density and potential of secondary active peak of stainless steel P853.

pH	i / mA/cm^2	E / mV
1	0.33	1073
2	0.05	959
3	0.04	796
7.7	0.02	774

Fig. 32 shows the results of anodic polarisation measurements for the stainless steel P720 at temperature 50 °C when the pH of the solution is 1, 2, 3 and 6. The change in pH affects the shape of the secondary active peak as for P853, but at pH 1 the secondary passive region is not so evident as in solutions of higher pH. The current densities and potentials at the secondary active peaks are shown in Table 8.

Table 8. Current density and potential of secondary active peak of stainless steel P720.

pH	i / mA/cm^2	E / mV
1	1.88	1102
2	0.19	936
3	0.09	853
6	0.02	804

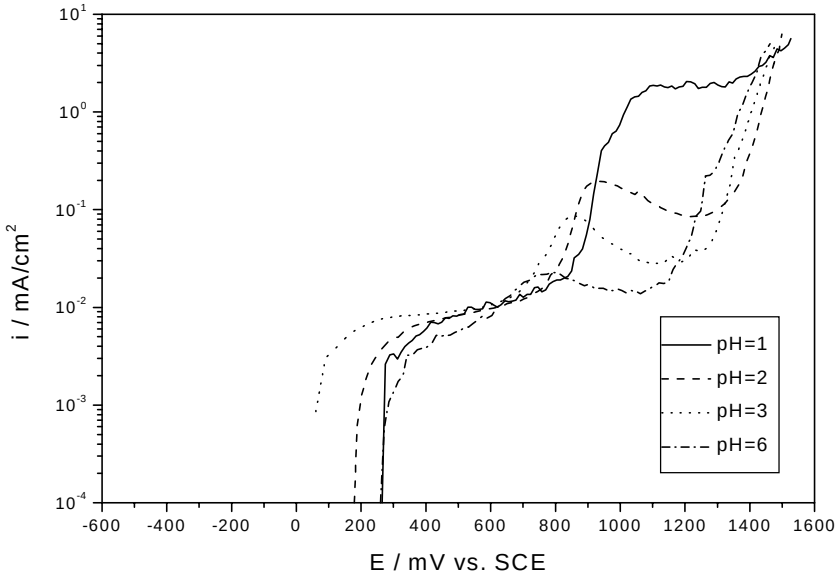

Fig. 32. Anodic polarisation behaviour of stainless steel P720 in ozonated solution at pH 1, 2, 3 and 6, 23 g/l Na_2SO_4, T=50 °C.

The behaviour of P752 in pH 1, 2, 3 and 6 is similar to P720 (Fig. 33). At pH 1 no secondary passive region is not found. The current densities are higher than for P720 and the peak potentials correspondingly lower (Table 9).

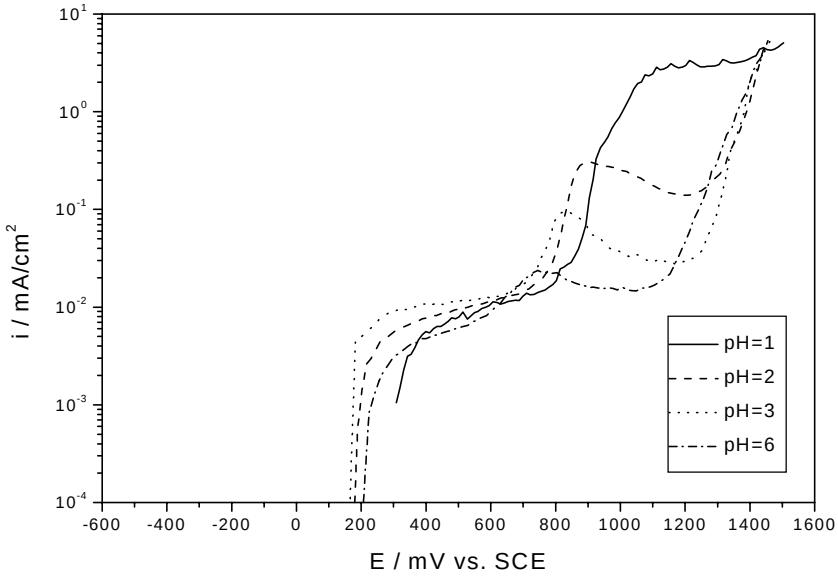

Fig. 33. Anodic polarisation behaviour of stainless steel P752 in ozonated solution at pH 1, 2, 3 and 6, 23 g/l Na_2SO_4, T=50 °C.

Table 9. Current density and potential of secondary active peak of stainless steel P752.

pH	i / mA/cm^2	E / mV
2	0.31	905
3	0.09	825
6	0.021	745

The corrosion potential of the higher alloyed Ralloy 654MO decreases when pH decreases. Likewise the secondary peak disappears already at pH 2 and the potential of the transpassive region decreases (Fig. 34).

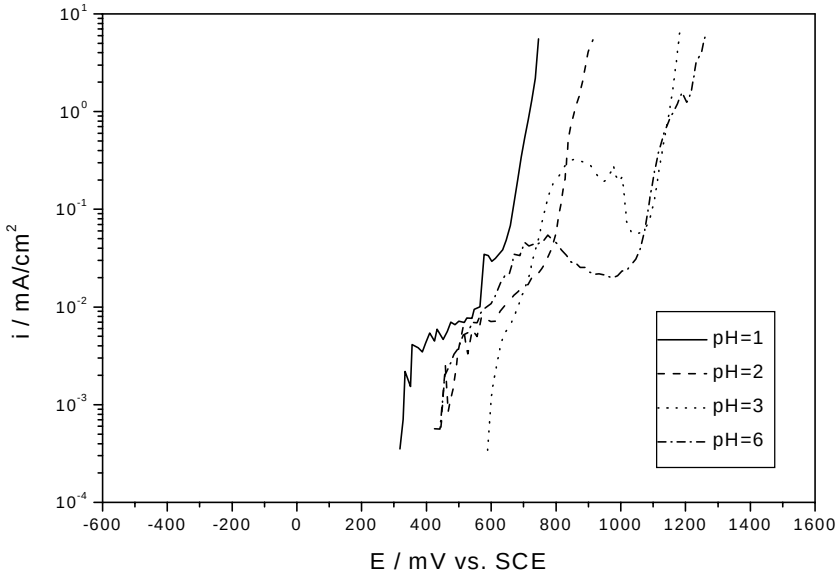

Fig. 34. Anodic polarisation behaviour of Ralloy 654MO at pH 1, 2, 3 and 6 in ozonated solution, 23 g/l Na_2SO_4, T=50 °C.

As the pH value decreases, the peak potential of the secondary active peak of stainless steels increases, as shown in Fig. 35. Differences between the potentials of the test materials are 50 - 90 mV and is obviously due to the variations in experiments. The potential of the secondary active peak is a function of pH and the composition of the material has only a minor effect.

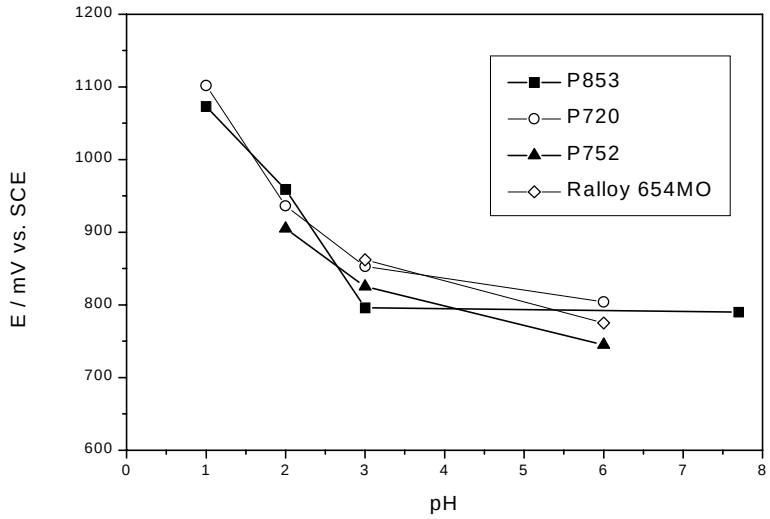

Fig. 35. The effect of pH on the potential of the secondary active peak of stainless steels P853, P720, P752 and Ralloy 654MO in solution, 23 g/l Na_2SO_4, T=50 °C.

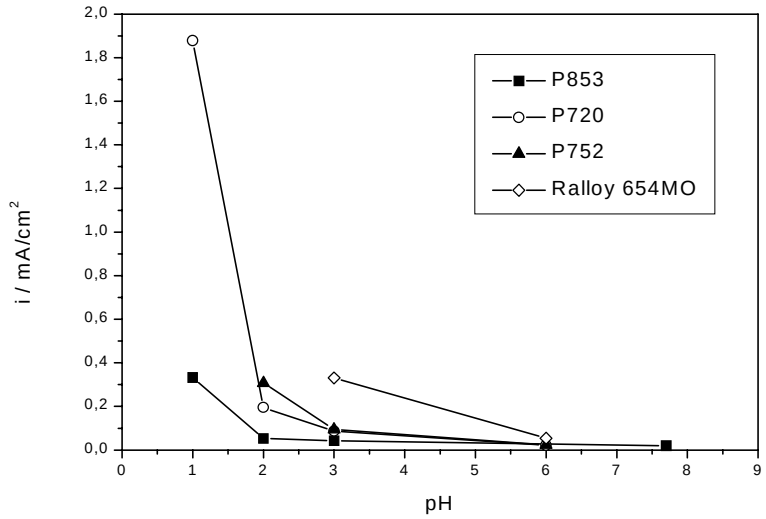

Fig. 36. The effect of pH on the current density of the secondary active peak of stainless steels P853, P720, P752 and Ralloy 654MO in solution, 23 g/l Na_2SO_4, T=50 °C.

The maximum current density of the secondary active peak clearly depends on the composition of the test materials (Fig. 36). The effect of composition decreases as pH increases: at pH 2 the current density of P752 (0.307 mA/cm^2) is about ten times compared with that of P853 (0.053 mA/cm^2) and at pH 6 the current density of Ralloy 654MO is only about two times higher than that of P720.

The reaction mechanism of the stainless steels changes as pH decreases. The real transpassive region begins without a secondary peak and secondary passive region below a critical pH value. This critical pH value is below 1 for P853 and P720, between 1 and 2 for P752 and for Ralloy 654MO it is between 2 and 3. This changes at low pH results according to Pourbaix diagrams [40] from the oxidation of chromium in stainless steel directly to trivalent ions, not to chromium oxide.

3.2.5 The effect of pressure

Anodic polarisation measurements were also carried out in a pressure vessel, with pressure up to 11 bar. The higher ozone concentration has no essential effect on the corrosion behaviour of the test materials. Results of the pressure experiments for stainless steels P752 and Ralloy 654MO are shown in Fig. 37 and Fig. 38. The experiments at 1 bar pressure were also done in pressure vessel equipment. At a pressure of 1 bar the current
density of the secondary passive region is lower and the transpassive region begins at lower potentials than in the Avesta cell. The potential and current density variations are larger in a pressure vessel than in the Avesta cell. The corrosion potential of Ralloy 654MO in particular at pressure 1 bar (Fig. 38) differs greatly from experiments made in the Avesta-cell.

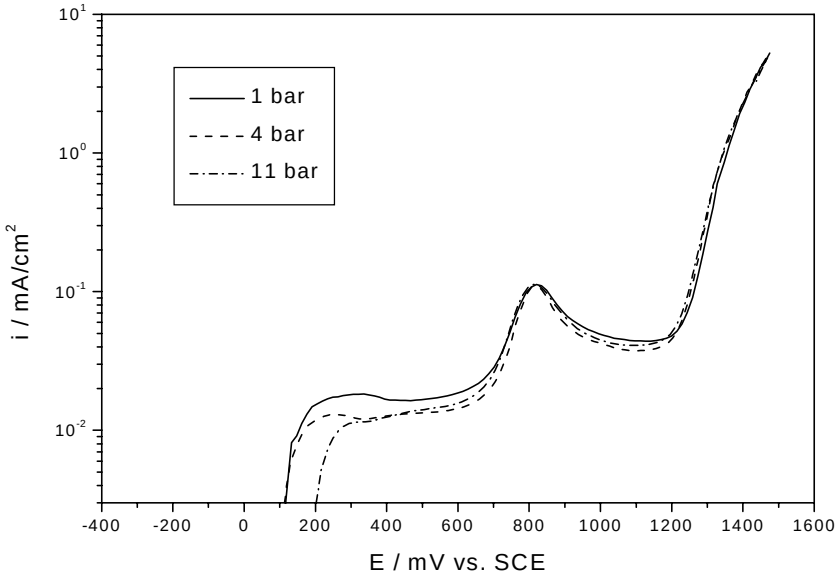

Fig. 37. The effect of pressure (1, 4 and 11 bar) on the polarisation behaviour of stainless steel P752 in ozone solution, 23 g/l Na_2SO_4, pH=3, T=25 °C.

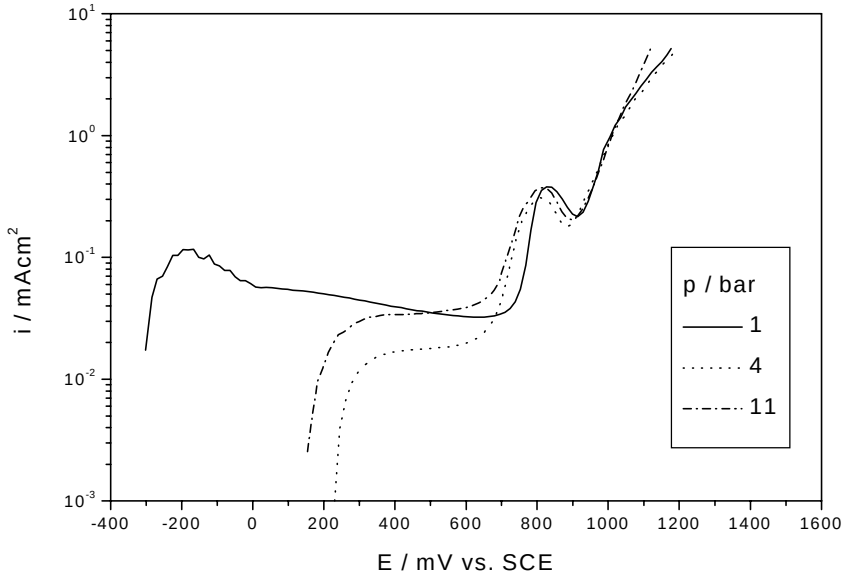

Fig. 38. The effect of pressure (1, 4 and 11 bar) on the polarisation behaviour of stainless steel Ralloy 654MO in ozone solution, 23 g/l Na_2SO_4, pH=3, T=25 °C

3.3 Cathodic polarisation experiments

Potentiodynamic cathodic polarisation measurements were carried out in order to investigate the effect of cathodic reactions on the corrosion behaviour of stainless steels. Experiments were carried out in oxygen bubbled solution after cathodic cleaning and in ozonated solution both after cathodic cleaning and after 22 h immersion. The solution was: pH=3, T=50 °C, Na_2SO_4 23 g/l. Cathodic cleaning was done at potential -1,5 V for 5 min, after which samples were held for 60 s at the open circuit potential and the polarisation was started in oxygen bubbled solution at potential -300 mV and in ozonated solution at 0 mV. After 22 h immersion in ozonated solution, polarisation was started at the corrosion potential. The scan rate was 100 mV/min.

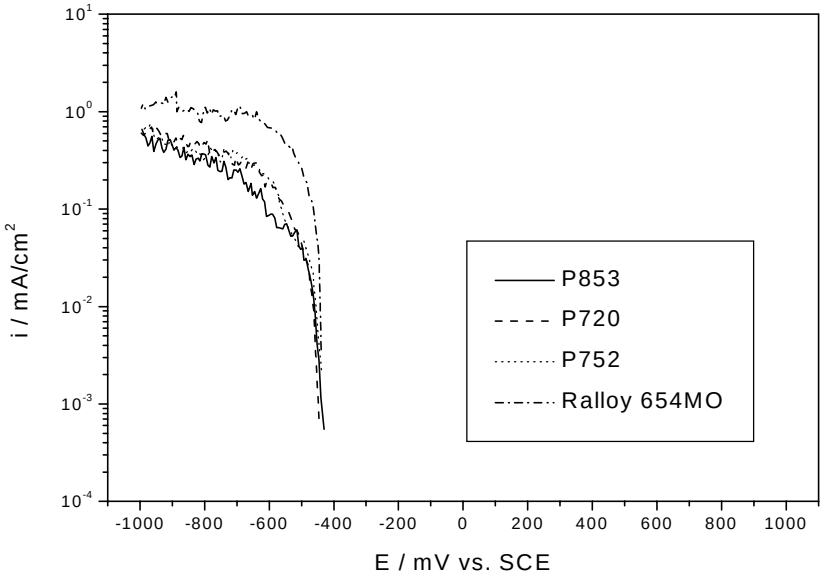

Fig. 39. Cathodic polarisation behaviour of stainless steels P853, P720, P752 and Ralloy 654MO in oxygen bubbled solution, 23 g/l Na_2SO_4, pH=3, T=50 °C.

In oxygen bubbled solution the cathodic polarisation behaviour of stainless steels P853, P720 and P752 after cathodic cleaning is similar (Fig. 39). The limiting current density of the oxygen reduction reaction for Ralloy 654MO is slightly higher than that for other steels, which means that Ralloy 654MO catalyses oxygen reduction more than other steels.

The shape of the cathodic polarisation curves in ozonated solution after cathodic cleaning is similar to that of oxygen bubbled solution (Fig. 40). The corrosion potentials are higher for steels P853, P720 and P752 but lower for Ralloy 654MO than in oxygen bubbled solution. In ozonated solution the cathodic reactions on cathodically cleaned stainless steels are the reduction of both oxygen and ozone.

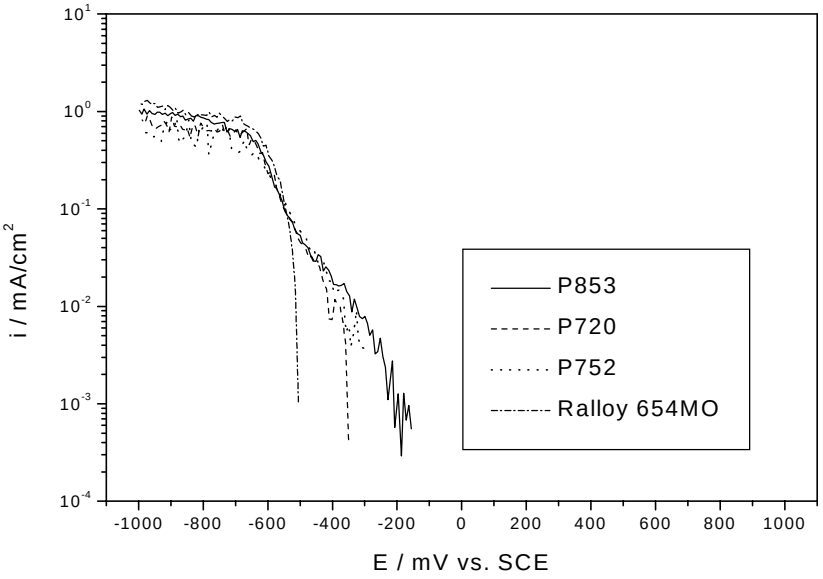

Fig. 40. Cathodic polarisation behaviour of stainless steels P853, P720, P752 and Ralloy 654MO in ozonated solution, 23 g/l Na_2SO_4, pH=3, T=50 °C.

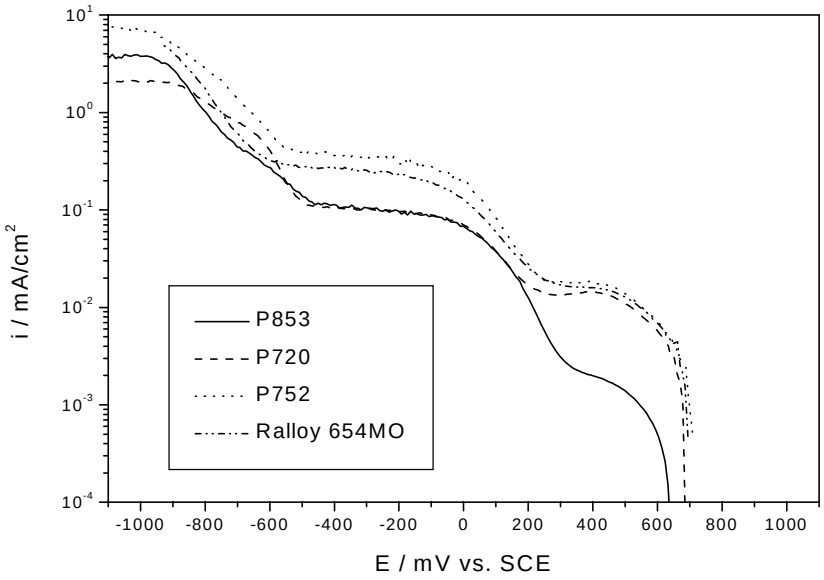

Fig. 41. Cathodic polarisation behaviour of stainless steels P853, P720, P752 and Ralloy 654MO after 22 h immersion in ozonated solution, 23 g/l Na_2SO_4, pH=3, T=50 °C.

The cathodic behaviour of steels after 22 h immersion in ozonated solution differs clearly from the behaviour of cathodically cleaned samples (Fig. 41). The corrosion potentials of the 22 h immersed steels are higher. The main difference in the polarisation behaviour of stainless steels is the lower current density of P853 immersed 22 h above potential +140

mV. This means that ferritic steel catalyses less the reduction of ozone than austenitic steels. The current density of the cathodic reaction is higher the more alloyed the steel.

The higher limiting current densities of oxygen reduction on stainless steels at potential regions below about -900 mV compared to the current densities after cathodic cleaning is due to the higher effective surface area formed in 22 h immersion in ozonated solution.

The reduction of hydrogen begins at a potential region below about -500 mV (Fig. 41 and Fig. 39). The cathodic reaction of the corrosion reaction of stainless steels in ozonated solution is the reduction of ozone to oxygen at higher potentials and at lower cathodic potentials mainly the reduction of oxygen.

3.4 Tafel slopes

The corrosion current densities of stainless steels P853, P720, P752 and Ralloy 654MO were determined with the Tafel method after 22 h immersion in ozonated solution (pH=3, T=50 °C, 23 g/l Na_2SO_4). Materials were polarised 150 mV in the cathodic direction from the corrosion potential. The potential sweep was then continued in the anodic direction to 150 mV above the corrosion potential. The potential was then returned to the corrosion potential. The second similar cycle followed immediately after the first cycle. The Tafel plots for the test materials are shown in Fig. 42 - 45.

.

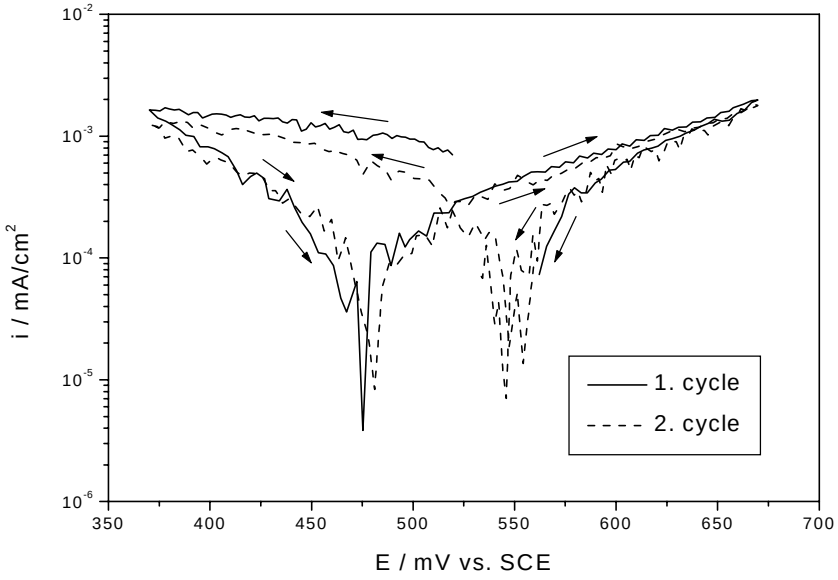

Fig. 42. The results of Tafel experiments for stainless steel P853 in ozonated solution, pH=3, 23 g/l Na_2SO_4, T=50 °C.

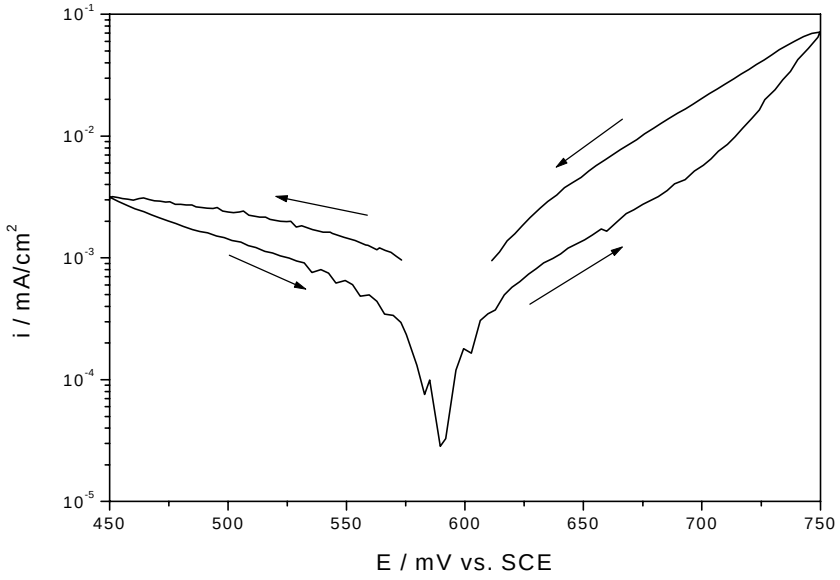

Fig. 43. The results of Tafel experiments for stainless steel P720 in ozonated solution, pH=3, 23 g/l Na_2SO_4, T=50 °C.

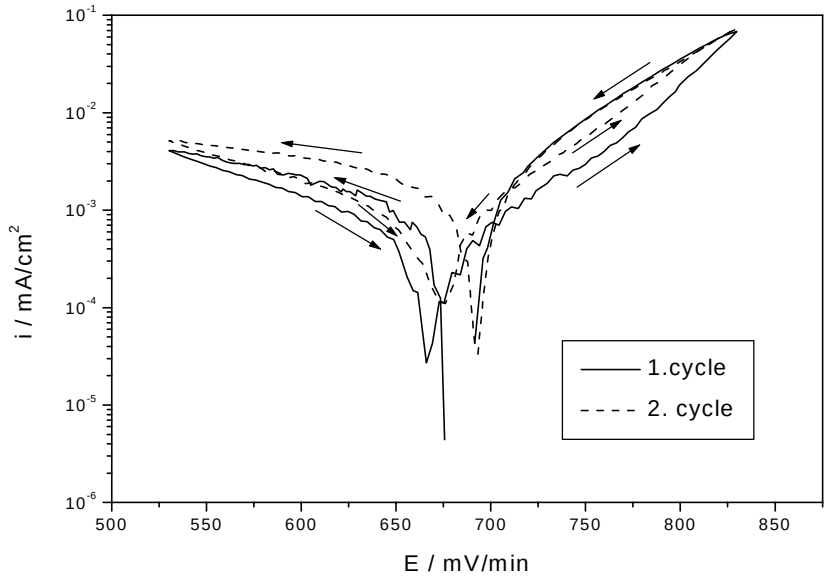

Fig. 44. The results of Tafel experiments for stainless steel P752 in ozonated solution, pH=3, 23 g/l Na_2SO_4, T=50 °C.

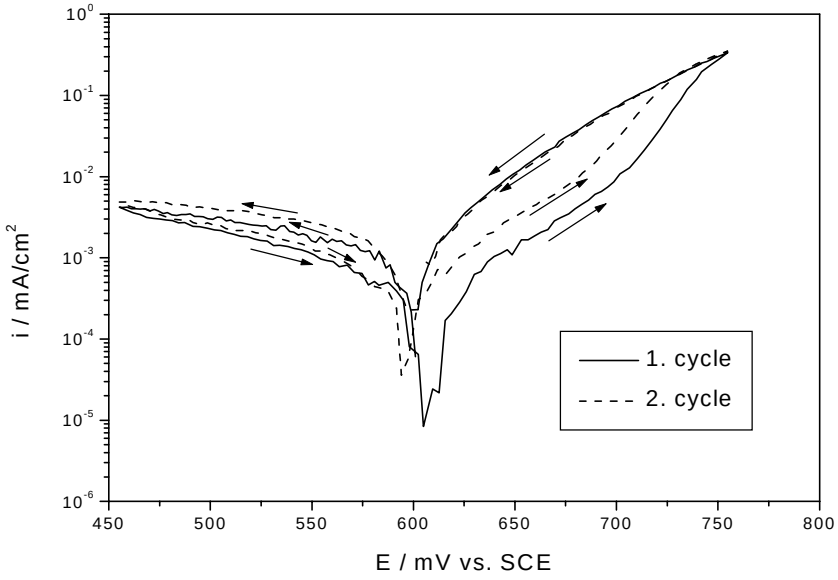

Fig. 45. The results of Tafel experiments for stainless steel Ralloy 654MO in ozonated solution, pH=3, 23 g/l Na_2SO_4, T=50 °C.

The differences in the corrosion potentials (i.e. the potential where the current changes the sign) between the first and the second cycle is the largest in stainless steel P853, about 20 -30 mV (Fig. 42). The corrosion potentials of Ralloy 654MO remain unchanged (Fig. 45). These differences indicate changes in the oxide layer or in the outer layer of the stainless steels during the Tafel experiments. In anodic polarisation the curve bends upwards; this increase in current density is more pronounced for Ralloy 654MO than the other stainless steels (Fig. 45). This change is caused by the secondary active peak (Fig. 30). After one days´s immersion in the ozonated solution the oxide layer is according to the GDOS measurements 52 nm for Ralloy 65MO and for P720 4 nm. The thickness on P853 was not measured, but it is near to that of P720. The outer oxide layer on Ralloy 654MO is depleted of chromium to a depth of about 30 nm (Fig. 80). The differences in oxide thickness and composition and therefore differences also in the effective surface areas of the samples affect also the results of the Tafel experiments by increasing the current densities, especially for higher alloyed steels.

The Tafel equation is strictly valid only for an activation controlled single electrode reaction. The cathodic Tafel plots for the stainless steels studied in ozonated solution show more mass transfer than activation controlled reactions. Tafel slopes have been calculated from the first cycle. The first cycle was used because some changes on the sample surfaces occur during the experiments with two cycles. The cathodic slope was taken from the curve towards the anodic direction and the anodic slope from the curve towards the anodic direction. The reason for this is was to get a clean surface on the cathodic sweep and avoid changes on the anodic sweep that may occur after the first cycle. In Fig. 46 - 49 the chosen parts of the curves are shown. The slopes have been calculated by fitting linear equations to E-log(i) points using the least squares method. Corrosion current densities were calculated by extrapolating these fitted lines to the corrosion potential. If the extrapolated corrosion current densities from the anodic and cathodic sweep were different, average values were calculated.

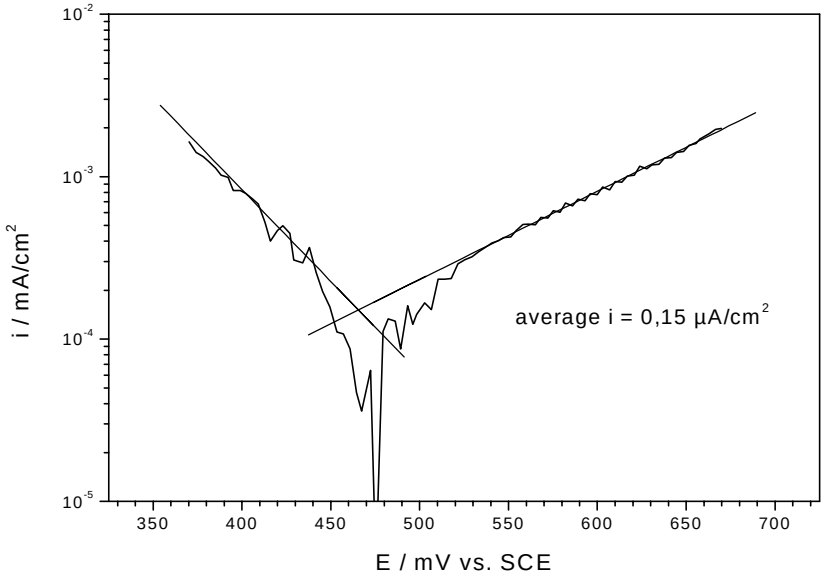

Fig. 46. Tafel plot for P853 in ozonated solution, pH=3, 23 g/l Na_2SO_4, T=50 °C.

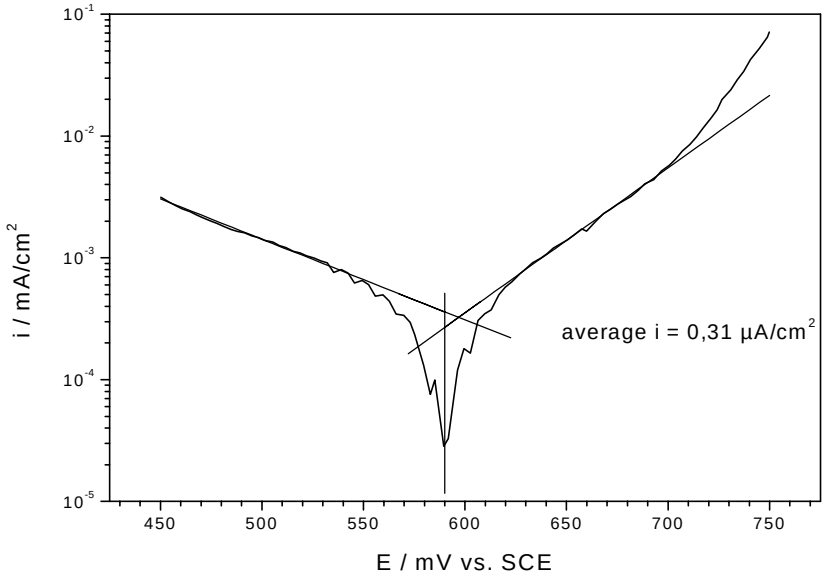

Fig. 47. Tafel plot for P720 in ozonated solution, pH=3, 23 g/l Na_2SO_4, T=50 °C.

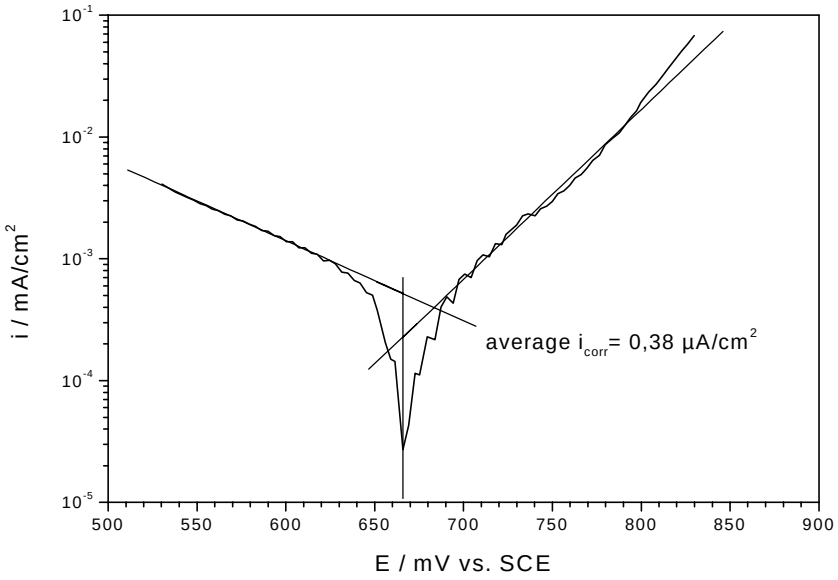

Fig. 48. Tafel plot for P752 in ozonated solution, pH=3, 23 g/l Na_2SO_4, T=50 °C.

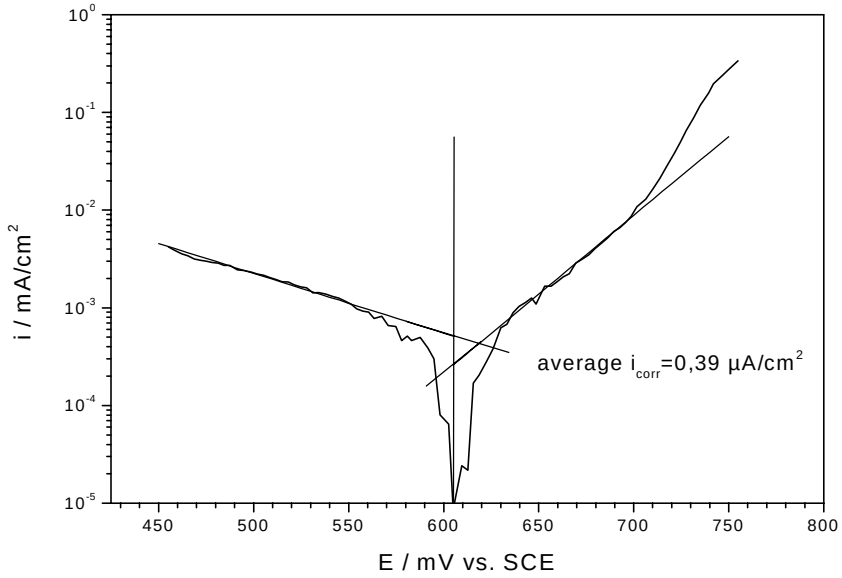

Fig. 49. Tafel plot for Ralloy 654MO in ozonated solution, pH=3, 23 g/l Na_2SO_4, T=50 °C.

The calculated current densities and the nominal corrosion rates calculated from the current densities are shown in table 10. Corrosion rates have been calculated from the current densities according to ASTM standard G 102 [49] with both the assumption that all metals (Fe, Cr, Ni, Mo and Mn) are oxidised to lowest (Fe^{2+}, Cr^{3+}, Ni^{2+}, Mo^{3+}, Mn^{2+}) and to highest (Fe^{3+}, Cr^{6+}, Ni^{2+}, Mo^{6+} and Mn^{4+}) valences.

Table 10. Current densities and corrosion rates according to Tafel experiments.

Steel	i / µA/cm^2	corr. rate/ µm/a	
		lowest valencies	highest valencies
P853	0.15	2	1
P720	0.31	3	2
P752	0.38	4	3
Ralloy 654MO	0.39	4	3

The anodic and cathodic Tafel slopes are given in table 11. The cathodic slopes are similar (150 - 170 mV/decade) for steels P720, P752 and Ralloy 654MO. The slope of ferritic P853 is lower (90 mV/decade). The Tafel slopes for cathodic reactions indicate that the cathodic reaction mechanism involves one electron, most likely the reduction of ozone.

Table 11. Anodic and cathodic slopes according to Tafel experiments.

	50 mV/min	
Steel	anodic slope / mV/decade	cathodic slope / mV/decade
P853	180	90
P720	80	150
P752	70	160
Ralloy 654MO	60	170

Anodic slope decreases as the amount of alloying metals in steels increases so that the slope of P853 is three times higher than that of Ralloy 654MO. For Ralloy 654MO and P752 the slope is 60 - 70 mV/decade, which means that about two electrons are involved in the rate determining anodic reaction. It is assumed that the oxidation rate of chromium is high and it is not the rate determining reaction in Tafel experiments. It is obvious that the anodic reactions vary according to the amount of alloying metals.

According to the Tafel experiments corrosion rates of stainless steels are low in the ozonated test solution. The lowest corrosion rate is for ferritic steel P853 and the highest is for highly alloyed Ralloy 654MO.

3.5 Pitting corrosion

The pitting corrosion resistance of materials was studied to determine the possibility for local corrosion as compared with the expected susceptibility based on literature [14]. Experiments were carried out in ozonated solutions at pH 3 and Na_2SO_4 concentration of 2.3 g/l. The scanning rate was 10 mV/min and the temperature of the solution was 20 °C.

In the polarisation curves for P853 (Fig. 50), no hysteresis loop exists and no pitting was found on the specimen surface after the experiment. At a potential range of up to about +1100 mV in anodic polarisation and under the same potential in cathodic polarisation, the fluctuation in current density is higher than in solution with 23 g/l Na_2SO_4. This is due to the low conductivity of the solution.

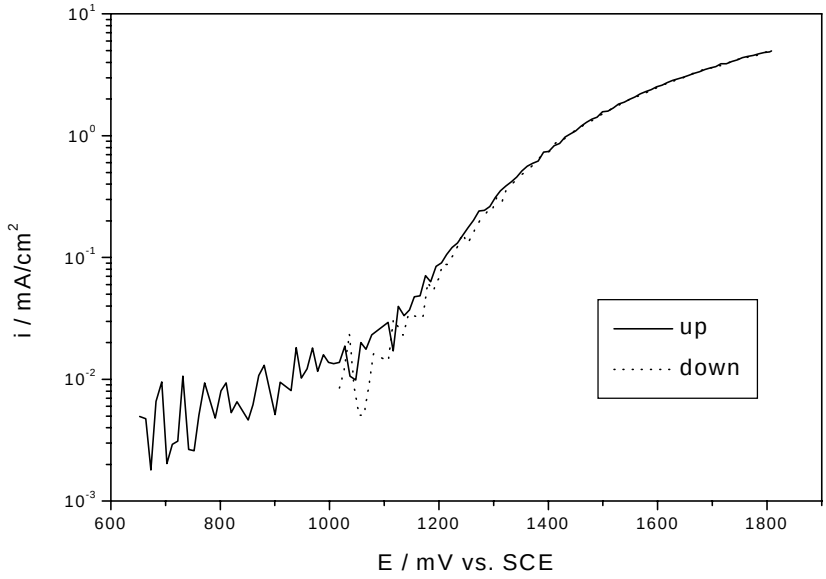

Fig. 50. The pitting polarisation behaviour of stainless steel P853 in ozonated solution 2.3 g/l Na_2SO_4, pH=3, T=20 °C.

No hysteresis is evident for steels P720 and P752 loop can be seen and no pits were found on the surface of the material (Fig. 51 and 52).

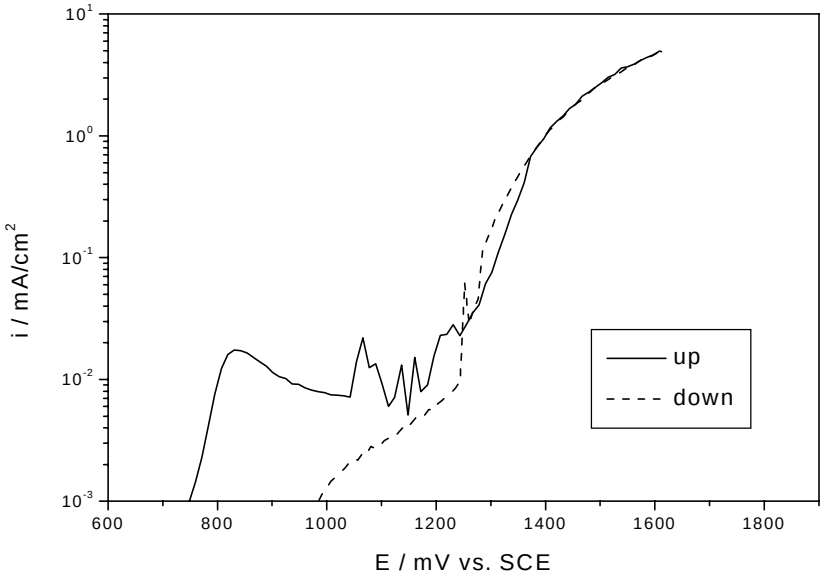

Fig. 51. The pitting polarisation behaviour of stainless steel P721 in ozonated solution, 2.3 g/l Na_2SO_4, pH=3, T=20 °C.

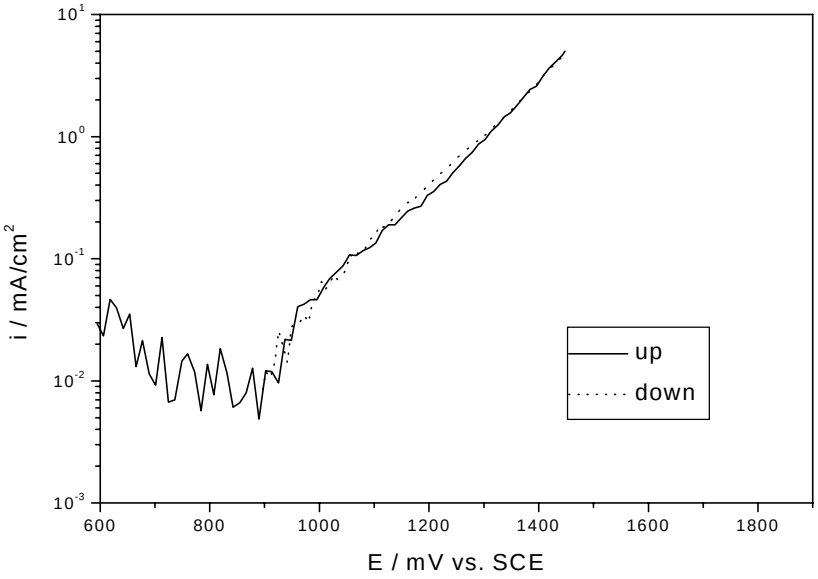

Fig. 52. The pitting polarisation behaviour of stainless steel P752 in ozonated solution 2.3 g/l Na_2SO_4, pH= 3, T=20 °C.

No hysteresis was found in the polarisation curve of Ralloy 654MO either (Fig. 53), but pits were clearly seen on the surface of the samples (Fig. 54). Pit size was up to above 200 µm and depth up to 70 µm. Pits were mostly similar to chloride induced pits.

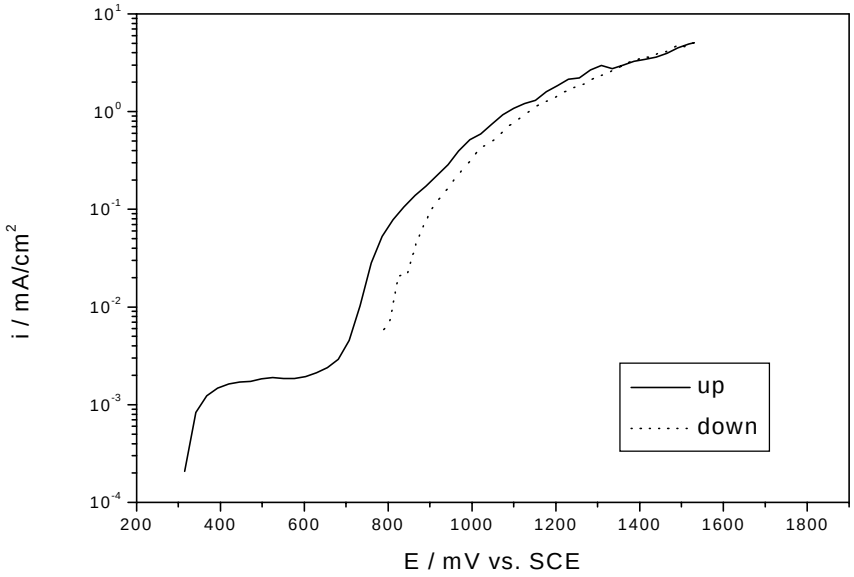

Fig. 53. The pitting polarisation behaviour of stainless steel Ralloy 654MO in ozonated solution, 2.3 g/l Na_2SO_4, pH= 3, T=20 °C.

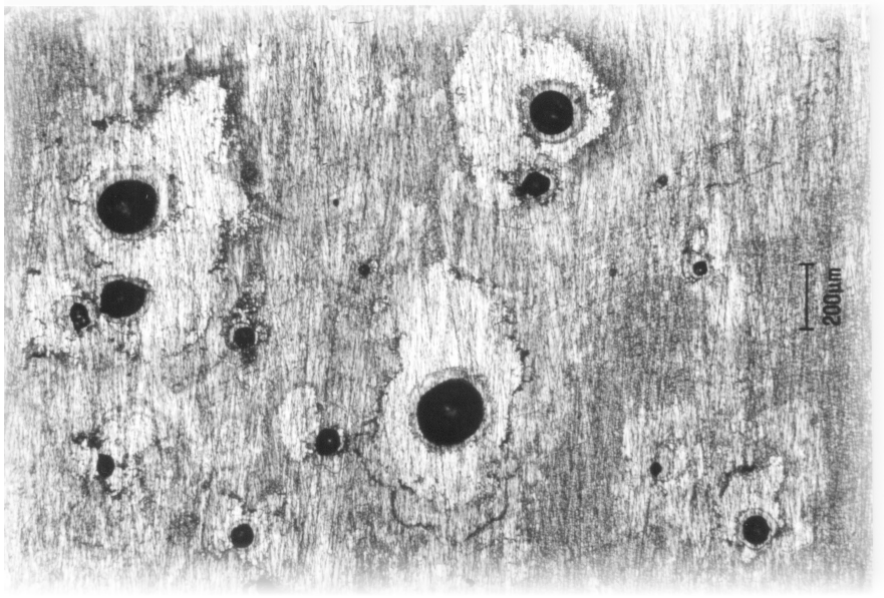

Fig. 54. Pitting in steel Ralloy 654MO after pitting corrosion experiment in ozonated solution, 2.3 g/l Na_2SO_4, pH= 3, T=20 °C.

According to the pitting polarisation measurements, the increase in the amount of alloying elements increases the susceptibility of stainless steels to pitting corrosion failure in ozonated solution without chloride. However, conclusions can be made on the basis of the shape of the polarisation curves only for stainless steels P853, P721 and P752 but not for Ralloy 654MO. Pits formed on Ralloy 654MO obviously repassivate during the pitting corrosion test, so no hysteresis can be seen in the curve.

Some evidence of intergranular corrosion was found after the pitting corrosion experiments. Grain boundaries were slightly etched but not clearly corroded. Due to the manufacturing method (HIP) it is not possible that Ralloy 654MO has suffered sensitisation.

The pits and intergranular corrosion are probably a result of the first stages of transpassive dissolution. Note that the experiment time from current increase at about 700 mV to the maximum potential and back is about 2.5 h.

3.6 Potentiostatic measurements

Potentiostatic experiments were carried out in solution with 23g/l Na_2SO_4 at temperature 50 °C and without at temperature 75 °C. Potential was +850 mV, which lies in the secondary active peak (Fig. 21). The test were done to verify the presumption that the oxidation of trivalent chromium in the oxide layer to hexavalent causes the increase in current density. At a potential region higher than the transpassivation potential, higher alloyed stainless steels should dissolve at a higher rate because of the higher chromium content. It was found in long term corrosion potential measurements that the stabilisation of the corrosion potential may take even 20 - 30 h and this potential is higher than the corrosion potential seen in the polarisation curves. Potentiostatic measurements where potential is kept in the "real" corrosion potential, may therefore give further information about the corrosion behaviour of stainless steels. Attention should be paid to the interpretation of the results, when stationary and not stationary situations are compared.

Without sodium sulfate in the solution, the current density decreases faster for alloys with low amounts of alloying elements (Fig. 55). The final current densities are affected by the low conductivity of the solution and they are not comparable.

In solution with 23 g/l sodium sulphate the current densities decrease in a way similar to that without Na_2SO_4(Fig. 56). The decrease is the faster the lower alloyed the steel. The current density of Ralloy 654MO is much higher than that of other steels. Also the current density stays at higher level (350 $\mu A/cm^2$) than in solution without sodium sulfate. The final current densities after 2.3 h are 0.3 $\mu A/cm^2$ for P853 and P720, 8 $\mu A/cm^2$ for P752 and 350 $\mu A/cm^2$ for Ralloy 654MO. After the experiment with Ralloy 654MO the solution is somewhat reddish, which means that chromium is oxidised to its hexavalent state.

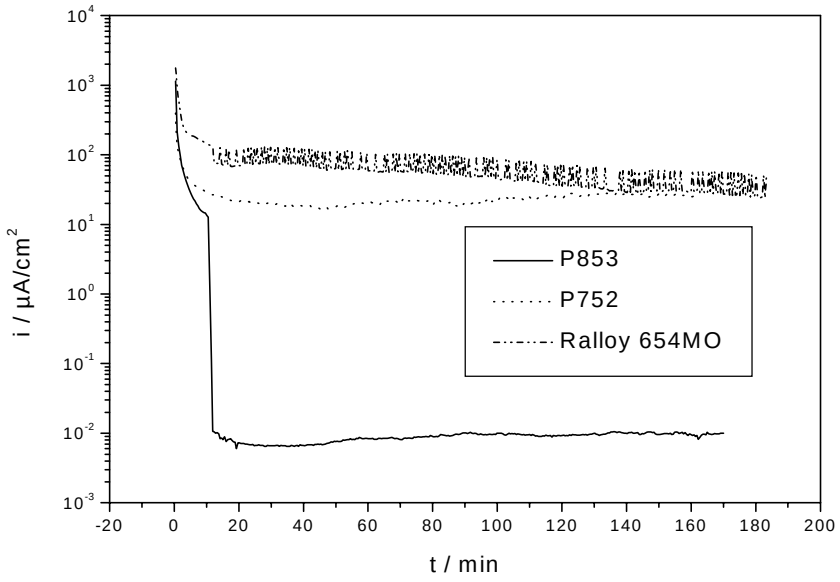

Fig. 55. The results of potentiostatic experiments for stainless steels P853, P752 and Ralloy 654MO at potential +850 mV in ozonated solutions without Na_2SO_4, at pH 3 at T=75 °C.

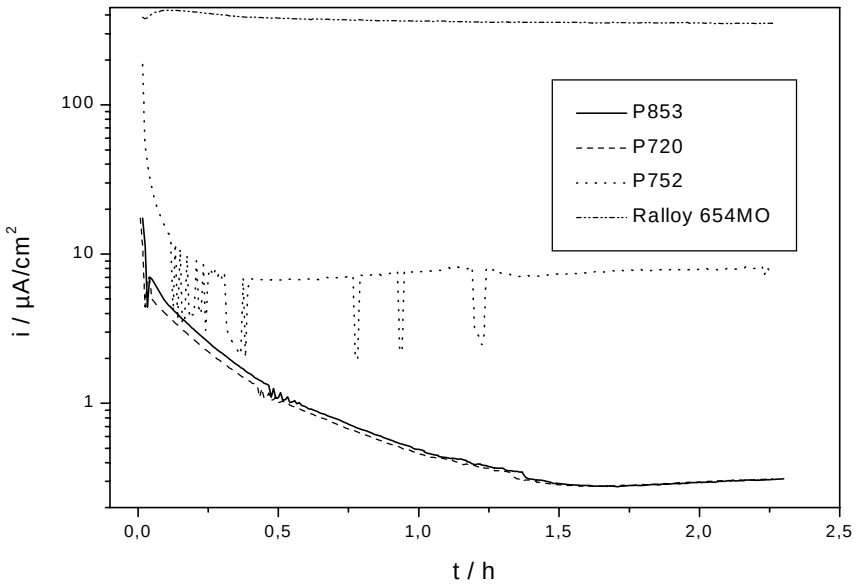

Fig. 56. The results of potentiostatic experiments for three stainless steels P853, P720, P752 and Ralloy 654MO at potential +850 mV in ozonated solutions with 23 g/l Na_2SO_4, pH=3, T=50 °C.

3.7 Immersion tests

Immersion tests were carried out at a temperature of 50 °C in a solution of pH 3 both with 23 g/l Na_2SO_4 and without. In long term immersion tests (60 days, without Na_2SO_4), the corrosion rate of Ralloy 654MO is the highest and that of P720 the lowest (Fig. 57). Weight losses after 60 days were: P720 0.46 mg/cm^2, P752 0.54 mg/cm^2 and Ralloy 654MO 0.56 mg/cm^2. Ferritic steel P853 was not investigated. The aim of the immersion tests was to gain information about the relative corrosion rates of test materials and to produce samples for surface analysis.

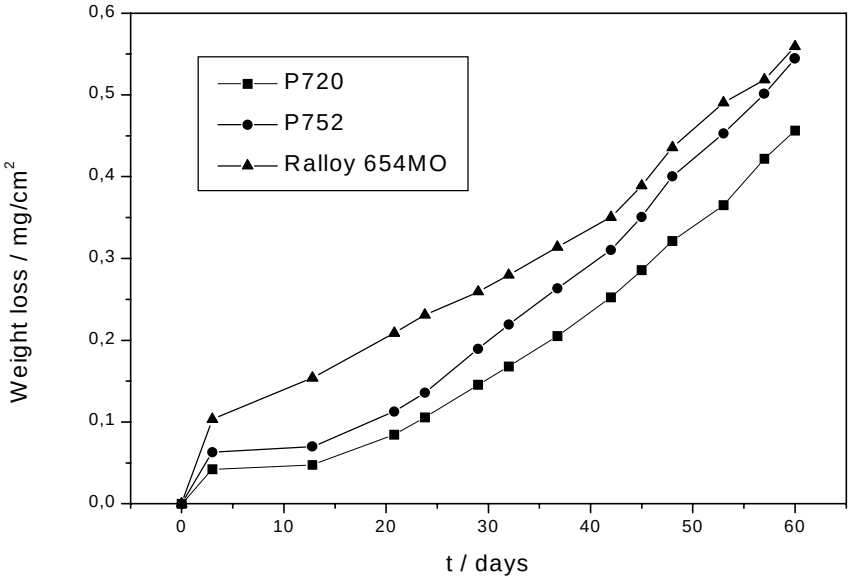

Fig. 57. Weight loss of stainless steels P720, P752 and Ralloy 654MO in ozonated solution, no Na_2SO_4, pH=3, T=50 °C.

After an initial high dissolution period of about three days the corrosion rates become lower. Corrosion rates after the higher initial rate are almost linear. Attention should be paid to sample preparation: the other sides of the plates of P720 and P752 had not been ground but were in pickled and prepassivated 2B state. This complicates the corrosion rate estimation and the comparison between Ralloy 654MO and the other steels. Experiments were also carried out mainly during week ends so that the samples were periodically removed from the solution and weighed, and then re-immersed after five days. In Fig. 57 time is immersion time. This also has an effect on the results of the experiments.

A sodium sulfate addition of 23 g/l increased the corrosion rate of Ralloy 654MO from 0.56 mg/cm^2 to 1.38 mg/cm^2 after 60 days, but those of P720 and P752 stayed at the same level, 0.43 mg/cm^2 and 0.46 mg/cm^2 respectively (Fig. 58). This increase in the corrosion rate of Ralloy 654MO occurs mainly during the first three days and the reason for this could be higher conductivity of the solution that causes less but larger corroded areas. In sodium sulfate solution the corrosion rates are after initial dissolution also almost linear.

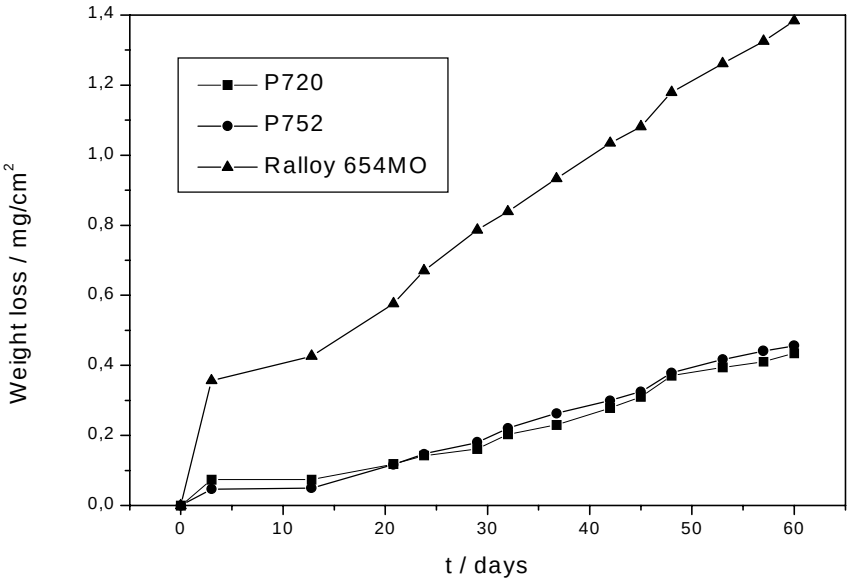

Fig. 58. Weight loss of stainless steels P720, P752 and Ralloy 654MO in ozonated solution, 23 g/l Na_2SO_4, pH=3, T=50 °C.

The corrosion rates, µm/a, from the weight loss test (Fig. 57 and 58) have been calculated using densities 8 g/cm^3 for P720 and P752 [47] and 7.9 g/cm^3 for Ralloy 654MO [48]. (table 12). In solution with 23 g/l Na_2SO_4 the corrosion rate of Ralloy 654MO is about three times that of P720 and P752. In solution without sodium sulphate corrosion rates are of similar magnitude for all three steels. Only the corrosion rate of Ralloy 654MO is affected by the dosage of Na_2SO_4.

Table 12. Corrosion rates of stainless steels P720, P752 and Ralloy 654MO in ozonated solution with 23 g/l Na_2SO_4 and without.

	Corrosion rate / µm/a	
Alloy	23 g/l Na_2SO_4	no Na_2SO_4
P720	3.2	3.5
P752	3.5	4.1
Ralloy 654MO	11	4.2

Stainless steels P720 and Ralloy 654MO were investigated in more detail by analysing dissolved elements in continuous immersion tests. Test were carried out for 1, 2, 4, 8, and 16 days so that each test was a separate experiment. Both materials were tested in separate cells, two samples in each. After the experiments, the test solutions were analysed using AAS, to determine of metal dissolution (Fe, Cr, Ni and Mo). Before analyses solid particles were dissolved by lowering the pH of the solution.

The main dissolved element from P720 (Fig. 59) according to analysis is iron. Chromium and nickel dissolve at a low rate. Between 4 and 16 days immersion the dissolution rate seems to be linear. Iron in Ralloy 654MO dissolves during the immersion test proportionally at a higher rate than the iron in P720. The dissolution rates of the alloying elements in Ralloy 654MO are also high at the beginning of the immersion and then decrease, but less than for P720. The total dissolution rate is higher than that of P720. Molybdenum dissolves first at a higher rate than expected according to the concentration in bulk metal. The dissolution rate of Mo decreases more than for other elements (Fig. 60

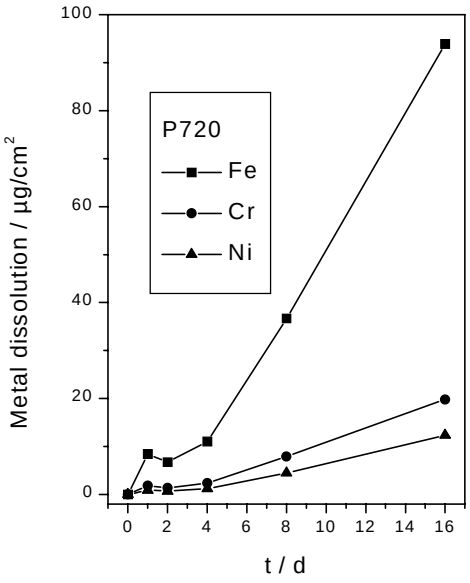

Fig. 59. Fe, Cr, Ni and Mo dissolved from P720 in immersion test per surface area in ozonated solution, pH=3, T=50 °C.

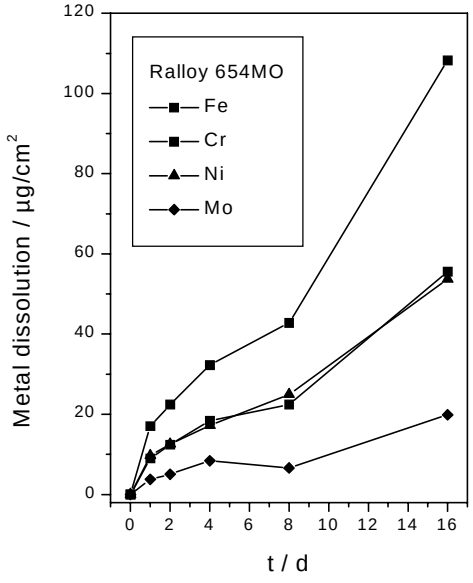

Fig. 60. Fe, Cr, Ni and Mo dissolved from Ralloy 654MO in immersion test per surface area in ozonated solution, pH=3, T=50 °C.

The corrosion rates calculated from weight loss measurements and analysis of dissolved metals clearly show that more alloyed stainless steels corrode at a higher rate than the lower alloyed steels.

The relative dissolution of elements was calculated from the solution analyses. In the alloy analyses the concentrations were calculated ignoring minor elements in steels. In both P 720 and Ralloy 654MO, all the analysed elements dissolve nearly in the same proportions as they are in the bulk metal. The dissolution rate of iron in P720 decreases with the immersion time and it is slightly higher than in bulk metal. Chromium dissolves less than the bulk concentration. The dissolution of nickel increases with the immersion time (table 13).

Table 13. Relative dissolution of P720 in ozonated solution, pH=3, T=50 °C.

	Fe / wt-%	Cr / wt-%	Ni / wt-%
metal analysis	72.1	18.6	9.3
1d immersion	76	16.1	7.9
2d immersion	76.5	15.5	8
4d immersion	75.7	16.1	8.1
8d immersion	74.7	16.2	9.1
16d immersion	74.5	15.7	9.8

In the dissolution of Ralloy 654MO, the variations are greater. Iron and chromium dissolve at a slightly lower relative rate than the concentrations in bulk metal. Nickel and molybdenum dissolve at higher rater (table 14).

Table 14. Relative dissolution of Ralloy 654MO in ozonated solution, pH=3, T=50 °C.

	Fe / wt-%	Cr / wt-%	Ni / wt-%	Mo / wt-%
metal analysis	44.6	25.8	22	7.6
1d immersion	43.2	22.7	24.5	9.6
2d immersion	42.7	23.7	24	9.6
4d immersion	42.3	24.1	22.6	11
8d immersion	44.2	23.2	25.8	6.8
16d immersion	45.6	23.4	22.6	8.4

After 16 days immersion in ozonated solution (pH=3, no Na_2SO_4) samples were examined by optical light microscope. On the surface of Ralloy 654MO two kinds of damage were found. Round pits of varying size and various shaped damages in the oxide layer with varying shape were noticed. The largest round pits were about 30 µm wide and about 6 µm deep (Fig.61). The various shaped damages in the oxide layer were under 50 µm in width and 1 - 6 µm in depth (Fig. 62).

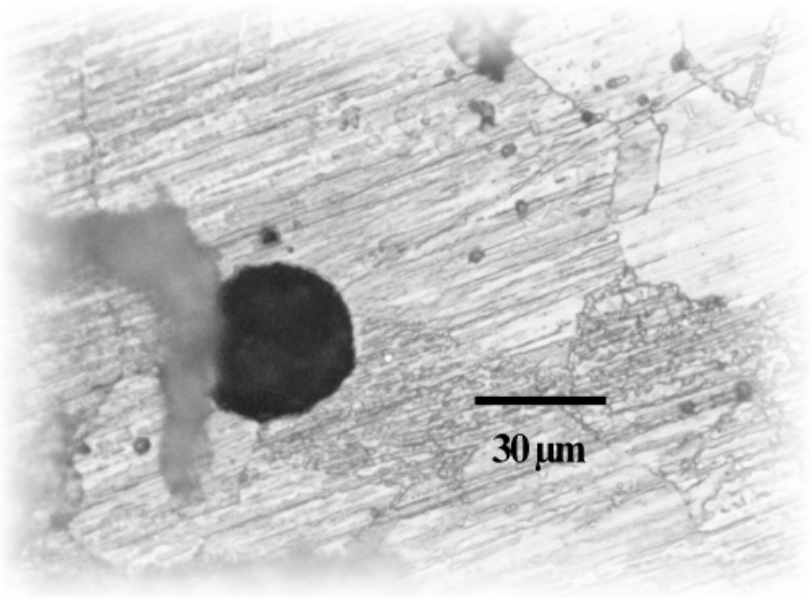

Fig. 61. A round corrosion damage in Ralloy 654MO after 16 days immersion in ozonated solution, pH=3, T=20°C.

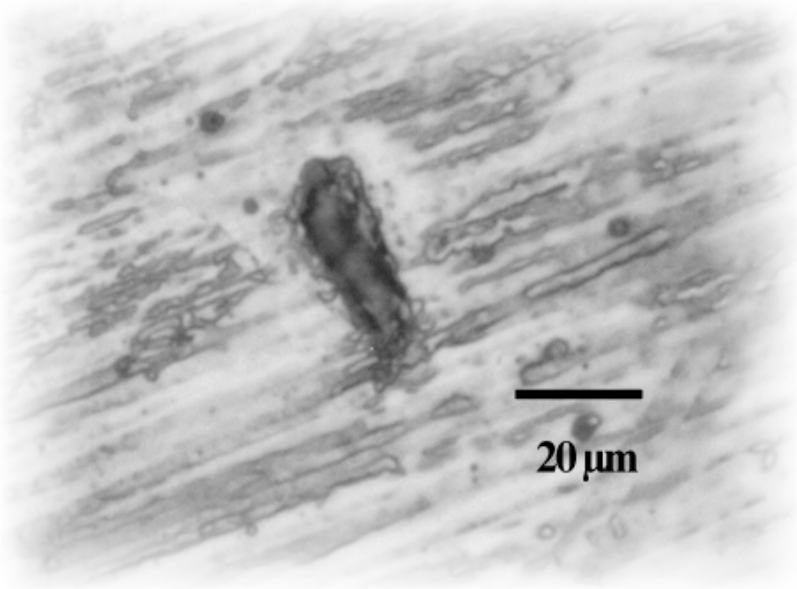

Fig. 62. Corrosion damages in Ralloy 654MO after 16 days immersion in ozonated solution, pH=3, T=20°C.

The number of damages in steel P752 is higher than in Ralloy 654MO. The damages are mainly circular in shape and the diameter under 20 µm. All the failures were shallow (1 - 2 µm) (Fig. 63).

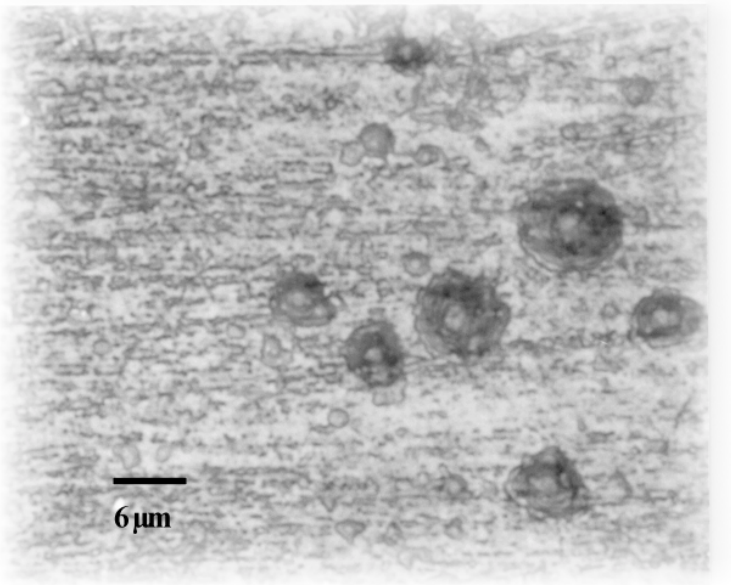

Fig. 63. Corrosion damages on P752 after 16 days immersion in ozonated solution, pH=3, T=20°C.

On P720 and P853 some circular and shallow damages were seen. The number was lower on P853, where only some failures were noticed. The failures were similar to P752 but smaller.

3.8 Structure of passive layers

The structure of the oxide layers formed in ozonated solution (pH=3, T=50 °C) after 16 days immersion in ozonated solution was investigated using SEM. The oxide layers were analysed by GDOS, ESCA and X-ray diffractometer methods.

In X-ray diffractometer measurements no peaks in the oxide layer samples were found. It seems that the oxide layer is amorphous. The oxide layer should be analysed separately from the bulk metal in order to identify the structure of the layer.

3.8.1 SEM examination

Ozone causes damage to the oxide layer of stainless steels. The number of damages per unit area was highest on stainless steel Ralloy 654MO samples ground to 800 grit, but damages were also found on the other stainless steels. SEM examination showed that the least alloyed steels had least damages. On ferritic stainless steel P853 the number of damages was negligible. The type of the damages on stainless steels in ozonated solution differed from pitting e.g. in chloride solution, where the pits are usually deep and small. In ozonated solution, the observed damages were wide and shallow (Fig. 64 b and c).

a)

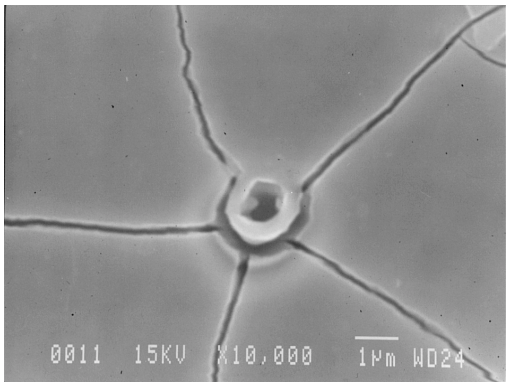

b)

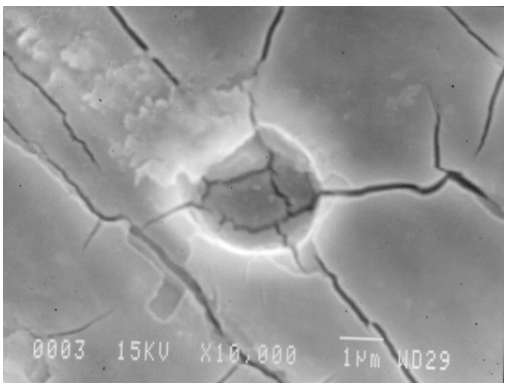

c)

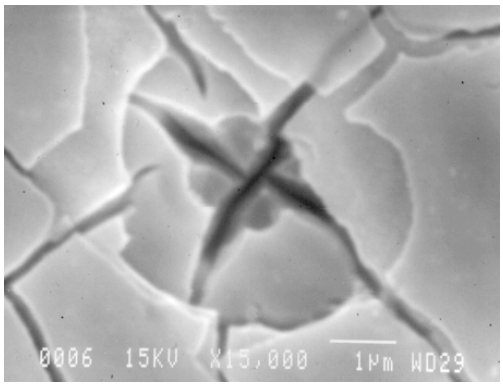

Fig. 64. Damage formation on Ralloy 654MO after 16 days immersion in ozonated solution, pH=3, T=50 °C.

Damages initiate obviously on grain boundaries and the already thick oxide layer begins to dissolve. In Fig. 64 a dissolution occurs both in the centre of the initial damage and outside the surrounding ring. Damage growth occurs both by dissolution of the oxide layer and by detachment of solid oxide after some dissolution. Dissolution and detachment of the oxide layer exposes bulk metal, which is oxidised further. If the area of the damage is large enough, the oxide layer may again dissolve or detach. According to Fig. 64 c, it may also be possible that the depth of the damage may increase only by the loosening of the oxide layer.

On stainless steel P720 and P752, surfaces as delivered (2B-condition: pickled and prepassivated), similar damages was found in a larger scale. The thickness of the oxide layer increases and the adhesion of the oxide decreases, which may be seen as a lighter colour around the damage in Fig. 65 on stainless steels P720. This oxide with low adhesion loosens and a large area of bare metal will be exposed. This area free of oxide begins to oxidize and the oxide may again later detach. This is illustrated in Fig. 66 for stainless steel P752. It may also be possible that as the thickness of the oxide increases, the oxide becomes fragile and cracks.

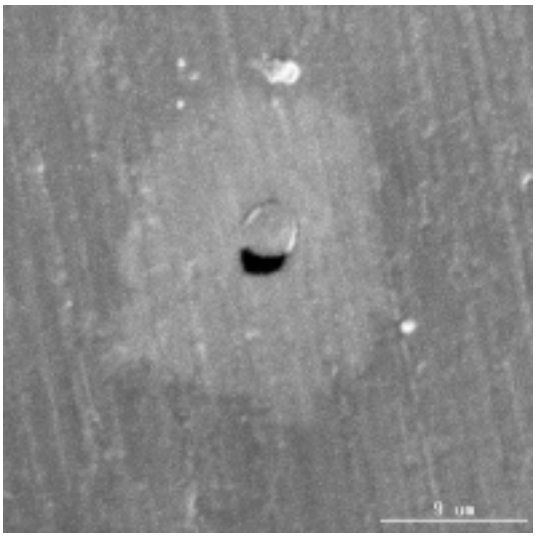

Fig. 65. Damage formation and detachment of the oxide layer on P720 after 16 days immersion in ozonated solution, pH=3, T=50 °C.

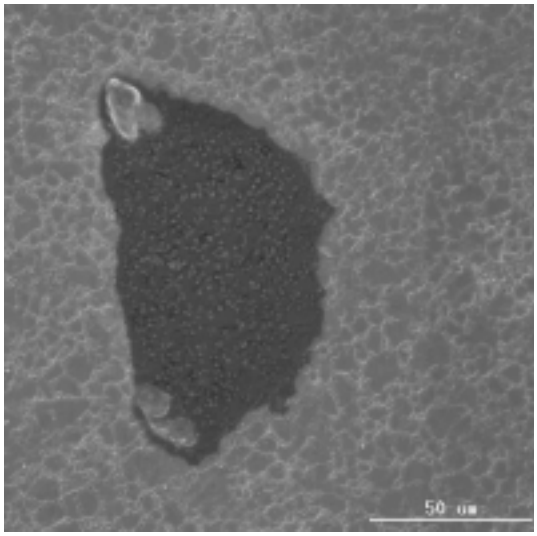

Fig. 66. Area of corrosion damage of P720 after 16 days immersion in ozonated solution, pH=3, T=50 °C.

According to the experiments the peeling mechanism of stainless steel in ozonated solution is the following: 1) increase in the thickness of the oxide layer, 2) local corrosion initiation, 3) increased corrosion damages resulting in weakened adhesion of the oxide layer, 4) peeling of the oxide from the surface, 5) further oxidation of the exposed steel with corrosion damage.

3.8.2 GDOS analyses

The chemical composition of oxide layers formed in ozonated solution was investigated by GDOS-method. Both the differences in the oxidised layers on the four test materials and the oxidising mechanism were examined. Test solution was pH=3, T=50 °C, no sodium sulfate. In GDOS-analyses the alloying elements and impurity profiles of stainless steels were measured to a depth of 500 - 1000 nm. Stainless steels immersed for 3 days in oxygen bubbled test solution, where the oxide layer is supposed to be a normal passive layer, were used as reference samples. O, Fe, Cr, Ni, Mo, Mn, P, S, Si and Cu concentrations were analysed.

The growth mechanism of oxide layers was investigated for 1, 2, 4, 8 and 16 day immersion tests so that every test was a separate experiment and each sample was analysed. Test materials were P720 and Ralloy 654MO. The differences in the oxide layers of all four test materials immersed for 16 days in ozonated solution was also studied. The analysis results (without Cu) are shown for each of the four test materials in appendix 1 - 8, immersed for 3 days in oxygen bubbled solution and 16 days in ozonated solution.

The variations in the results of samples immersed in oxygen bubbled solution were not significant. A typical example is the iron concentration profile of three separate analyses for ferritic stainless steel P853 shown in Fig. 67. Results indicate no great variations in the thickness of the oxide layers on all steels investigated.

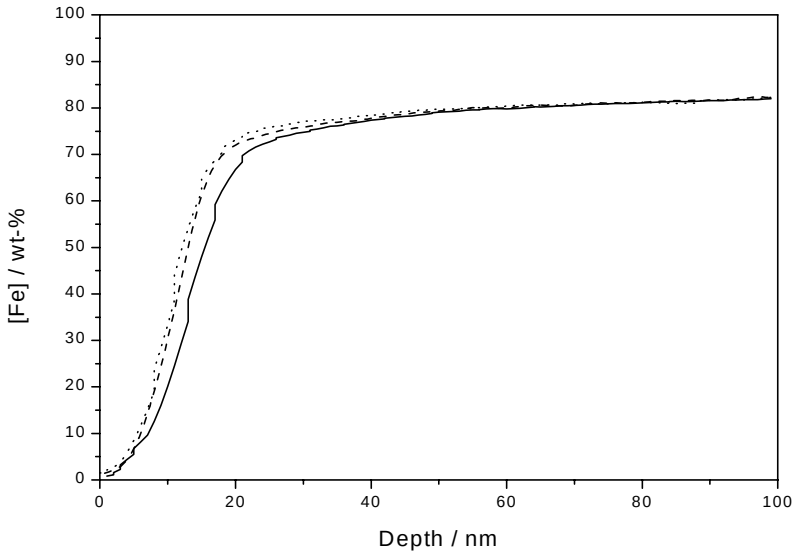

Fig. 67. Fe profiles of P853 immersed 3 days in oxygen bubbled solution, pH=3, T=50 °C.

Major variations were found in the outermost layer (less than about 5 nm) for some oxide layers formed in oxygen bubbled solution. For example in Fig. 68 the oxygen concentration of the outer layer on stainless steel P720 varies from about 30 to about 43 wt-%. This is partly due to error in the analysis method. In GDOS method inaccuracies occur if large differences in chemical composition between the outer layer and the bulk material exist, especially in O concentrations. It is also obvious that the oxide layer is not uniform and the chemical composition varies also in a certain range.

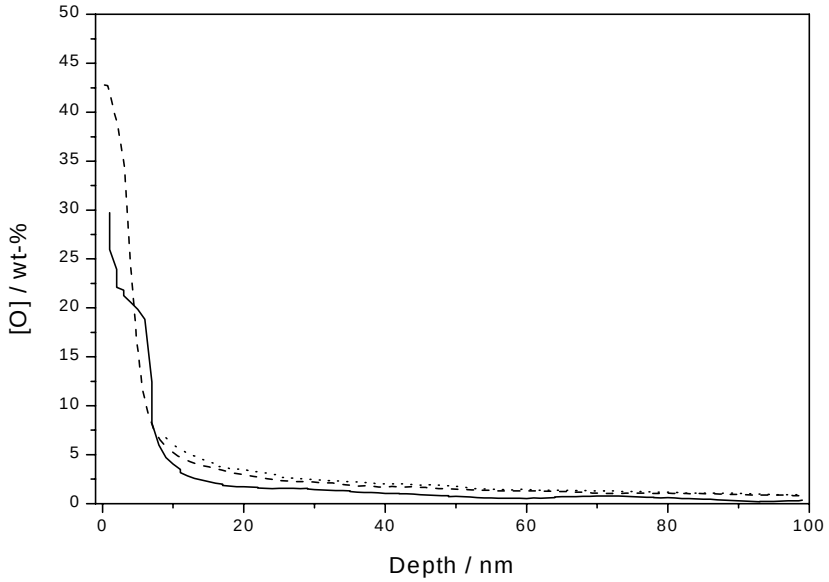

Fig. 68. O profiles of P720 immersed 3 days in oxygen bubble solution, pH=3, T=50 °C.

The variations in alloying elements, e.g. molybdenum (Fig. 69) in the oxide layer of P752, were also minor in oxygen bubbled solution. Variations for Ralloy 654MO were greater. This is shown in Fig. 70, where the nickel concentration profiles are shown.

In ozonated solutions the variations of the element profiles were greater than in oxygen bubbled solutions. The reason for this is the greater thickness of the oxide layers in ozonated solutions than in oxygen bubbled solutions. The local corrosion defects have also an effect on the analyses, because it was not possible to detect the defects on the sample surfaces in the analysis. GDOS analyses have also been done on areas, where defects occur, especially for more alloyed steels P752 and Ralloy 654MO. As an example O and Fe profiles of P720 are shown in Fig. 71 and 69. The greatest variations in results are in the O concentration profiles on the outer layer; it varies on P720 from about 68 to 86 wt-%. Fe profiles vary below a depth of about 40 nm from 0 to about 25 wt-%. This makes the interpretation of results difficult.

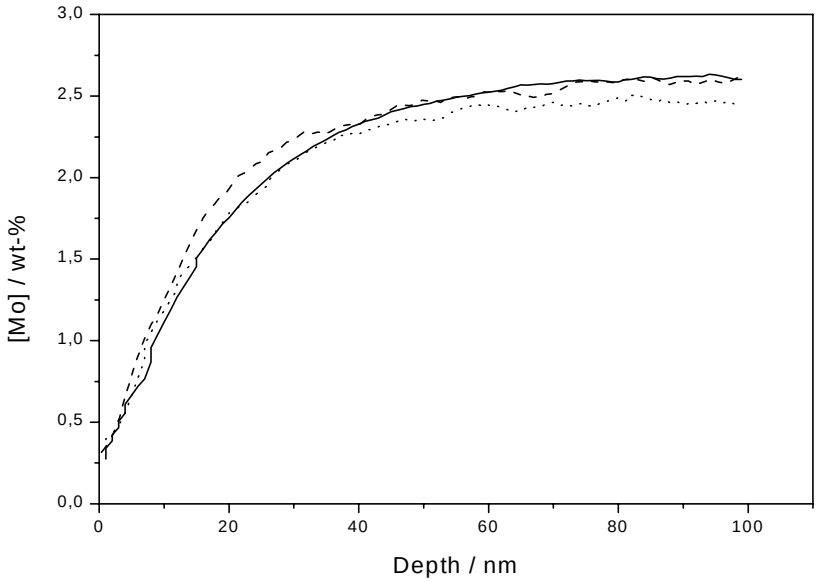

Fig. 69. Mo profiles of P752 immersed 3 days in oxygen bubbled solution, pH=3, T=50 °C.

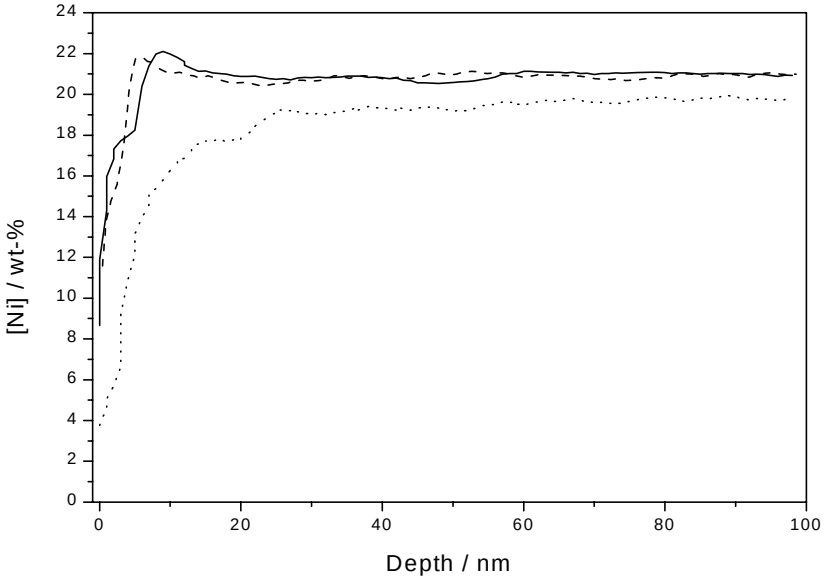

Fig. 70. Ni profiles of Ralloy 654MO immersed 3 days in oxygen bubbled solution, pH=3, T=50 °C.

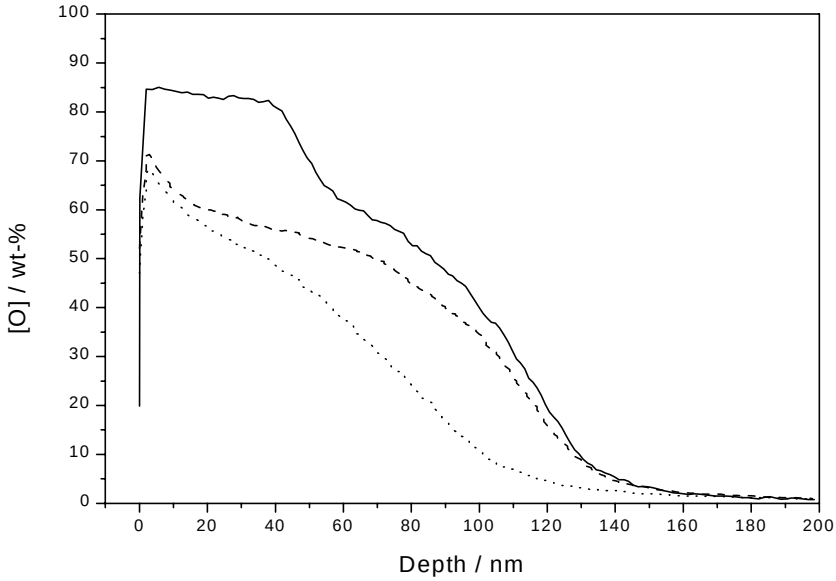

Fig. 71. O profiles of P720 immersed 16 days in ozonated solution, pH=3, T=50 °C.

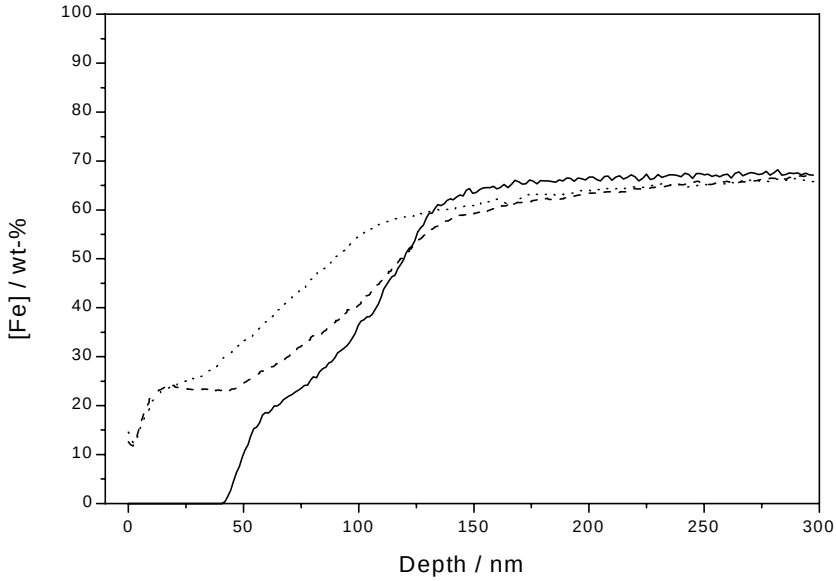

Fig. 72. Fe profiles of P720 immersed 16 days in ozonated solution, pH=3, T=50 °C.

The thickness of the oxide layers formed in ozonated solution were defined using the oxygen profiles from GDOS analyses. This was done by fitting linear equations for the oxygen concentration profiles, as in Fig. 73. The thickness of the oxide layer was taken as the intersection of these two slopes. In Fig. 70 the O profiles are the median profiles of three separate oxygen analyses. This does not give the real thickness of the oxides; the

exact thickness is impossible to determine from GDOS analyses. The main aspect in the examination is to compare the differences in thickness on different steels and the effect of immersion time.

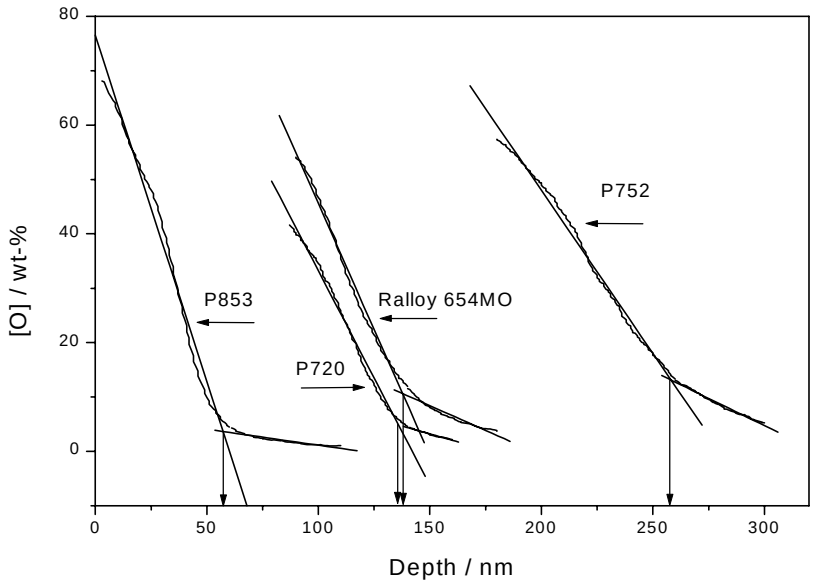

Fig. 73. Thickness of the oxide layers of stainless steels P853, P720, P752 and Ralloy 654MO in ozonated solution, pH=3, T=50 °C, after 16 days.

The calculated thickness of the oxide layers in ozonated solution after 16 days immersion are shown in table 15. On ferritic stainless steel P853 the oxide layer (57 nm) is about one third of that on austenitic steels P720 (136 nm) and Ralloy 654MO (141 nm). The thickness of the oxide of austenitic stainless steel P752 is about five times higher (258 nm) than that of P853. One would have thought that the thickness of the oxide layer would increase as the amount of alloying elements increases. This is, however, not always valid. The oxide on Ralloy 654MO is thinner than on less alloyed P752. This is obviously caused by the peeling of the oxide seen in SEM pictures.

Table 15. Thickness of the oxide layers in ozonated solution, pH=3, T=50 °C, after 16 days.

Material	Thickness / nm
P853	57
P720	136
P752	258
Ralloy 654MO	141

The chemical concentrations in the outermost layer (< 2 nm) formed in ozonated solution in 16 days is discussed here briefly, because it is very difficult to determine the composition due to great variations caused by the ineffectiveness of GDOS when used for thin oxide layers. Some estimations of the changes in chemical composition in ozonated

solution compared with oxygen bubbled solution are given. The surface analyses in ozonated solution are shown in table 16 and in oxygen bubbled solution table 17. Results are the average values of three analyses.

Table 16. The chemical concentration (wt-%) of the outer oxide layers (< 2 nm) of P853, P720, P752 and Ralloy 654MO after 16 days immersion in ozonated solution, pH=3, T=50 °C.

Material	Fe	Cr	Ni	Mo	O	C	Mn	P	S	Si
P853	14	1	0.2	0.5	51	27	0	1.5	2	2.8
P720	13	1.7	0.3	0.5	55	21	0.9	1.2	2.3	4
P752	13	1.8	0.3	0.6	50	29	0.1	1	1.8	2.4
Ralloy 654MO	12	1.3	0.3	2.9	60	17	2.1	1.1	1.2	2.1

Table 17. The chemical concentration (wt-%) of the outer oxide layers (<2 nm) of P853, P720, P752 and Ralloy 654MO after 3 days immersion in oxygen bubbled solution, pH=3, T=50 °C.

Material	Fe	Cr	Ni	Mo	O	C	Mn	P	S	Si
P853	1.4	5.7	0.2	0.4	50	27	0	3.3	5.2	7
P720	20	22	6.4	0.1	33	12	1.1	0.9	1.3	3.6
P752	14	17	6.7	0.4	32	22	0.9	0.7	1.1	5.4
Ralloy 654MO	14	28	10	1.3	28	11	2.9	0.8	1.1	2.3

Carbon and oxygen concentrations on the outermost layer are high on samples from both oxygen and ozone solutions. The origin of carbon on the outer layer is obviously partly from the analysis equipment, where some grease has been leaking onto the sample and partly from sample handling. The most important differences between layers formed in ozonated solution compared to oxygen bubbled solution, besides the thickness, are lower Cr concentration, lower Ni concentration. Where the Cr concentration is between 6 - 28 wt-% in oxygen bubbled solution, it is only 1 - 2 wt-% in ozonated solution. Fe concentration of P853 increases in ozonated solution. Mo concentrations are slightly higher in ozonated solutions. On the surface of samples immersed in ozonated solutions some very high Mo concentrations (up to 50 w-%) were found. It is obvious, that these high concentrations are real, because also in ESCA analyses high Mo concentrations (up to 16 %) were found. The values of the Mo concentrations in GDOS analyses are probably higher than the real values.

The growth rate of the oxide layers were studied for stainless steels P720 and Ralloy 654MO. GDOS surface analyses were done after 1, 2, 4, 8 and 16 days immersion in ozonated solution. The same steels immersed for 3 days in oxygen bubbled solution were used as reference samples. The thickness of the oxide layer of P720 begins to increase between 4 and 8 days immersion. This is shown in Fig. 74. Before day 4 only minor changes occurs in the oxide layer and it is quite similar to that formed in the oxygen bubbled solution.

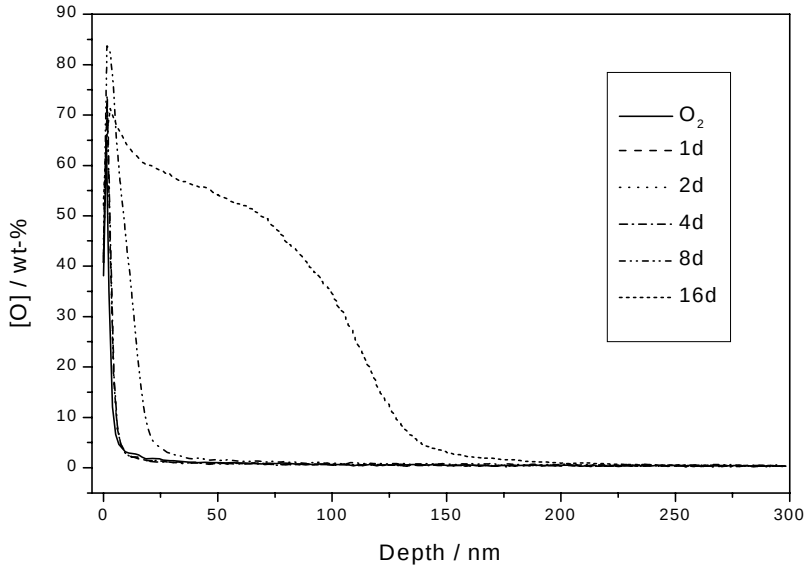

Fig. 74. The effect of immersion time on the oxidation of P720 according to O profile in ozonated solution, pH=3, T=50 °C.

The oxidation rate of the more alloyed Ralloy 654MO is higher (Fig. 75). The thickness of the oxide layer begins to increase already during the first day: after 24 h immersion the thickness of the oxide layer is 52 nm. This is about 7 times thicker than in oxygen solution after 3 days. After 16 days the thickness is similar to P720 (Ralloy 654MO 141 nm, P720 136 nm). The depth of high oxygen concentration in 4 days experiments is about 15 times greater than in oxygen bubbled solution.

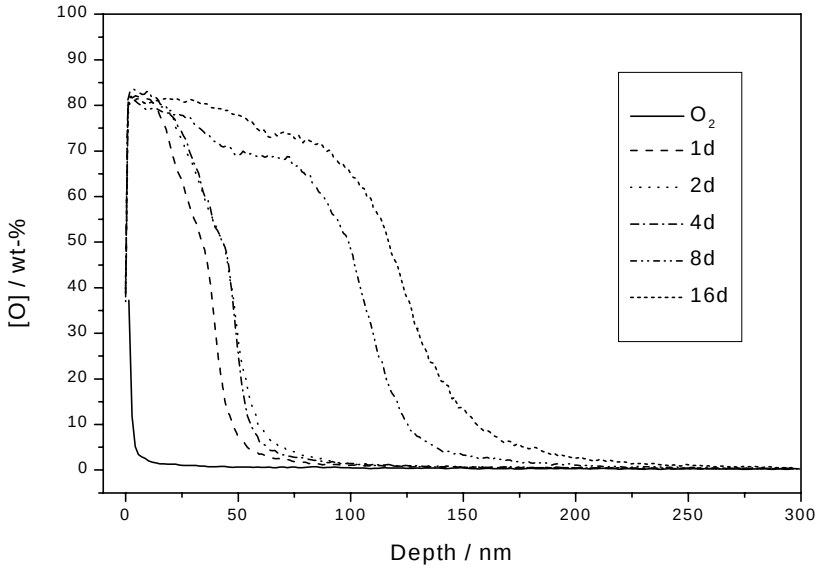

Fig. 75. The effect of immersion time on the oxidation of Ralloy 654MO according to O profile in ozonated solution, pH=3, T=50 °C.

The depth of the oxidised layer of stainless steels P720 and Ralloy 654MO can be seen in table 18.

Table 18. The depth of the oxidised layer from oxygen profiles on P720 and Ralloy 654MO.

	Depth / nm	
Immersion time / days	P720	Ralloy 654MO
3 d in O_2	4.3	4.2
1d in O_3	4.3	52
2 d in O_3	6.1	64
4 d in O_3	6.2	62
8 d in O_3	19	129
16 d in O_3	136	141

The growth of the oxide layer on P720 and Ralloy 654MO as a function of immersion time is shown in Fig. 76. The growth on P720 follows an exponential function (depth growth = $3{,}505e^{0.2215x}$ with R^2 =0,9805). As the oxidation depth increases all the time, the protection given by the oxide layer is not very good. The oxidation rate of Ralloy 654MO differs from that of P720. Ralloy 654MO oxidises at a higher rate at the beginning of the immersion. The thickness of the layer decreases after 2 days immersion. This is assumed to be due to the partial detachment of oxide from the base metal, as has been observed in SEM investigations. After a certain area has become bare of oxide, the oxidation rate increases again as in Fig. 76. The oxidation of Ralloy 654MO is breaking oxidation. The oxide layer is protective, but as it detaches frequently, oxidation can continue.

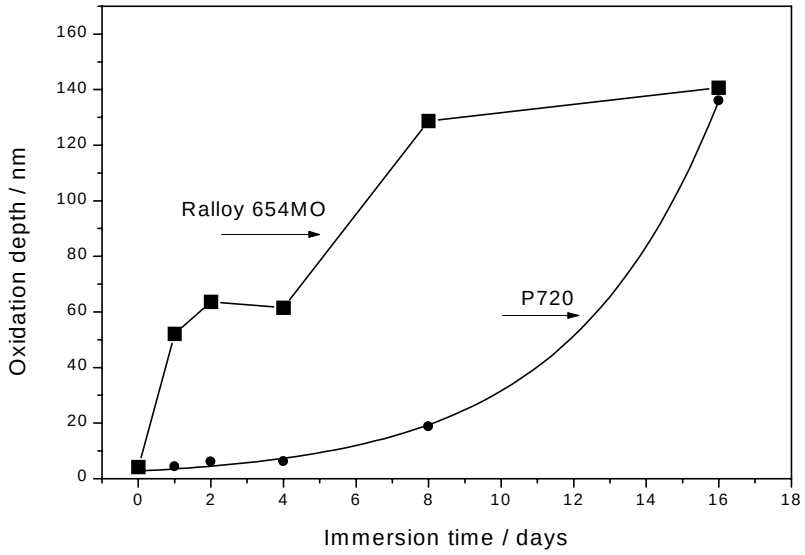

Fig. 76. The oxidation rate of P720 and Ralloy 654MO in ozonated solution, pH=3, T=50 °C.

In order to determine the exact mechanism of the oxidation of stainless steels in ozonated solution, longer and more immersion tests should have been carried out. It is not possible that the oxidation of P720 continues further at an exponential rate as the first 16 days would indicate. SEM analyses show that detachment of the oxide layer occurs also on less alloyed stainless steels. It is assumed that the oxidation behaviour of lower alloyed steels will in longer experiments follow the oxidation of more alloyed Ralloy 654MO.

The concentration profiles of Fe, Cr, Ni and Mo from stainless steel P720 after 3 days immersion in oxygen bubbled solution and after 1, 2, 4, 8, and 16 days immersion in ozonated solution are shown in Fig. 77 - Fig. 80. Analysis of the 16 day experiment was carried out separately from those others. This has caused the differences in the bulk concentration of Fe, Cr and Ni seen in the figures. The behaviour of all analysed elements is similar: the major changes in concentrations begin between 4 and 8 days.

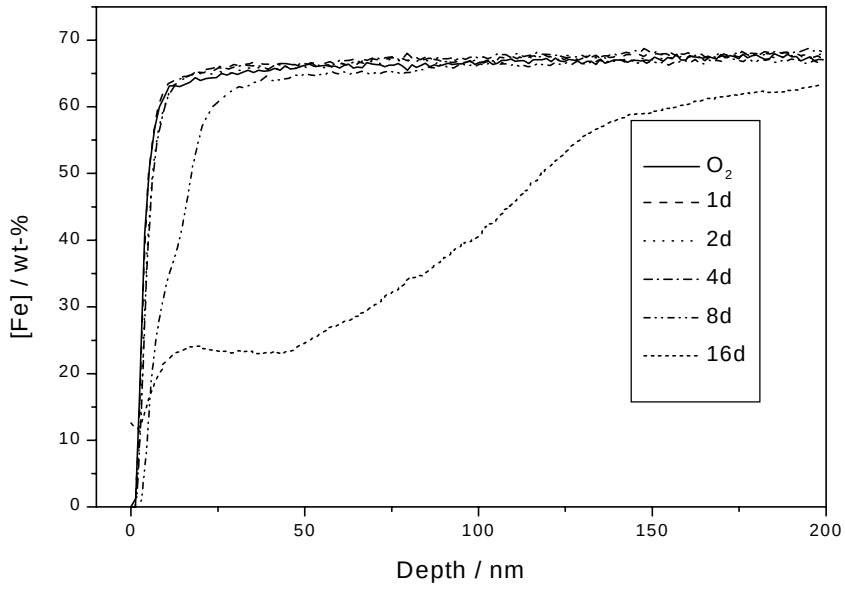

Fig. 77. Fe profiles of P720 after 3 days in O_2 and 1, 2, 4, 8, and 16 days in O_3 solution, pH=3, T=50 °C.

Iron in the 16 day sample has a plateau from about 15 nm to about 40 nm, where Fe concentration is about 23 % (Fig. 77).

Chromium concentration on the very outer surface varies, but a maximum 29 - 34 wt-% occurs at a depth between 2.5 and 5.5 nm on O_2, 1, 2 and 4 days specimens (Fig. 78). This chromium enriched oxide dissolves in ozonated solution so that after 8 days no enriched layer can be noticed, but the depth of the chromium deficient Cr-layer increases to about 140 nm in 16 days.

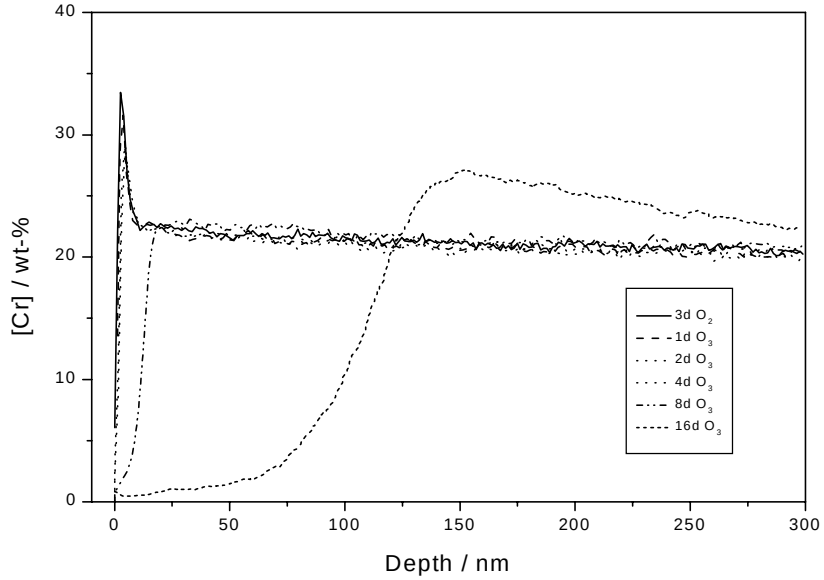

Fig. 78. Cr profiles of P720 after 3 days in O_2 and 1, 2, 4, 8, and 16 days in O_3 solution, pH=3, T=50 °C.

The behaviour of nickel is similar to that of chromium (Fig. 79). Nickel concentration reaches a maximum at a depth of 5 to 8 nm. This maximum concentration depth goes to about 20 nm after 8 days immersion and disappears between 8 and 16 days immersion.

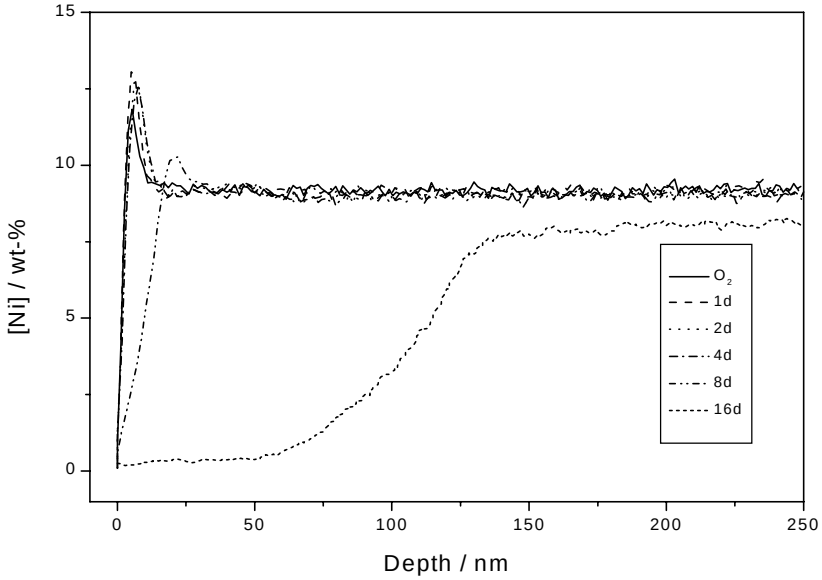

Fig. 79. Ni profiles of P720 after 3 days in O_2 and 1, 2, 4, 8, and 16 days in O_3 solution, pH=3, T=50 °C.

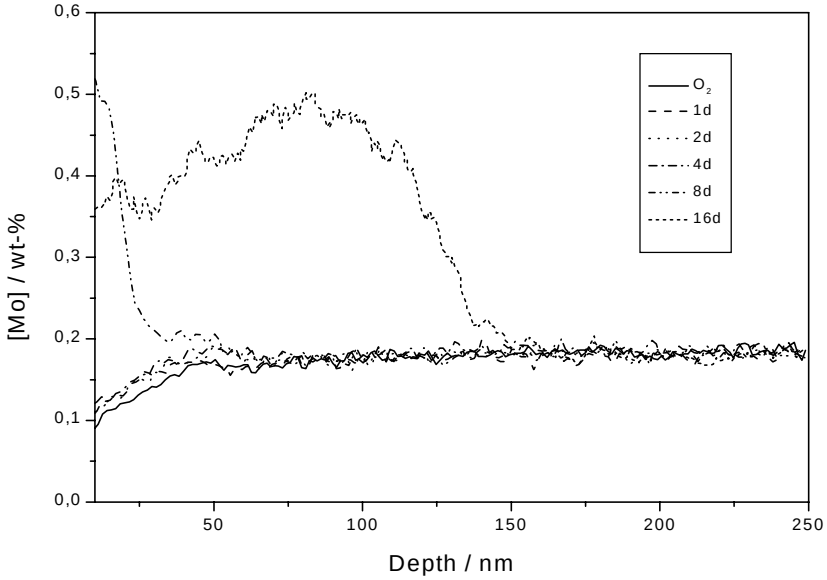

Fig. 80. Mo profiles of P720 3 days in O_2 and 1, 2, 4, 8, and 16 days in O_3 solution, pH=3, T=50 °C.

The Mo concentration in stainless steel P720 is low (0.19 wt-%) but nevertheless is a cause for comment. In Mo concentration profile a larger change occurs after 4 days immersion (Fig. 80). The changes in Mo concentration profiles during 0 - 4 day experiments are minor; in ozonated solution Mo has a low concentration range and reaches the nominal concentration at a depth of about 40 nm. In 8 and 16 day experiments Mo concentration increases clearly so that after 16 days Mo concentration is 0.4 - 0.5 wt-% to a depth of 120 nm and reaches the nominal bulk concentration at about 150 nm. Molybdenum concentrates on the surface.

The depths of oxide layers from the Fe analyses were defined by the intersection of linear fittings of the Fe profile from depth of zero with the nominal Fe concentration of the alloy. This intersection was chosen to the thickness of the Fe depleted range. In the Fe profile from the 16 day immersion test, the depth was chosen according to the intersection of the nominal Fe concentration and the linear fitting between 70 and 110 nm in the Fe profile. The corresponding values for Cr and Ni were defined by intersections of linear fittings in the alternation zone of element profiles with the nominal concentration. The changes of O, Cr, Fe and Ni profiles are plotted in Fig. 81 similar to Fig. 76. The changes in O, Fe, Cr and Ni concentrations are similar and seem to follow exponential equations. After 16 days immersion, changes in Fe concentration are the largest; the depletion of Fe reaches deeper (168 nm) in the alloy than nickel (143 nm) and change in chromium concentration is shallower (122 nm).

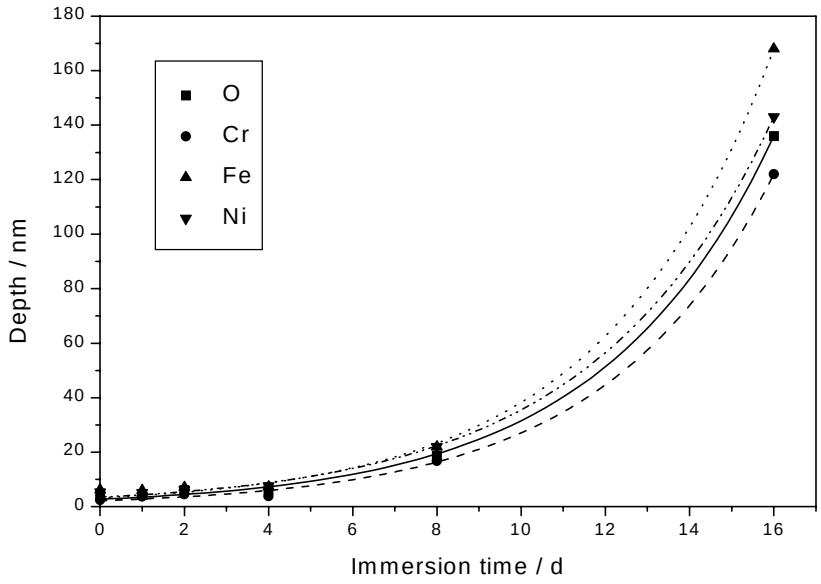

Fig. 81. The thickness of the oxide layer of P720 according to O, Cr, Fe and Ni profiles in ozonated solution, pH=3, T=50 °C.

The corresponding element profiles for Ralloy 654MO are shown in Fig. 82 - Fig. 85. The iron concentration reaches its nominal concentration at a depth of about 8 nm in oxygen bubbled solution. After 1 day immersion in ozonated solution, the Fe concentration is zero to 12 nm, 2 days 17 nm, 4 days 9 nm, 8 days 28 nm and after 16 days 52 nm (Fig. 82). In stainless steel P720 no similar Fe-depleted range was found.

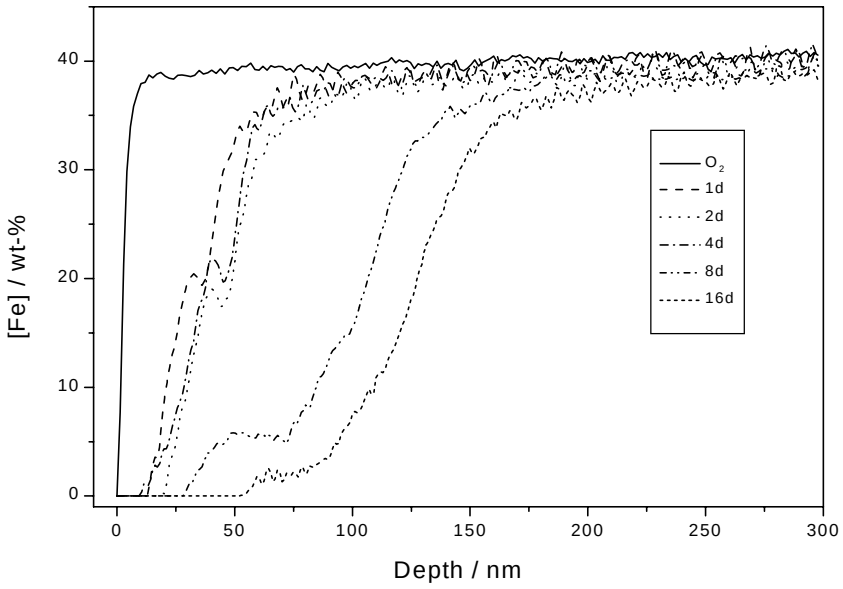

Fig. 82. Fe profiles of Ralloy 654MO 3 days in O_2 and 1, 2, 4, 8, and 16 days in O_3 solution, pH=3, T=50 °C.

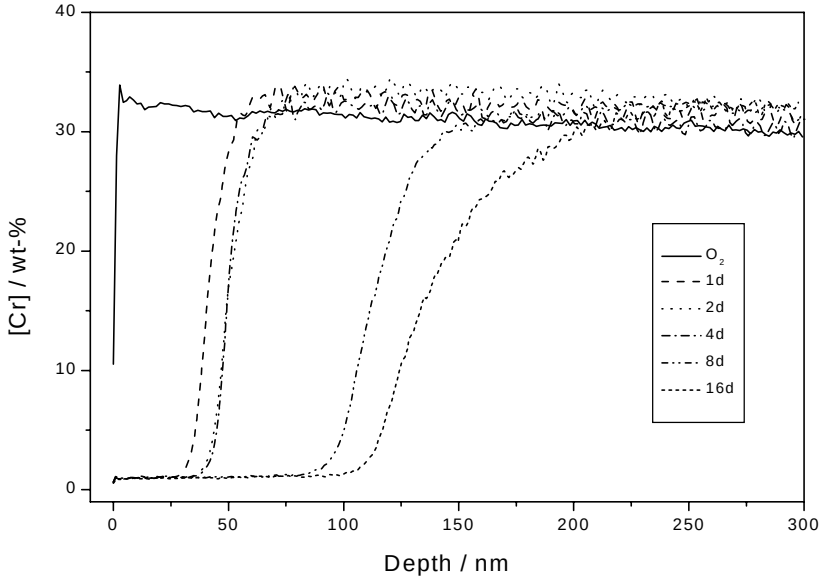

Fig. 83. Cr profiles of Ralloy 654MO 3 days in O_2 and 1, 2, 4, 8, and 16 days in O_3 solution, pH=3, T=50 °C.

The concentration profiles for Cr differ also between P720 and Ralloy 654MO (Fig. 78 and Fig. 83). On Ralloy 654MO, with higher Cr concentration, no maximum in Cr profiles was found. The Cr concentration was decreased by ozone from a concentration of about 33 wt-% in oxygen bubbled solution (if the outermost layer < 2 nm is not considered) to a concentration of about 1 wt-%; this low Cr concentration depth increased with the immersion time.

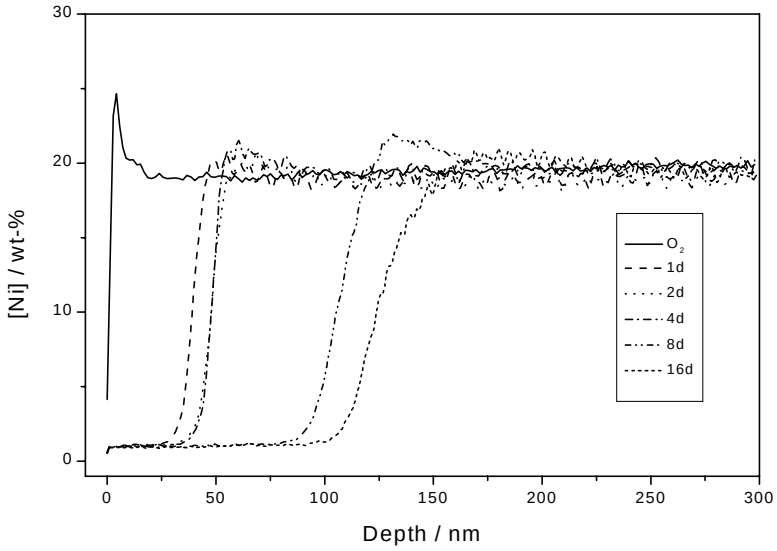

Fig. 84. Ni profiles of Ralloy 654MO 3 days in O_2 and 1, 2, 4, 8, and 16 days in O_3 solution, pH=3, T=50 °C.

The difference in Ni concentration profiles between P720 and Ralloy 654MO is smaller. A maximum in Ni concentration occurs also in the oxide layer of Ralloy 654MO. The depth of this maximum increases and the concentration maximum decreases with the immersion time so that after 16 days immersion no maximum exists (Fig. 84 The depth of the nickel depleted layer increases with immersion time.

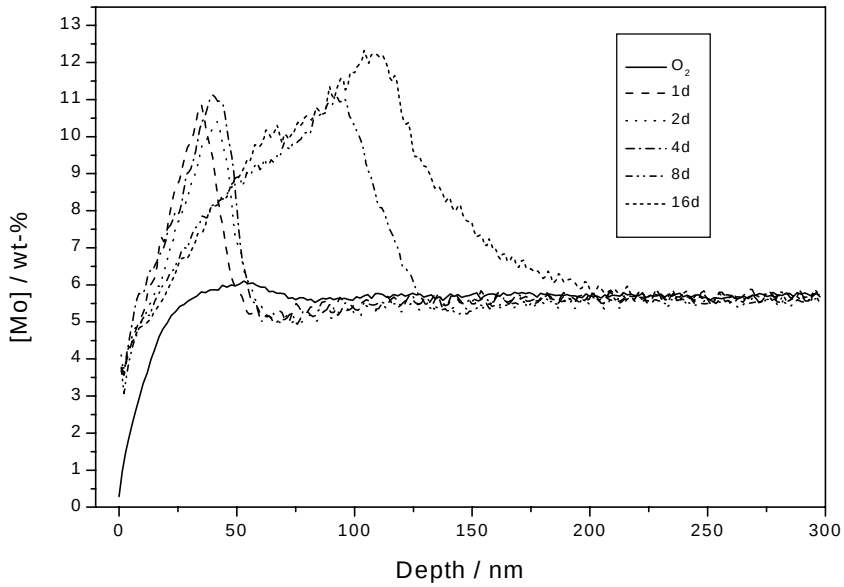

Fig. 85. Mo profiles of Ralloy 654MO 3 days in O_2 and 1, 2, 4, 8, and 16 days in O_3 solution, pH=3, T=50 °C.

The effect of ozone on the Mo profile of Ralloy 654MO is similar to that of P720 (Fig. 85). For Ralloy 654MO, where the bulk Mo concentration is 5.8 wt-%, the concentration in the maximum range is 11 - 13 wt-%. Both the depth and value of the maximum concentration increases with immersion time. The depth of this maximum is 31 - 41 nm in samples immersed for 1, 2 and 4 days in ozonated solution and about 90 nm after 8 days immersion and about 110 nm after 16 days. In oxygen bubbled solution a minor maximum at 50 nm can be seen and below this the outer layer down to about 40 nm is depleted of Mo.

The changes of O, Cr, Fe and Ni profiles for Ralloy 654MO are plotted in Fig. 86 as for P720 in Fig. 80. The oxidation patterns are similar for the changes in oxygen and alloying elements. All elements follow the same behaviour pattern.

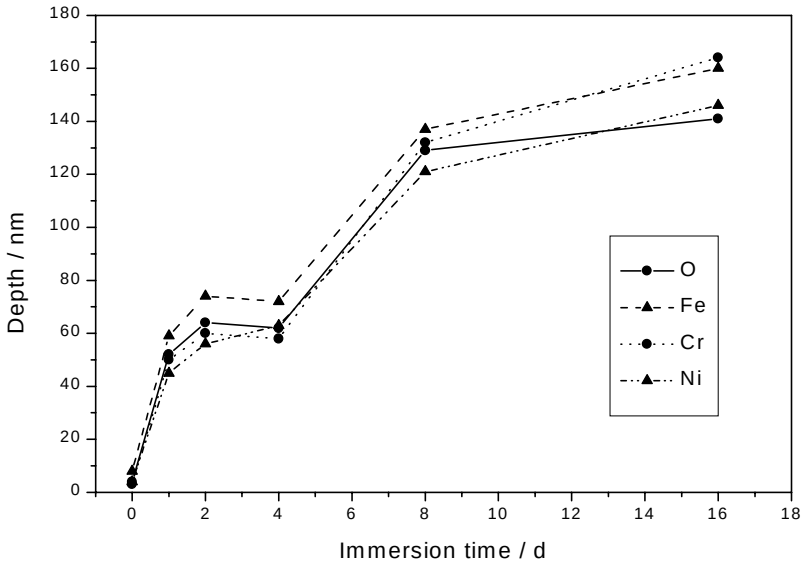

Fig. 86. The oxidation rate of Ralloy 654MO according to O, Cr, Fe and Ni profiles in ozonated solution, pH=3, T=50 °C.

The oxide films after 3 days immersion in oxygen solution and after 16 days in ozonated solution were compared. The oxide layer from the oxygen bubbled solution on stainless steel P853 is thicker than layers on other steels (Fig. 87). Thickness of oxide layers are: P853 13 nm, P720 4.3 nm, P752 6.0 nm and Ralloy 654MO 4.2 nm; thickness calculations were done as for the samples in the ozonated solutions. In oxygen bubbled solution the thickness of the oxide layer increases as the amounts of the alloying elements decrease. P752 is an exception, as was the case in the ozonated solution.

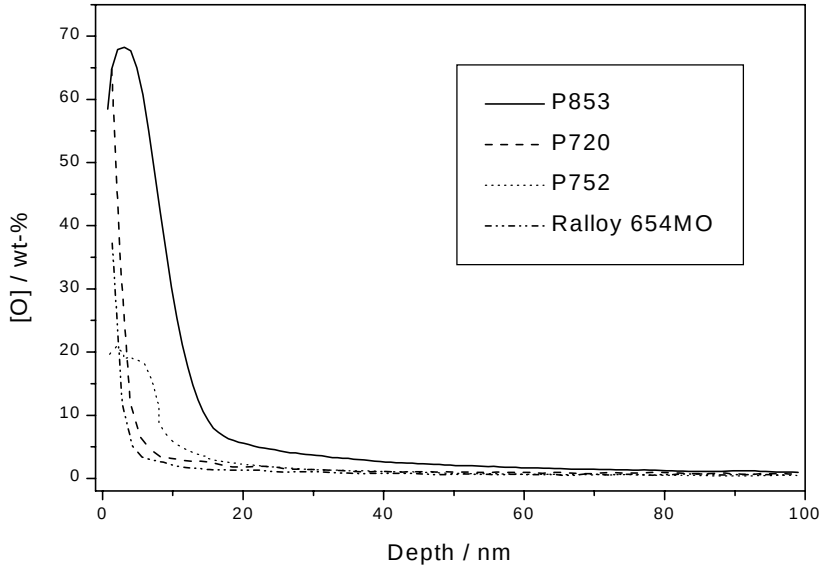

Fig. 87. O profiles of test materials immersed 3 days in O_2 solution, pH=3, T=50 °C.

The concentration profiles of Fe, Cr, Ni and Mo are shown as deviations from the nominal concentrations, where the bulk metal concentrations are from corresponding GDOS analyses. The iron concentration profiles follow the oxygen profiles. The depth of the Fe depleted range is relative to the oxidation depth (Fig. 88).

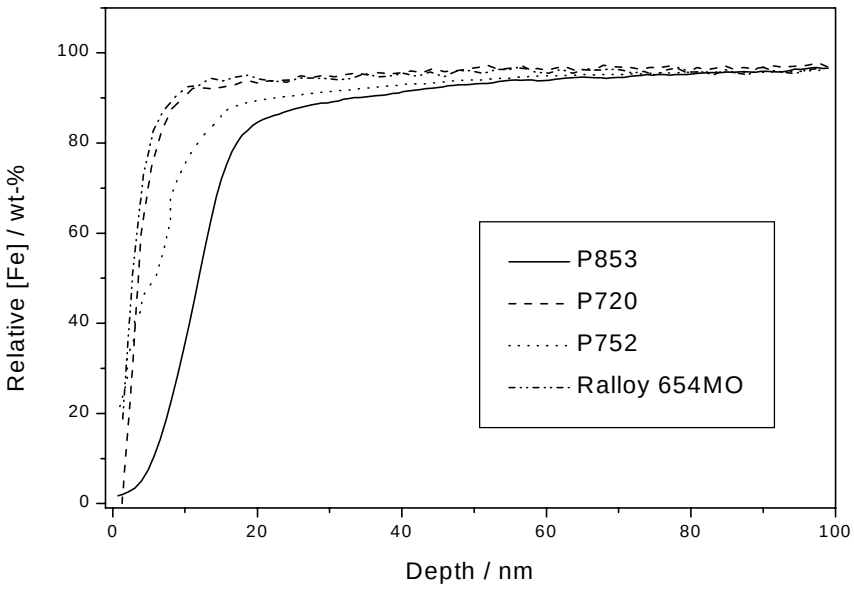

Fig. 88. Relative Fe concentration profiles of test materials immersed 3 days in O_2 solution, pH=3, T=50 °C.

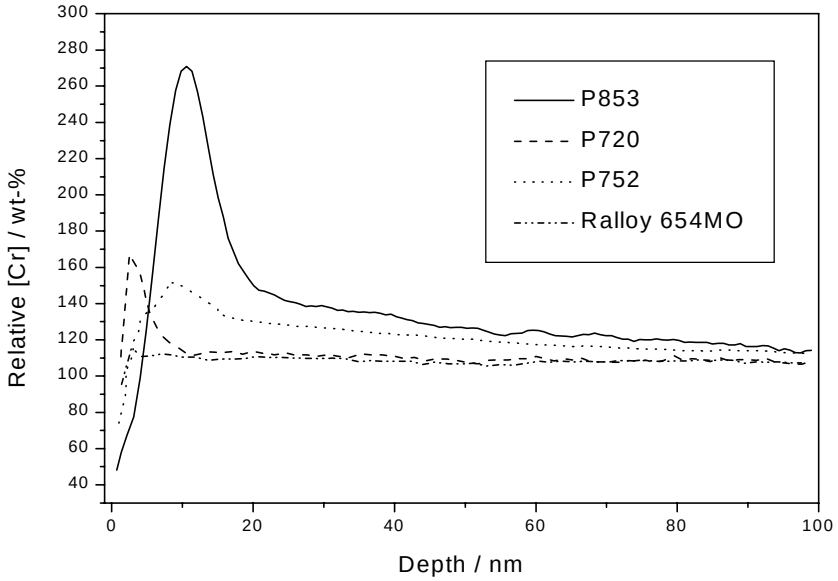

Fig. 89. Relative Cr concentration profiles of test materials immersed 3 days in O_2 solution, pH=3, T=50 °C.

More differences can be seen in the Cr concentration profiles (Fig. 89). On the surface of every test material a maximum concentration occurs. This maximum is inversely related to the alloying element concentrations in the bulk metal. Chromium concentrates more in the oxide layers of less alloyed steels.

A maximum also occurs in the Ni profiles (Fig. 90). This maximum is highest on P853, where Ni concentration was only 0.20 wt-%. On P720 and Ralloy 654MO a smaller peak can be seen.

Mo concentrates in a very large quantity in the oxide layer of stainless steel P853. The relative Mo concentration on the outer layer is about 1800 wt-%. On other steels a Mo depleted range can be seen (Fig. 91).

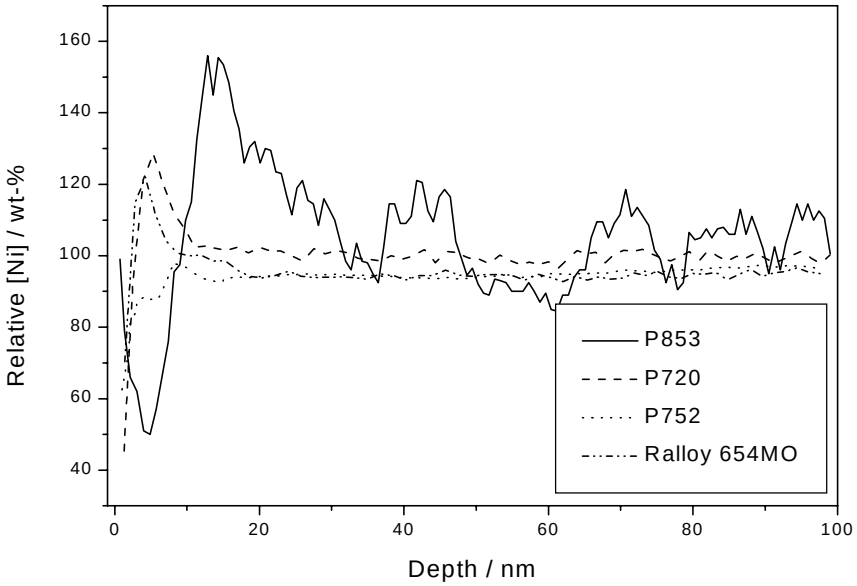

Fig. 90. Relative Ni concentration profiles of test materials immersed 3 days in O_2 solution, pH=3, T=50 °C.

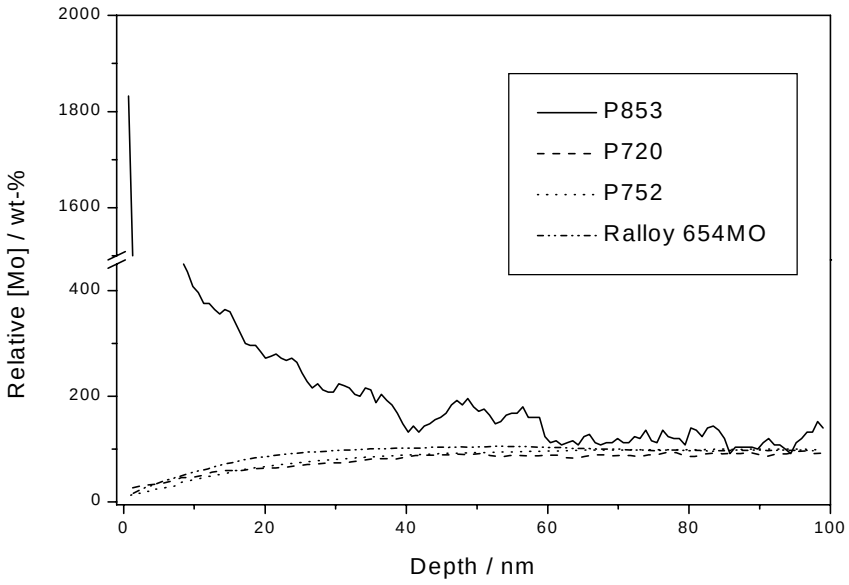

Fig. 91. Relative Mo concentration profiles of test materials immersed 3 days in O_2 solution, pH=3, T=50 °C

The differences between bulk metal and the oxide layer composition increase as the depth of the oxidised layer increases. Oxidation is stronger on less alloyed stainless steels. As oxidation progresses, the relative concentration changes of Ni and especially Mo between bulk metal and the oxide layer increase.

After 16 days immersion in ozonated solution, the oxide layer on test materials is thinnest on P853 and thickest on P752 (Fig. 92). On Ralloy 654MO iron has dissolved completely to a depth of 50 nm. A plateau in Fe concentration on P720 of about 27 wt-% is evident from 10 nm to 50 nm and from 60 to 160 nm on P752 50 wt-%.

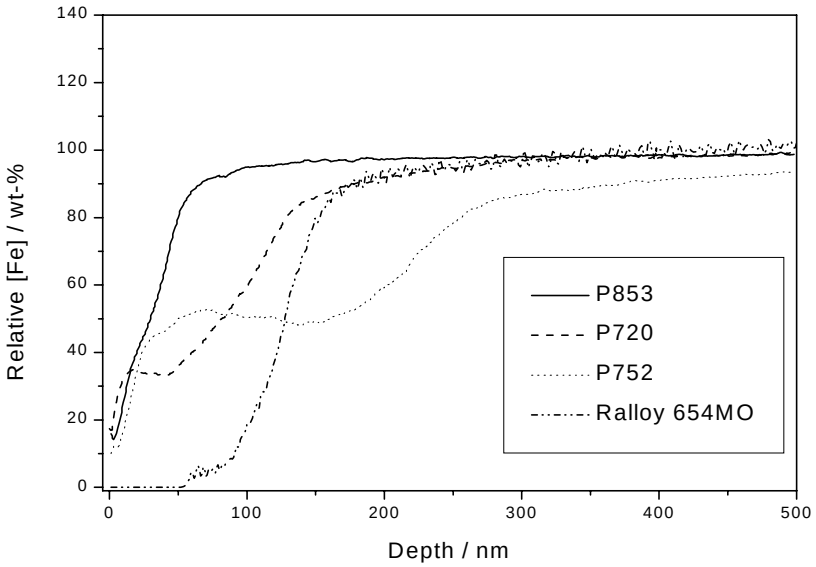

Fig. 92. Relative Fe concentration profiles of test materials immersed 16 days in O_3 solution, pH=3, T =50 °C

Chromium concentration in the outer oxide layer is very low in each test material (Fig. 93). This Cr depleted range is for P853 about 20 nm, for P720 about 60 nm, for P752 about 180 nm and for Ralloy 654MO about 110 nm. In these ranges, Cr concentration is below 5 wt-% for P720, P752 and Ralloy 654MO. For P853 a minimum of about 6 wt-% can be seen. A maximum in nominal Cr concentration occurs below this Cr depleted range in P853 and P720. Cr concentration of P752 reaches its bulk concentration at a depth of about 700 nm.

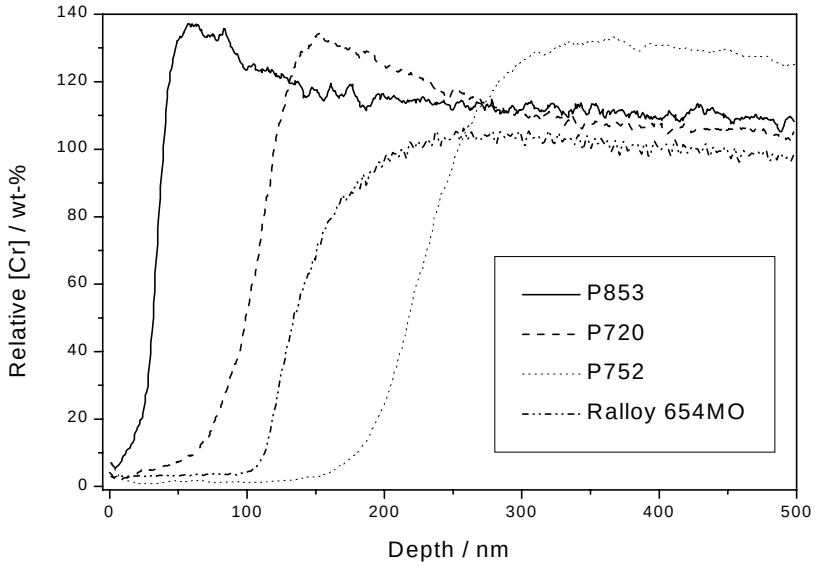

Fig. 93. Relative Cr concentration profiles of test materials immersed 16 days in O_3 solution, pH=3, T=50 °C.

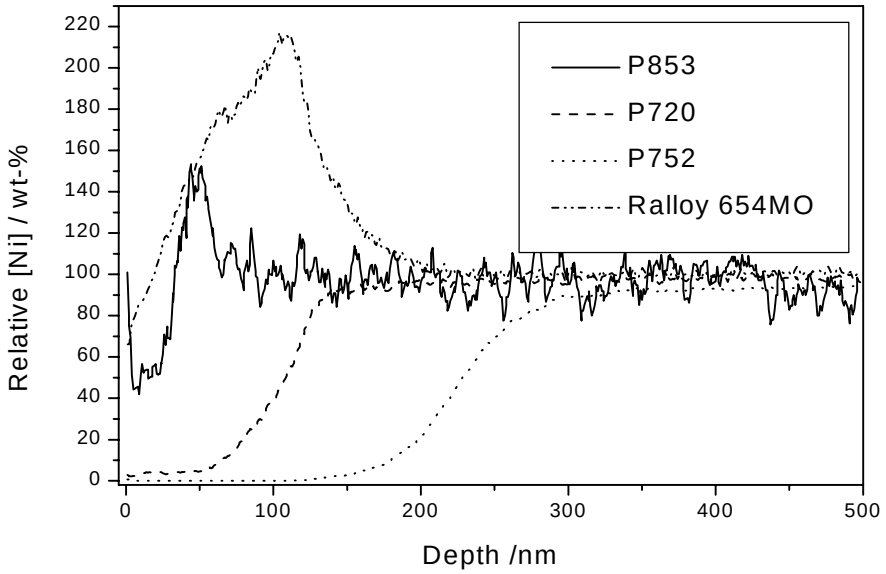

Fig. 94. Relative Ni concentration profiles of test materials immersed 16 days in O_3 solution, pH=3, T=50 °C.

Large differences in the relative Ni concentration profiles can be seen (Fig. 94). In the oxide layers of P752 on the very outer layer (0 - 4 nm) a low Ni concentration (< 1 wt-%) can be found. Below this layer to a depth of 110 nm Ni is completely dissolved. On P720 Ni the concentration is also low (< 5 wt-%) to 50 nm. On stainless steel P853 and Ralloy 654MO, the relative Ni concentrations are higher in the outer oxide layer and a maximum can be seen on both materials.

Molybdenum concentrates most on the surface of steel P853 compared with the bulk concentration. The more the material has oxidised, the lower is the Mo concentration on the surface (Fig. 95).

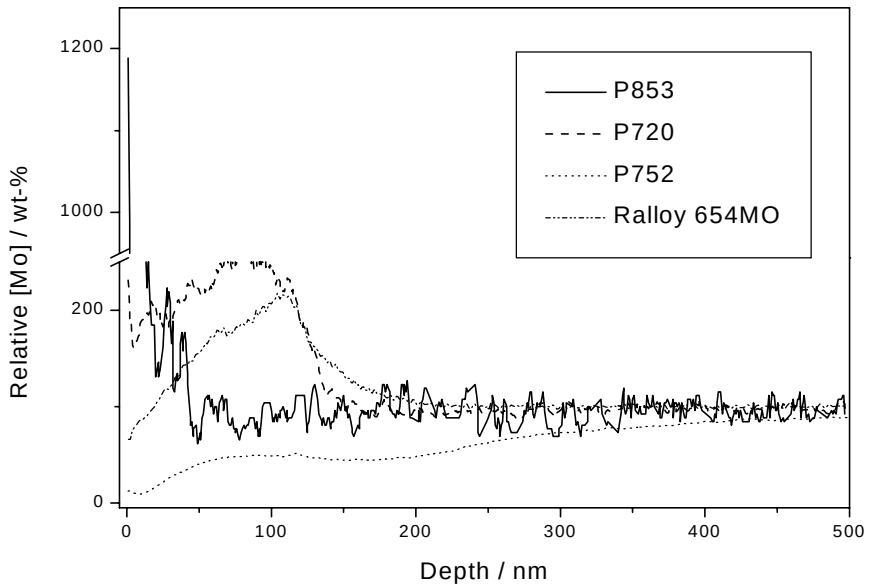

Fig. 95. Relative Mo concentration profiles of test materials immersed 16 days in O_3 solution, pH=3, T=50 °C.

The concentration profiles of P, Mn, Si and S are discussed briefly. The concentration of phosphorus on the surface (< 4 nm) varies in oxygen bubbled solution. On P853, P concentration is higher (1 - 4.5 wt-%) than on the other materials (0.1 - 0.8 wt-%). The nominal concentration of P on Ralloy 654MO at a depth of about 10 nm is 0.024 wt-%.

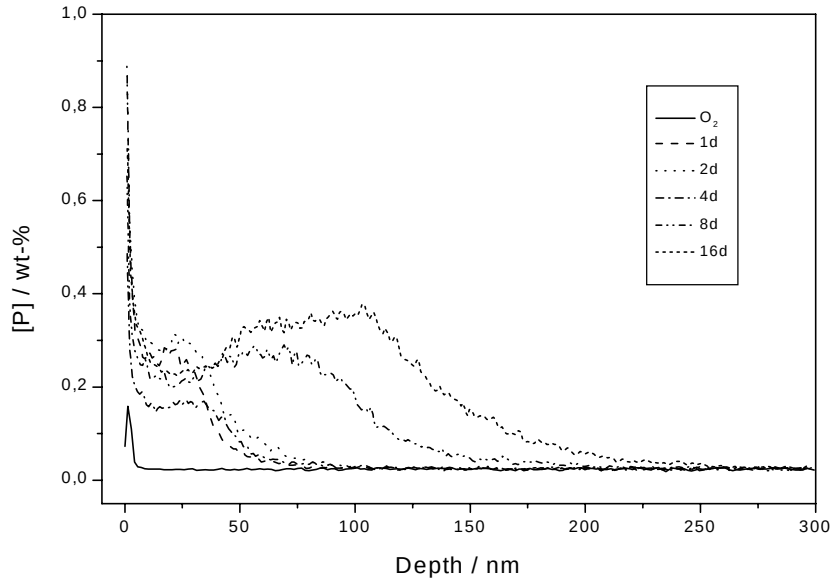

Fig. 96. P profiles of Ralloy 654MO after 3 days in O_2 and 1, 2, 4, 8, and 16 days in O_3 solution, pH=3, T=50 °C.

In ozonated solution, P begins to concentrate in the oxide layer so that in the outermost layer P concentration is 0.5 - 0.9 wt-% and under this layer P concentration increases to a value of 0.15 - 0.38 wt-%. As the immersion time increases, the depth of this high P concentration increases. After 16 days immersion in ozonated solution, high P concentration occurs to a depth of 110 nm, after which it decreases and reaches the nominal P concentration at a depth of about 300 nm (Fig. 96).

The behaviour of P is similar for the other stainless steels studied. Phosphorous concentration in the outermost layer is high; P has concentrated in the oxide layer and reaches its nominal concentration for steel P853 at a depth of 80 nm, P720 200 nm, P752 400 nm in ozonated solution. The high phosphorous concentration is even deeper than the thickness of the estimated oxide layer. This means, as is explained in literature [3], that corrosion on the grain boundaries found in pitting corrosion tests is obviously caused by the precipitation of phosphides and other compounds.

The behaviour of manganese in the oxide layers varies widely. In oxygen bubbled solution, Mn concentration is near the bulk concentration on the surface of P720, P752 and Ralloy 654MO. On the outer surface (< 10 nm) of P853 Mn concentration is zero. The Mn concentration on the surface of P720 and Ralloy 654MO has increased already after 3 days immersion in oxygen bubbled solution. The maximum value increases as the immersion time in ozonated solution increases up to 8 days for P720 and 4 days for Ralloy 654MO after which the concentration decreases. The depth of the maximum also moves deeper in the oxide layer and is after 16 days immersion in ozonated solution at 110 nm for P720 and at 120 nm for Ralloy 654MO. The width of the maximum concentration peak increases, which also indicates that Mn is concentrated in the layer. This Mn maximum occurs in both P720 and Ralloy 654MO to a depth, where the oxygen concentration is 25 wt-%. Mn concentration profiles of stainless steels Ralloy 654MO are shown in Fig. 97.

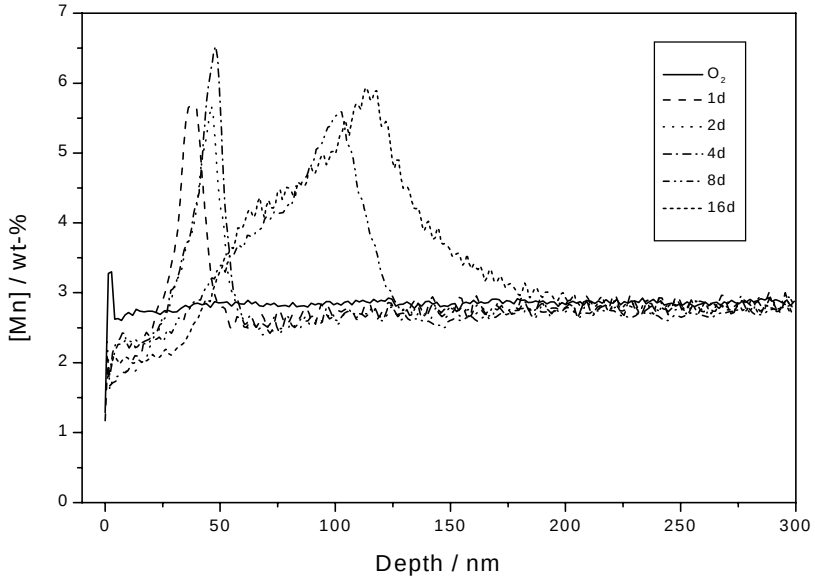

Fig. 97. Mn profiles of Ralloy 654MO after 3 days in O_2 and 1, 2, 4, 8, and 16 days in O_3 solution, pH=3, T=50 °C.

Silicon concentration on the surface is high on all four stainless steels after immersion in oxygen bubbled solution. The nominal concentrations of the alloys according to GDOS analysis, maximum Si concentration in the oxide layer, and the depth of this maximum are shown in table 19. The maximum Si concentrations are 3 - 10 times higher than the nominal concentration.

Table 19. Nominal Si concentration of alloys, maximum concentration and the depth of maximum concentrations after 3 days immersion in oxygen bubbled solution, pH=3, T=50 °C.

material	nom. conc. / wt-%	max. conc. / wt-%	max. depth / nm
P853	0.65	7.8	3
P720	0.44	1.6	1
P752	0.5	5.2	1
Ralloy 654MO	0.26	2.6	0

In ozonated solution the silicon concentration of the oxide layer on Ralloy 654MO decreases already after 1 days immersion to a level corresponding to the nominal concentration. Si concentration varies from 0.1 wt-% to about 0.4 wt-% to a depth of about 200 nm in all ozone immersion tests The concentration profiles for P720 vary widely in ozonated solution. Similar maximum levels exist for oxygen bubbled solution with Si concentrations from 1.1 to 1.4 wt-% at a depth of 1 - 3 nm. After 16 days immersion larger changes occur: the highest Si concentration is on the surface (2.8 wt-%) and below this a minimum of 0.8 wt-% at 13 nm. Further below is a large area with higher Si concentration so, that the maximum concentration is 1.8 wt-% at 55 nm. Si concentration reaches the nominal concentration at a depth of about 200 nm. Silicon concentration on the outer layer of P853 after 16 days immersion in ozonated solution has decreased and varies between 1.9 and 2.5 wt-% to about 30 nm and below this decreases so that it reaches the nominal concentration at depth of about 80 nm. Steel P752 has the same tendency: Si concentration decreases from about 1.2 wt-% in the outer layer to the nominal concentration at depth of about 90 nm.

The effect of thinning due to the dissolution of elements is not possible to consider in the inspection of GDOS results. However, as the weight losses for all stainless steels studied in this investigation are small, it is obvious that the thinning of the specimens is low.

3.8.3 ESCA analyses

The aim of ESCA analysis was to determine the compounds of the outer oxide layers formed during immersion. The concentration profiles of elements were also analysed. Analyses were carried out for stainless steel P720 and Ralloy 654MO immersed both 3 days in oxygen bubbled solution and 16 days in ozonated solution. Surface ESCA analysis was done form about 2 nm to 10 nm depth.

Surface ESCA analysis for P720 immersed 3 days in oxygen bubbled solutions shows that the main elements on the surface are O, C, Cr, Fe, Mo and Ni. Results of three separate analyses are shown in table 20. The amount of Mo is rather high even though the concentration of the bulk metal is low (about 0.19 wt-%).

Table 20. ESCA surface analysis for stainless steel Polarit 720 in oxygen bubbled solution.

peak	meas.1/ wt-%	meas.2/ wt-%	meas.3/wt-%	average wt-%
Sp O 1s	49.4	22	46	39.1
Sp C 1s	22	46.7	22.8	30.5
Sp Ni 2p	1.2	1.5	1.9	1.5
Sp Fe 2p	7.7	7.8	8.1	7.9
Sp Mn 2p	0.2	0	0.1	0.1
Sp Cr 2p	17.5	20.5	19.9	19.3
Sp Mo 3d	2	1.5	1.2	1.6

The main changes in the chemical composition of the sample immersed for 16 days in ozonated solution are the great decrease in Cr concentration from 19.3 to 0.8 wt-% and increase in Fe concentration from 7.9 to 15.6 wt-% (table 21). Also the concentration of Mn has increased (from 0.1 to 2.6 wt-%) and Ni concentration decreased (from 1,5 to 0,2 wt-%). A slight increase in Mo concentration may also be seen.

Table 21. ESCA surface analysis for stainless steel Polarit 720 in ozonated solution.

peak	meas.1/ wt-%	meas.2/ wt-%	meas.3/wt-%	average wt-%
Sp O 1s	47.6	32	48.2	42.6
Sp C 1s	31.6	46.6	30.9	36.4
Sp Ni 2p	0.2	0.5	0	0.2
Sp Fe 2p	15.2	16	15.5	15.6
Sp Mn 2p	2.7	2.6	2.5	2.6
Sp Cr 2p	0.9	0.7	0.7	0.8
Sp Mo 3d	1.9	1.7	2.2	1.9

The surface of stainless steel Ralloy 654MO immersed for 24 h in oxygen bubbled solution contains in addition to O and C mainly Cr but also Mo, Fe and Ni (table 22).

The interpretation of the results for Ralloy 654MO becomes more complicated because of the large increase of carbon concentration from 16.9 wt-% in oxygen bubbled solution to 39.4 wt-% in ozonated solution and oxygen decrease from 43.2 to 30.9 wt-% respectively (table 23). However, the Cr concentration has decreased dramatically (from 21.1 to 0.3 wt-%) and the Mo concentration doubled compared with that in oxygen bubbled solution (from 8.3 to 16.9 wt-%). Also the Ni concentration has decreased (from 3,2 to 0,6 wt-%) and Mn concentration has increased (from 0.3 to 4.2 wt-%).

Table 22. ESCA analysis for stainless steel Ralloy 654MO immersed in oxygen bubbled solution.

peak	meas.1/ wt-%	meas.2/ wt-%	meas.3/wt-%	average wt-%
Sp O 1s	42.1	43.9	43.7	43.2
Sp C 1s	17.1	16.3	17.2	16.9
Sp Ni 2p	3.4	2.9	3.2	3.2
Sp Fe 2p	7.3	7.1	6.8	7.1
Sp Mn 2p	0.6	0.1	0.2	0.3
Sp Cr 2p	21.3	21.2	20.8	21.1
Sp Mo 3d	8.2	8.5	8.2	8.3

Table 23. ESCA surface analysis for stainless steel Ralloy 654MO in ozonated solution.

peak	meas.1/ wt-%	meas.2/ wt-%	meas.3/wt-%	average wt-%
Sp O 1s	27.6	25.4	39.6	30.9
Sp C 1s	52.6	39.7	25.9	39.4
Sp Ni 2p	0.7	0.4	0.8	0.6
Sp Fe 2p	4.8	8.9	9.4	7.7
Sp Mn 2p	2.8	4.7	5.1	4.2
Sp Cr 2p	0.3	0.4	0.3	0.3
Sp Mo 3d	11.2	20.5	18.9	16.9

A clear change can be seen in the surfaces of both stainless steel samples immersed in ozonated solution compared with samples immersed in oxygen bubbled solution. These changes are compatible with GDOS results. In ozonated solution chromium is depleted in the outer oxide layer and Mo concentrations are higher. Mn is found in higher concentration on the surface of samples from ozonated solution. Some trace amounts of phosphorous were also found in Ralloy 654MO samples in ozonated solution, but not in oxygen bubbled solution immersed sample.

After immersion in ozonated solution the oxide layers of P720 and Ralloy 654MO have some marked differences. In P720 immersed in ozonated solution iron is in oxidised form during sputtering throughout the layer, but in the inner oxide layer ofR alloy 654MO the oxide, iron is partly metallic. This may mean that iron oxides in P720 are in a more stabile form than in Ralloy 654MO. The other reason may be the differences in the oxide thickness. Iron oxides in both materials after immersion in oxygen bubbled solution seems to reduce easier than oxides formed in ozonated solutions.

Chromium does not reduce during sputtering in P720 and reduces partly in Ralloy 654MO.

Nickel is, according to ESCA analyses, mostly in metallic form both in oxygen and in ozonated solutions.

Molybdenum is highly oxidised in samples after immersion in ozonated solution and reduces in sputtering through many stages. This means that molybdenum is its hexavalent form on the surface and in lower valences in the oxide.

The term “reduce” means here the unfastening of oxygen atoms from the oxides during sputtering [50].

The high C concentrations are attributed to the contamination of the surface before analysis. Carbon is drifted to metal surface during the oxidation after oxide removal. The origin of some carbon is the methanol purification of the sample before analysis [50]. The high sulphur concentrations may also be due to the inclusion of sulfate anions into the oxide layers [46].

4 CONCLUSIONS

Dissolved ozone at concentrations above about 0.5 ppm increases the redox-potential to about +1200 mV in a solution of pH 3. Cathodic reactions in ozonated solutions are the reduction of ozone and oxygen. Anodic reactions are both the oxidation of metals in the passive layer to higher valency and the oxidation of base metal under the oxide layer. Metals oxidise to the highest valency (Fe^{3+}, Cr^{6+}, Ni^{2+}, Mo^{6+}) in the outermost oxide layer. Chromium oxidises to $Cr(OH)_4$ and dissolves as hexavalent $HCrO_4^-$ or $Cr_3O_7^{2-}$ or Cr^{3+} ions, nickel as bivalent Ni^{2+} ions and iron as trivalent ions. Molybdenum oxidizes to solid MoO_3, which dissolves partly as $HMoO_4^-$.

Corrosion potentials of stainless steels are increased by dissolved ozone to +660 - +750 mV in a solution with 23 g/l Na_2SO_4 at pH 3 and temperature 50 °C, where the dissolved ozone concentration is 24 - 28 ppm. The further increase in the ozone concentration in a pressure vessel has no effect. Corrosion potentials of stainless steels are in the transpassive region but below the oxygen evolution potential. The corrosion potential of Armco iron is -720 mV, commercial pure chromium +740 mV, commercial pure Ni -190 mV and commercial pure molybdenum +20 mV. The increase in the corrosion potentials of stainless steels to the final value is a slow process and may take up to 20 h. Pure metals reach their corrosion potentials in about 5 minutes.

In the anodic and cathodic polarisation experiments, current the densities of stainless steels are close to each other in ozonated solutions. The current densities of higher alloyed steel are, however, higher in the cathodic and anodic polarisation curves than low alloyed steels. When the results in ozonated solutions are compared with results in oxygen bubbled solutions, the differences are minor, but ozone does increase the current densities slightly in anodic and cathodic polarisation.

When pH is lowered from value 3, the corrosion rates of higher alloyed steels begin to increase at higher pH than lower alloyed steels.

Cyclic polarisation experiments at slow scanning rate (10 mV/min) are not suitable for evaluating the susceptibility of stainless steels towards pitting. No hysteresis was found in any of the test material curves. On the surface of higher alloyed steels, pits were nevertheless formed. The reason for this is the high redox-potential of the solution. Pits initiated during polarisation passivate after a certain dissolution and this does not increase the current density in cyclic polarisation.

Potentiodynamic polarisation measurements together with corrosion potential measurements can be used in evaluating the electrochemical corrosion behaviour of stainless steels in ozonated solutions. Potentiodynamic polarisation experiments are a good tool to compare the behaviour of different alloys in ozonated solutions and to investigate the effect of changes in solution.

Corrosion rates measured by the Tafel method, weight loss tests and analysing the amount of dissolved elements give similar results (Table 24). The corrosion rate increases as the amount of alloying elements in stainless steels increase. Corrosion rates of stainless steels P720 and P752 determined by the Tafel method and by weight loss measurements are very close to each other. The corrosion rate of P720 in solution without Na_2SO_4 is somewhat higher measured from solution analysis than in weight loss experiments, but both are close to the results in Na_2SO_4 solution. The corrosion rate of Ralloy 654MO in sodium sulphate solution is higher in weight loss tests than in Tafel experiments. This is caused by the peeling of the thick oxide layer and local corrosion in long the term immersion tests,

which does not take place in the short term Tafel experiments or which can´t be detected in the electrochemical experiments, because peeling is not an electrochemical phenomenon. The corrosion rate of Ralloy 654MO measured by solution analysis is two times higher than that in weight loss experiments and again close to the corrosion rates in sodium sulphate containing solution.

Table 24. Corrosion rates of stainless steels in ozonated solution with 23 g/l Na_2SO_4.

	Corrosion rate / µm/a			
Alloy	Tafel method (Na_2SO_4)	weight loss (Na_2SO_4)	weight loss (no Na_2SO_4)	solution analysis (no Na_2SO_4)
P853	1.7 / 1.1			
P720	3.2 / 2.0	2.6	2.8	3.6
P752	3.9 / 2.5	3.4	3.3	
Ralloy 654MO	4.5 / 2.8	10.6	3.4	6.8

The predominant factor in the corrosion behaviour of stainless steels in ozonated solutions is the strong growth of oxide layers to a high thickness. After 16 days immersion in the ozonated solution the thickness of oxide layers are 60 nm for P853, 140 nm for 720, 260 nm for P752 and 140 for Ralloy 654MO. The thickness of the layer increases as the amount of alloying elements increases. However, on Ralloy 654MO the oxide is thinner than on P752. This is obviously due to the peeling of the layer.

The chemical structure of the oxide layer is also changed by ozone during immersion. Dissolved ozone drastically decreases the Cr concentration of the oxide layer. The relative Fe concentration decreases most in Ralloy 654MO and increases in less alloyed steels. The relative increase in Mo concentration is the highest in the oxide layer of P853 and decreases when the amount of alloying elements increases. In the oxide layer of P752 the Mo concentration is lower than the nominal bulk concentration. This is obviously due to the thick oxide layer, from which MoO_6 has dissolved completely. The most important differences in the outermost layers (< 5 nm), besides thickness, are the lower Cr concentrations, lower Ni concentration (except Ralloy 654MO) and the enrichment of Mo. In some analyses very high concentrations (up to Mo 50 w-%) were found on the surfaces. The main components in the oxide layers are iron oxides, and MoO_6 occurs ramdomly on the surfaces. The slopes of the concentration profiles are higher for Ralloy 654MO than for P720. Thus, the change from oxide to bulk metal occurs in a more narrow region for Ralloy 654MO. This may cause greater internal stresses, which may increase the peeling of the oxide on Ralloy 654MO.

The interpretation of the concentration profiles becomes more difficult because of the peeling of the oxide layer, which occurs most in Ralloy 654MO. After 16 days immersion so much oxide has peeled off (and also dissolved) that it is obvious this is the reason for the oxide layer of P752 being thicker than that of Ralloy 654MO.

The mechanism for transpassive corrosion is conventionally regarded to be intergranular corrosion or e.g. etching, where potential has a major effect. The corrosion phenomenon is different in ozonated solutions, where the corrosion potential of stainless steels is only slightly higher than the transpassivation potential. General corrosion rates of stainless steels are low and the oxide layers peel off slightly. These corrosion damages formed in ozonated solution are shallow; unlike pitting caused by chlorides. The number of damages is low in P853 and P752. In P752 damages are 1 - 2 µm deep and in Ralloy 654MO up to 6 µm. The peeling mechanism in ozonated solution is assumed to be the following: The peeling mechanism is as follows: 1) increase in the thickness of the oxide layer, 2) local corrosion initiation, 3) increased corrosion damages resulting in weakened adhesion of the oxide layer, 4) peeling of the oxide from the surface, 5) further oxidation of the exposed steel with corrosion damage. This detachment of the oxide layers can be seen both in SEM

pictures and obviously also in GDOS analyses, where the thickness of Ralloy 654MO may also decrease during immersion. Corrosion rates of these metals are, according to weight loss oxidation measurements, low and the depth of the corrosion damages will remain low. This means that local corrosion is not a continuous process and metals are able to repassivate.

Corrosion of stainless steels in ozonated solution is partly an electrochemical and partly a physical phenomenon. Because of this both electrochemical methods and surface analyses need to be used in order to acquire comprehensive information on the phenomenon. By using polarisation and potentiostatic measurements together with the Tafel method the electrochemical corrosion behaviour can be measured. Surface analysis methods, e.g. SEM, GDOS and ESCA are also needed to analyse the major changes in the thickness and chemical composition of the oxide layer and in local corrosion damage due to peeling.

5 SUMMARY

The information available prior to this investigation on the effect of dissolved ozone on the corrosion behaviour of stainless steels and some metals in pure solutions and at high concentration was very limited. The subject has been studied mainly in impure solutions, such as sea and river water used in industrial cooling systems, where dissolved ozone concentrations are low.

Test materials were four different stainless steels: ferritic stainless steel Polarit 815 and austenitic stainless steels Polarit 720, Polarit 752 and Ralloy 654MO. Also Armco iron and pure Mo, Ni and Cr were tested. The pH of the test solution was 1, 2, 3 and neutral (adjusted by H_2SO_4). 2.3 and 23 g/l Na_2SO_4 was added to increase the conductivity in anodic and cathodic polarisation measurements. The temperature of the test solution was 20, 50 and 75 °C. The dissolved ozone concentration was 24 - 28 ppm at temperature 25 °C,15 -20 ppm at 50 °C. The ozone concentration in pressure vessel at 10 bar was 100 - 200 ppm, but this was not possible to determine by measurements. Avesta cell was mainly used as a test cell.

The electrochemical behaviour of stainless steels and pure metals was studied using potentiodynamic cyclic polarisation at scanning rates 1, 10 and 100 mV/min and pitting behaviour at 10 mV/min. Potentiostatic experiments and long term corrosion potential measurements were also used. The corrosion rates of steels were also investigated by the Tafel method. Immersion tests were carried out mainly to produce test samples for surface examination but also to measure the weight losses. The structure and thickness of the oxidized surfaces were examined and analysed using SEM, GDOS, ESCA and X-ray diffractometer methods.

Dissolved ozone increases the redox-potential of test solutions to about +1200 mV vs. SCE at dissolved ozone concentrations above about 0.5 ppm and the corrosion potential of stainless steel to the transpassive region below the oxygen evolution potential. The current density of stainless steels is higher the higher alloyed the steel. On the other hand, dissolved ozone slightly increases current densities compared to experiments in oxygen bubbled solutions. Higher ozone concentration obtained under high pressure has no effect on the corrosion behaviour of stainless steels.

As the pH of the solution is decreased, the current density in the transpassive region increases in higher alloyed stainless steels at higher potentials than in low alloyed steel. This critical pH value is below 1 for P853 and P720, between 1 and 2 for P752 and for Ralloy 654MO it is between 2 and 3.

The oxide layer formed in 22 h immersion in ozonated solution clearly increases the current densities in anodic polarisation experiments compared to experiments carried out immediately after cathodic cleaning.

The cathodic behaviour of steels after 22 h immersion in ozonated solution differs clearly from the behaviour of cathodically cleaned samples. The corrosion potentials of steels are higher and the main difference in the polarisation behaviour of stainless steels is the lower current density of P853 up to potential +140 mV. This means that ferritic steel catalyses less the reduction of ozone than austenitic steels. The cathodic reaction of the corrosion reaction of stainless steels in ozonated solution is the reduction of ozone to oxygen at higher potentials and at lower cathodic potentials mainly the reduction of oxygen.

According to the Tafel experiments corrosion rates of stainless steels are low in ozonated test solution. The lowest corrosion rate is for ferritic steel P853 and the highest for highly alloyed Ralloy 654MO. However, oxide layers of stainless steels peel off locally in ozonated solutions, which means that the calculated corrosion rates are not reliable.

Cyclic polarisation experiments at slow scanning rate (10 mV/min) are not suitable to evaluate the tendency of stainless steels to pitting. No hysteresis was found in any of the test material curves.

On the surface of higher alloyed steels, pits were nevertheless formed. The reason for this is the high redox-potential of the solution. Pits initiated during polarisation passivate after a certain dissolution and this does not increase the current density in cyclic polarisation.

Corrosion of stainless steels is mainly general but some indications of intergranular corrosion were also found. Also peeling of oxide layers occur. Wide shallow corrosion damages are formed during both in cyclic polarisation and in immersion tests. Damages are able to passivate.

Dissolved ozone greatly increases the thickness of the oxide layers. In oxygen bubbled solution at pH 3 the thickness of the layer is a few nanometers and in ozonated solution 60 - 260 nm. Marked changes in the chemical concentrations of the layers great changes have been found. The Cr concentration is negligible in the oxide layers especially for Ralloy 654MO and P752. Molybdenum concentrates in the outer layer, in partivcular with lower alloyed steels. Also Fe concentration has increased in the oxide. Iron and alloying elements have oxidised to the highest valencies.

REFERENCES

1. Landolt, D., Transpassivity. In Passivity of metals, eds. Frankenthal, R.P., Kruger, J. The Electrochemical Society, Princeton 1978, pp. 484-504.

2. Sedriks, A.J., Corrosion of stainless steels. A Wiley-Interscience Publication. John Wiley & Sons, Inc., New York 1996. 437 p.

3. Okada, H., Mechanistic understanding and prevention of localized corrosion. Materials Performance, 37(1998) 12, pp. 54-61.

4. Cowan, R.L., Tedmon, C.S., Intergranular corrosion of iron-nickel-chromium alloys. In Advances in corrosion science and technology; Volume III, eds. Fontana, M.G., Staehle, R.W., Plenum Press, New York 1973, pp. 293-400.

5. Herbsleb, G., Der Einfluss von Legierungselementen auf das Passivieringsverhalten nichtrostender Stähle. VDI-Z. Zeitschrift des vereins Deutscher Ingenieure für Maschinenbau und Metallbearbeitung, 123(1981) 12, pp. 505-511.

6. Sedriks, A.J., Effects of alloy composition and microstructure on the passivity of stainless steels. Corrosion, 42(1986) 7, pp. 376-389.

7. Kirchheim, R., Heine, B., Fischmeister, H., Hofmann, S., Knote, H., Stolz, U., The passivity of iron-chromium alloys. Corrosion Science, 29(1989) 7, pp. 899-917.

8. Metikos-Hukovic, M., Ceraj-Ceric, M., p-type and n-type behaviour of chromium oxide as function of the applied potential. Journal of the Electrochemical Society, 134(1987) 9, pp. 2193-2197.

9. Montermor, M.F., Simoes. A.M.P., Ferreira, M.G.S., Da Cunha Belo, M., The role of Mo in the chemical composition and semiconductive behaviour of oxide films formed on stainless steels. Corrosion Science, 41(1999) 1, pp. 17-34.

10. Bojinov, M., Betova, I., Raicheff, R., Influence of molybdenum on the transpassivity of a Fe + 12% Cr alloy in H_2SO_4 solutions. Journal of Electro-analytical Chemistry, 430(1997) 1-2, pp. 169-178.

11. Puckorius, P.R., Ozone use in cooling tower systems - current guidelines. Where it works. Ozone science and engineering, 15(1993) 1, pp. 81-93.

12. Strittmatter, R.J., Yang, B., Johnson, D.A., A comprehensive investigation on the application of ozone in cooling water systems - correlation of bench-top, pilot and field application data. Ozone science and engineering, 15(1993) 1, pp. 47-79.

13. Yang, B., Johnson, D.A., Shim, S.H., Effect of ozone on corrosion of metals in cooling towers. Corrosion, 49(1993) 6, pp. 499-513.

14. Brown, E.E., Lu, H.H., Duquette, D.J., Effect of flow rates on localized corrosion behaviour of 304 stainless steel in ozonated 0.5 N NaCl. Corrosion, 48(1992) 12, pp. 970-975.

15. Wyllie, W.E., Duquette, D.J. The effects of dissolved ozone on the corrosion behaviour of stainless steels in artificial seawater. In Corrosion´97, NACE, March 10-14, 1997, New Orleans. Paper No. 436, 33 p.

16. Brown, B.E., Stevens, J.H., Duquette, D.J., Wyllie, W.E. The effects of dissolved ozone on the corrosion behaviour of nickel, stainless steels, and aluminium-based alloys in artificial seawater. In 1977 Tri-service conference on corrosion, November 17-21. Wrightsville. Pp.1:35-1:50.

17. Brown, B.E., Duquette, D.J. A review of the effects of dissolved ozone on the corrosion behaviour of metals and materials. In Corrosion`94, NACE, February 28 - March 4, 1994, Baltimore. Paper No. 486, 19 p.

18. Lu, H.H., Duquette, D.J., The effect of dissolved ozone on the corrosion behaviour of Cu-30Ni and type 304L stainless steel in 0,5 NaCl solutions. Corrosion 46(1990) 10, pp. 843-.852.

19. Videla, H.A., Viera, R.M., Guiamet, P.S., de Mele, M.F.L., Effect of dissolved ozone on the passive behaviour of heat exchanger structural materials. biocidal efficacy on bacterial biofilms. In Corrosion`95, NACE, March 26-31, 1995. Orlando. Paper No. 199, 10 p.

20. Videla, H.A., Viera, M.R., Guiamet, P.S., Using ozone to control biofilms. Materials Performance, 34(1995) 7, pp. 40-44.

21. Herbert, D., Whillock, G.O.H., Worthington, S.E., Zero resistance ammetry - its application in preventing the corrosion of stainless steel in cooling waters. Materials Science Forum, 192-194(1995), pp. 469-476.

22. Andreasson, P., Troselius, L., The corrosion properties of stainless steels and titanium in bleach plants, 1995, Korrosionsinstitutet: Stockholm. 25 p.

23. Sato, Y., Suzuki, M., Matsudaira, M., Dissolved ozone effect on corrosion of metals in water. Boshoku Gijutsu, 31(1982) 5, pp. 319-324.

24. Tyupalo, N.F., Velichko, E.A., Alekseev, E.A., Influence of ozone on passivation of 0Cr23Ni28Mo3Cu3Ti steel. Journal of applied chemistry of the USSR, 50(1978) 9, part 2, pp. 2001-2002.

25. Kurtepov, M.M., Bochareva, E.F., The influence of ozone on the corrosion of stainless steel in nitric acid. Corrosion on metals and alloys, (1966) 2, pp. 134-137.

26. Matsudaira, M., Suzuki, M., Sato, Y., Dissolved ozone effects on corrosion of metals in water. Materials Performance, 20(1981) 11, pp. 55-56.

27. Litvinova, E.I., Marukhno, L.G., Study of the dissolution of steel in ozonized solutions of sulfuric acid. Protection of metals, 7(1971) 2, pp. 184-186.

28. Zhuravlev, V.K., Kurtepov, M.M., Bochareva, E.F., Effect of cerium and silver ions on the electrochemical corrosion behaviour of stainless steel in ozonized solution of nitric acid. Protection of metals, 10(1974) 3, pp. 274-275.

29. Gru, B.W., Tatarchenko, G.O., Tyupalo, N.F., Effect of ozonization and some additions on the corrosion and electrochemical behaviour of steel 12Kh18N10T in sulfuric acid. Soviet Materials Science, 27(1992) 2, pp. 121-123.

30. Kashcheeva, T.P., Sologub, L.V., Gadasina, L.Yu, Pitting corrosion of equipment for catalytic final purification of effluent with ozone. Protection of metals, 17(1981) 2, pp. 161-162.

31. Horváth, M., Bilitzky, L., Hüttner, J., Ozone. 1985, Budapest: Elsevier. 350 p.

32. Rice, R.G., Wilkes, J.F. Fundamental aspects of ozone chemistry in recirculating cooling water systems. In Corrosion´91, NACE, March 11 - 15 1991. Cincinnati. Paper No. 205, 43 p.

33. Wyllie, W.E., Brown, B.E., Duquette, D.J. Ozone in sea water. In Corrosion`95, NACE, March 26-31, 1995. Orlando. Paper No 269, 18 p.

34. Clayton, C.R., Olefrojd, I., Passivity of austenitic stainless steels. In Corrosion mechanisms in theory and practice, eds. Marcus, P., Oudar, J. Marcel Decker Inc., New York, pp. 175-199.

35. Lu, Y.C., Clayton, R., Brooks, A.R., A bipolar model of the passivity of stainless steels - II. The influence of aqueous molybdate. Corrosion Science, 29(1989) 7, pp. 863-880.

36. Ürgen, M., Çakir, A.F.,, The effect of molybdate ion ton the temperature dependent pitting potential of austenitic stainless steels in neutral chloride solutions. Corrosion Science, 32(1991) 8, pp. 841-852.

37. Clayton, C.R., Lu, Y.C., A bipolar model of the passivity of stainless steels - III. the mechanism of MoO_4^{2-} - formation and incorporation. Corrosion Science 29(1989) 7, pp. 881-898.

38. Gaben, F., Oltra, R. The influence of the electronic properties of passive films on the localized depassivation transients. In Passivity and its breakdown, vol. 97-26, September 1 - 5 1997. Paris. Pp. 21 - 33.

39. Kruger, J., Passivity of metals - a materials science perspective. International Materials Review, 33(1988) 3, Pp. 113-130.

40. Pourbaix, M., Atlas of electrochemical equilibria in aqueous solutions, Oxford: Pergamon Press 1966. 644 p.

41. Beverskog, B., Puigdomenech, I., Pourbaix diagrams for the ternary system of iron-chromium-nickel. Corrosion, 55(1999) 11, pp. 1077-1087.

42. Qvarfort, R., New electrochemical cell for pitting corrosion testing. Corrosion Science, 28(1988) 2, pp. 135-140.

43. Marshall, K., Valensi, D., Surface analysis: glow discharge spectroscopy. Materials World, 3(1995) 10, pp. 471-473.

44. Angeli, J., Haselgrüber, E.M., Achammer, E. M., Burger, H., Surface analysis of steel with GDOS and EPMA. Fresenius Journal of Analytical Chemistry, 346(1993) 1-3, p. 138-143.

45. Handbook of chemistry and physics, 57th ed., Ed. Weast, R.C. CRC press Inc. 1976.

46. Wolff, U., Schneider, F., Mimmert, K., Schultz, L., Stability electrochemical properties of passive layers on Fe-Si. Corrosion, 56(2000) 12, pp 1195 -1201.

47. Peckner D., Bernstein, I.M., Handbook of stainless steels. McGraw-Hill Inc.1977.

48. Homepages of Metso Powdermet, Http://www.raumamaterials.com/.

49. Standard practice for calculation of corrosion rates and related information from electrochemical measurements, G 102. 1993 Annual book of ASTM standards. Section 3 Metals test methods and analytical procedures. Volume 03.02 Wear and erosion; metal corrosion.

50. Private communication. Leena-Sisko Johansson, D.Sc., head of Center of Chemical Analysis, Helsinki University of Technology. 2.10. 2001.

Appendix 1a: P853 3 days in O_2

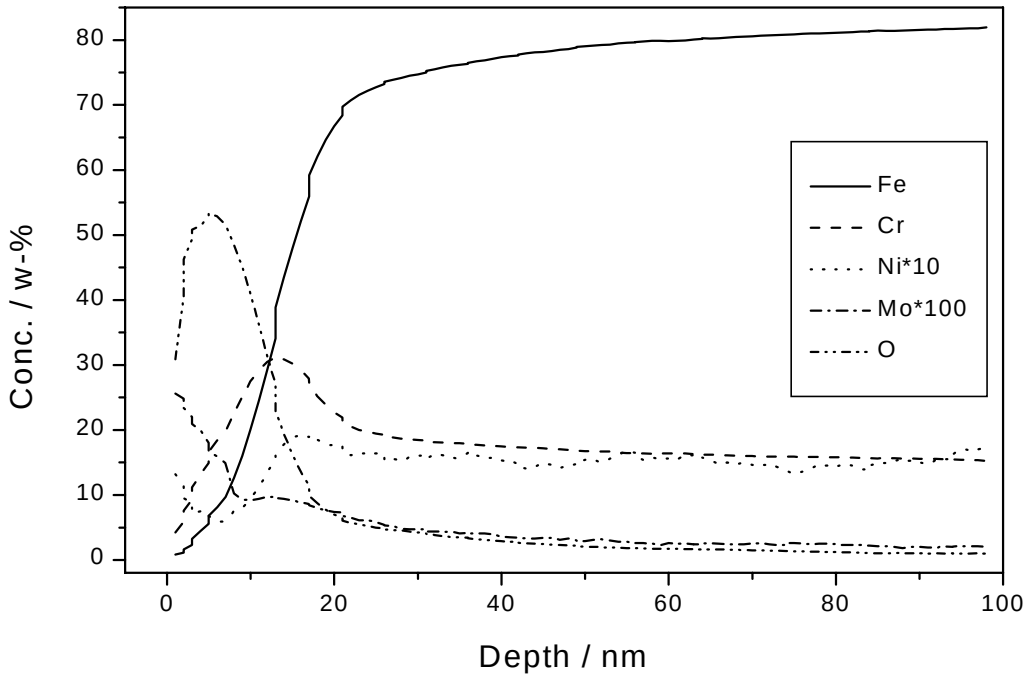

Appendix 1b: P853 3 days in O_2

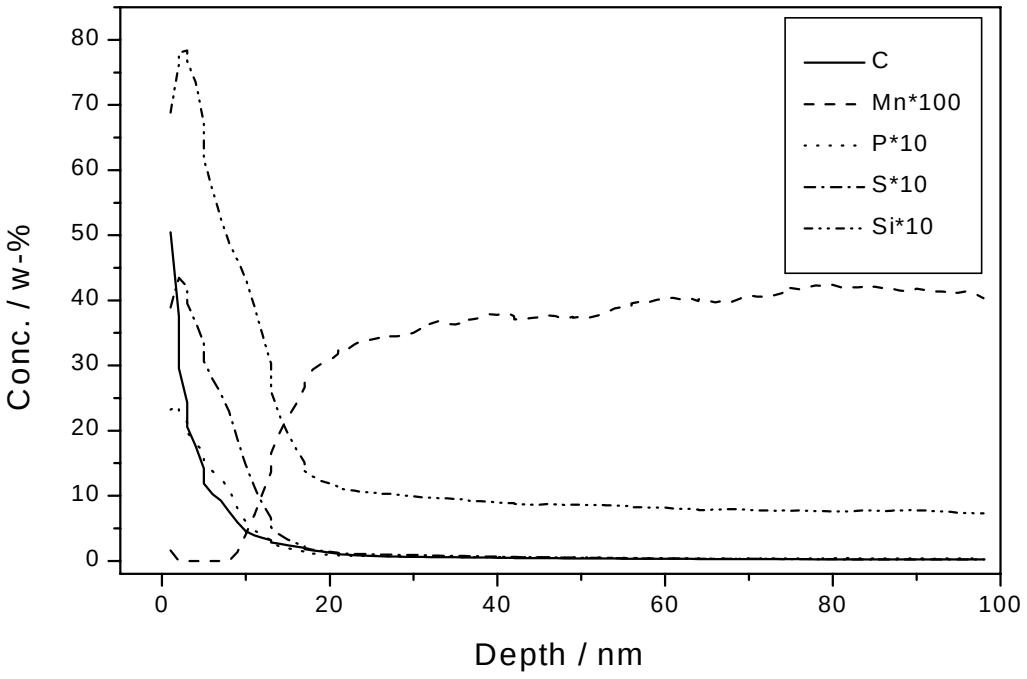

Appendix 2a: P853 16 days in O_3

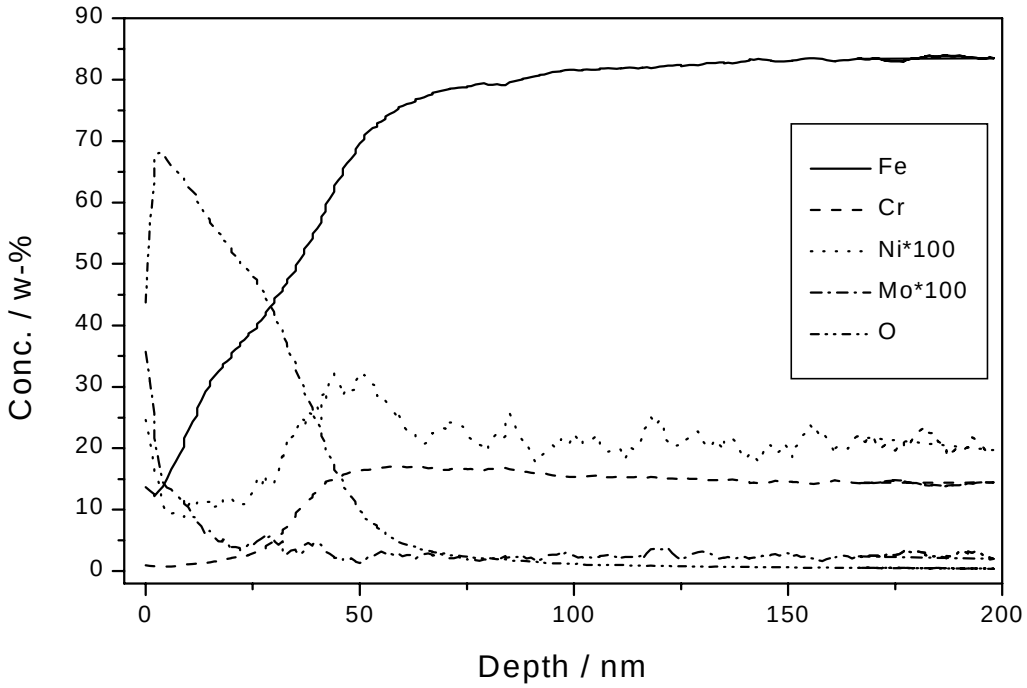

Appendix 2b: P853 16 days in O_3

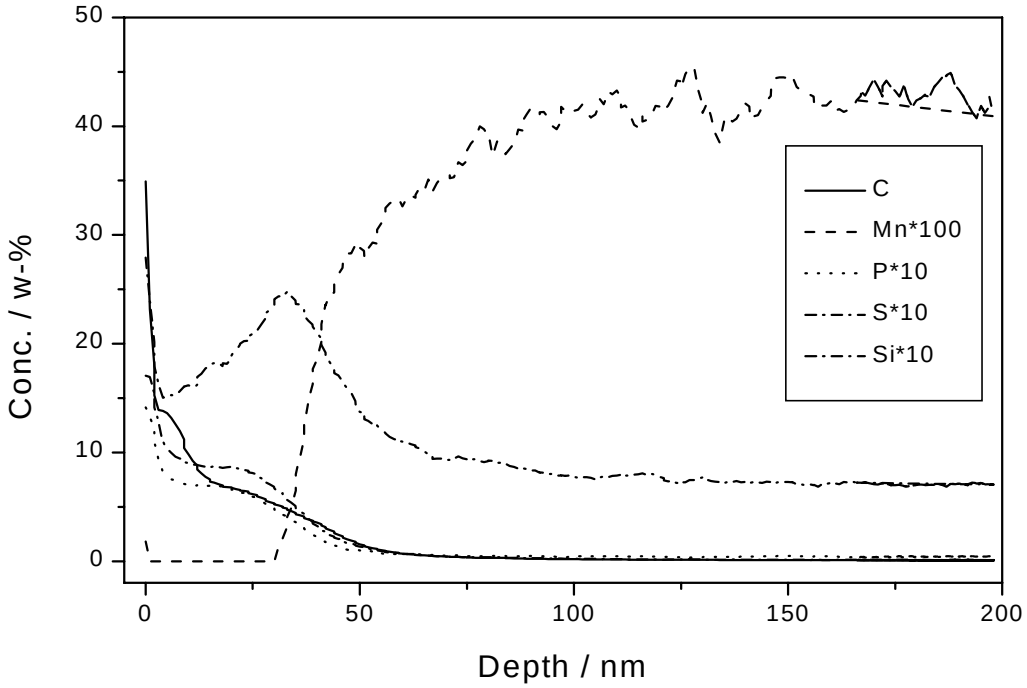

Appendix 3a: P720 3 days in O_2

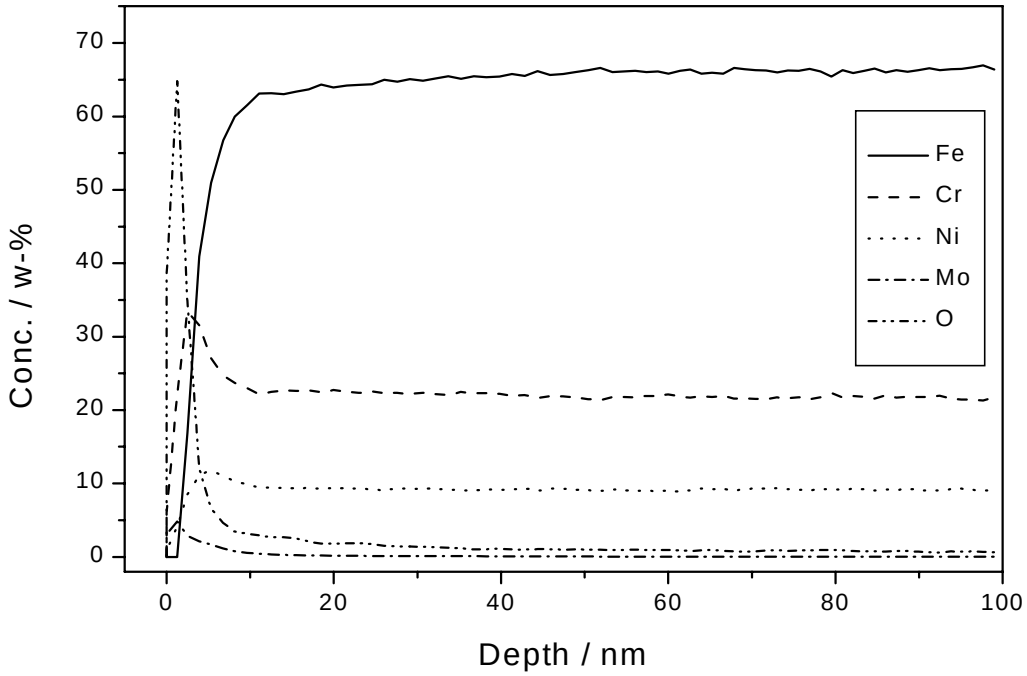

Appendix 3b: P720 3 days in O_2

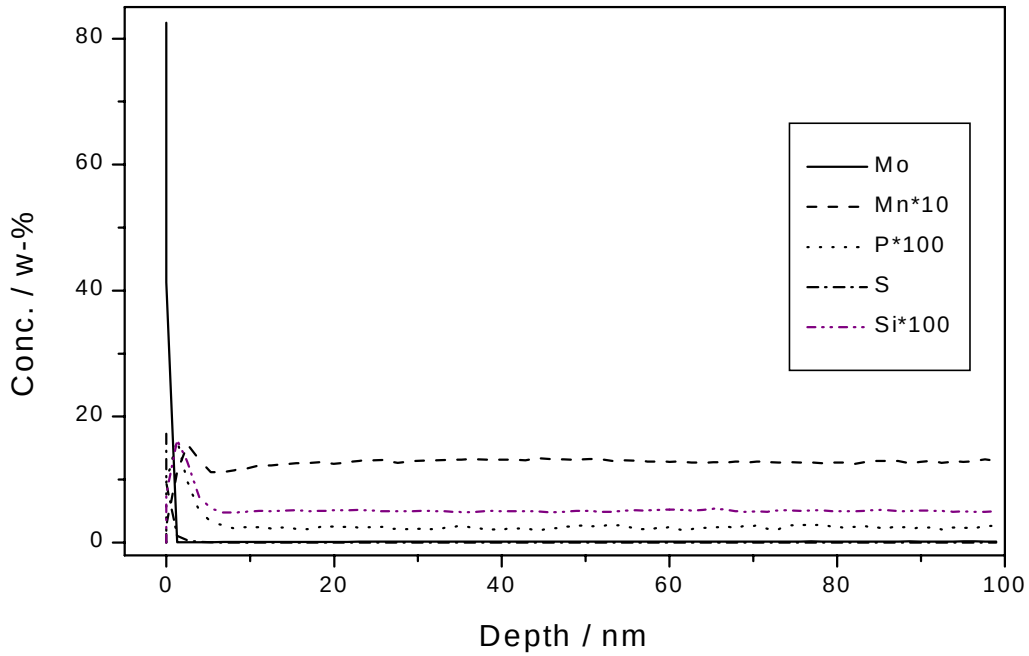

Appendix 4a: P720 16 days in O_3

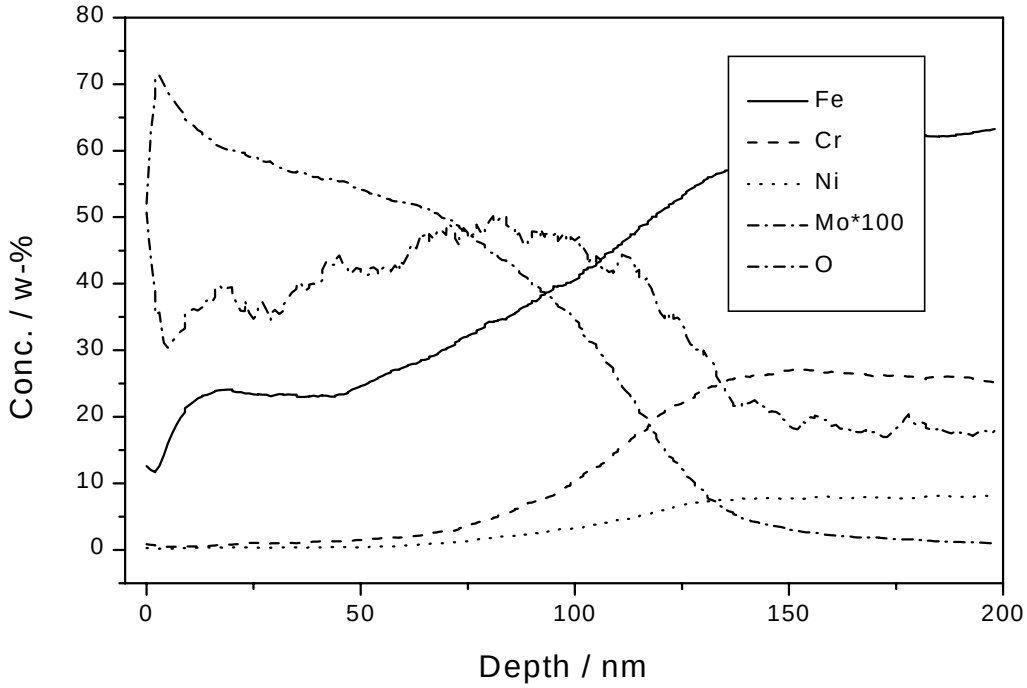

Appendix 4b: P720 16 days in O_3

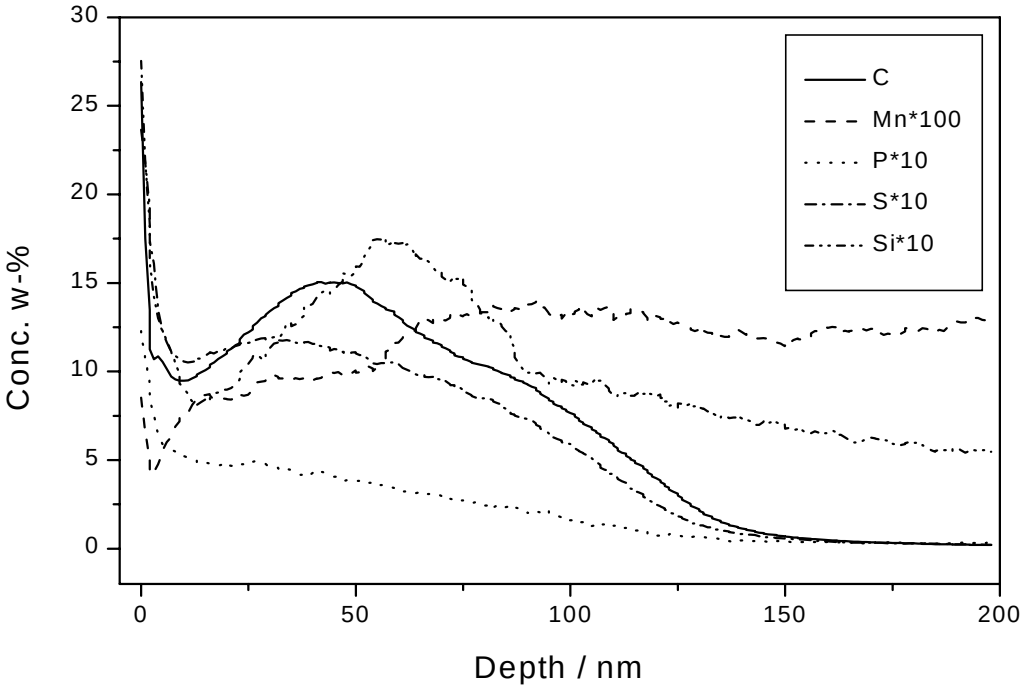

Appendix 5a: P752 3 days in O_2

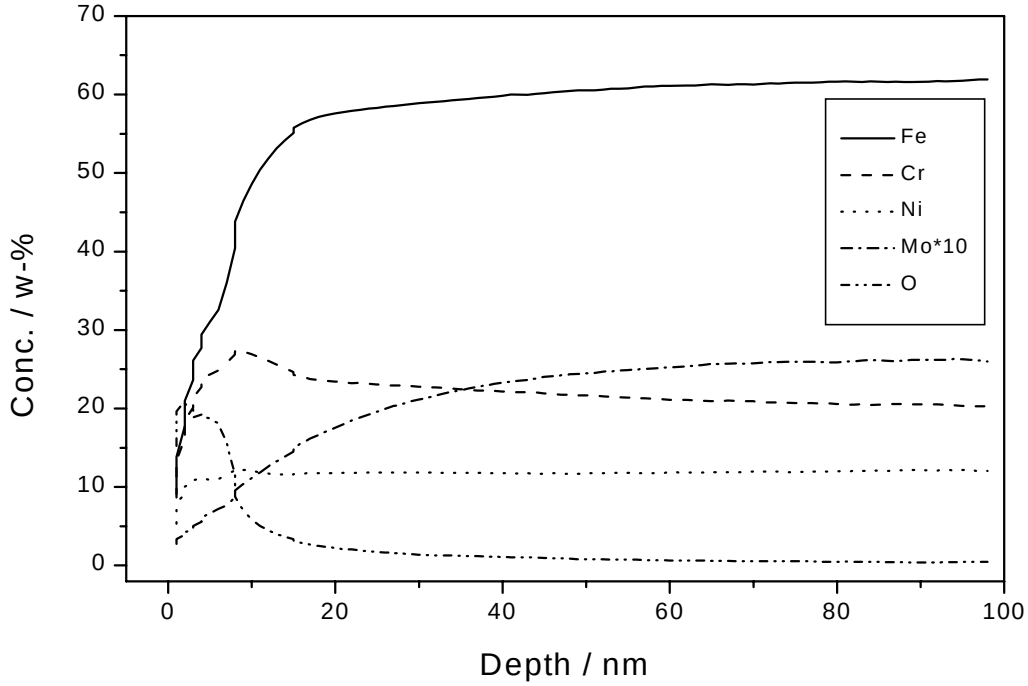

Appendix 5b: P752 3 days in O_2

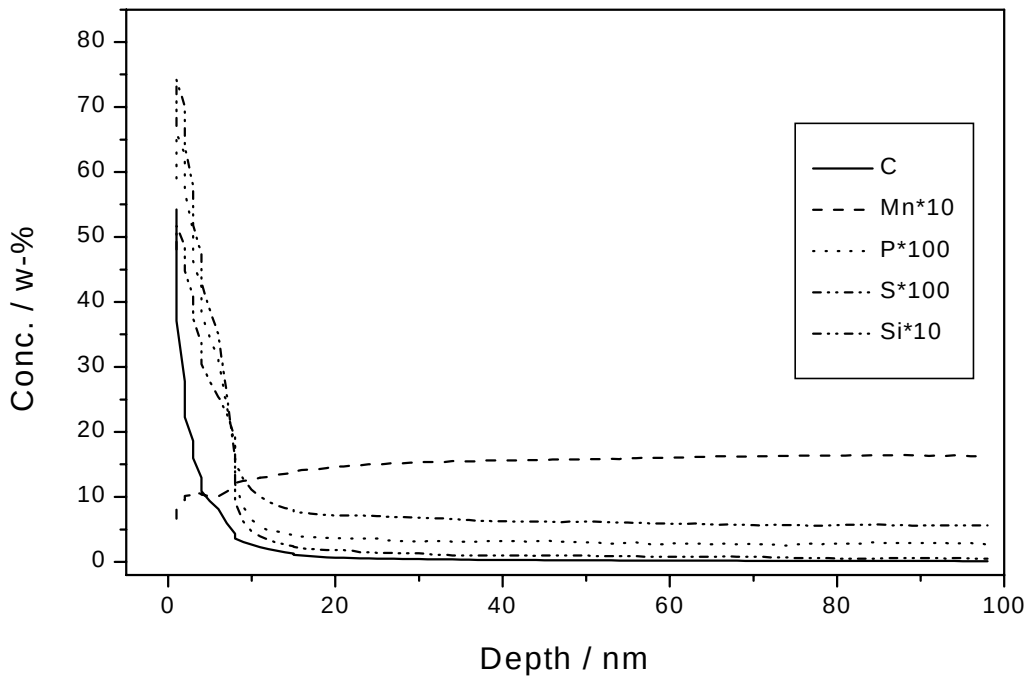

Appendix 6a: P752 16 days in O_3

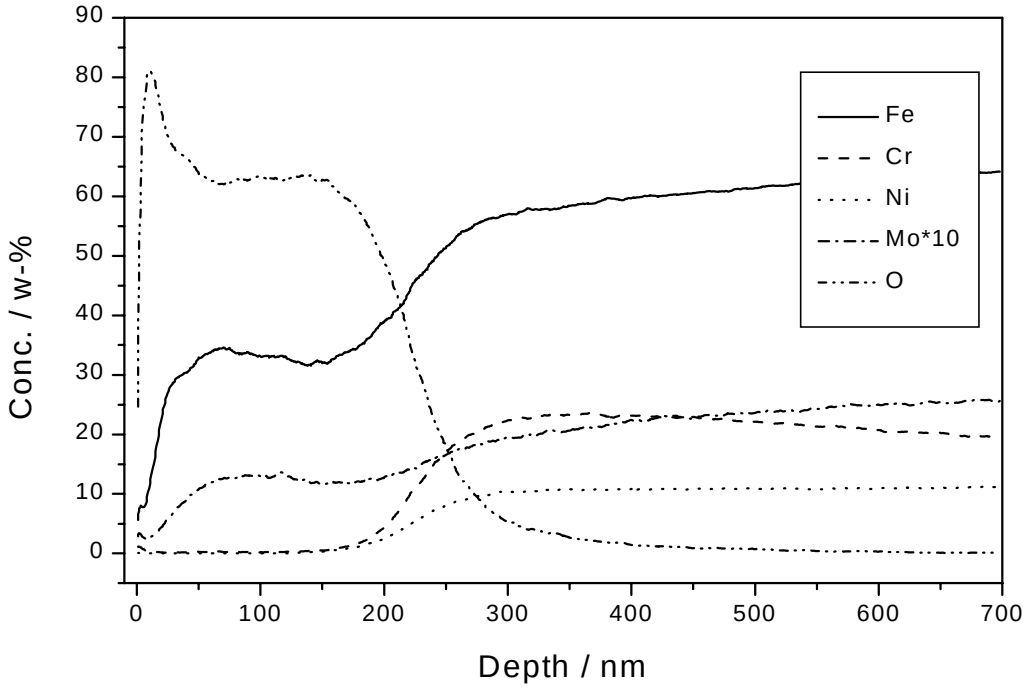

Appendix 6b: P752 16 days in O_3

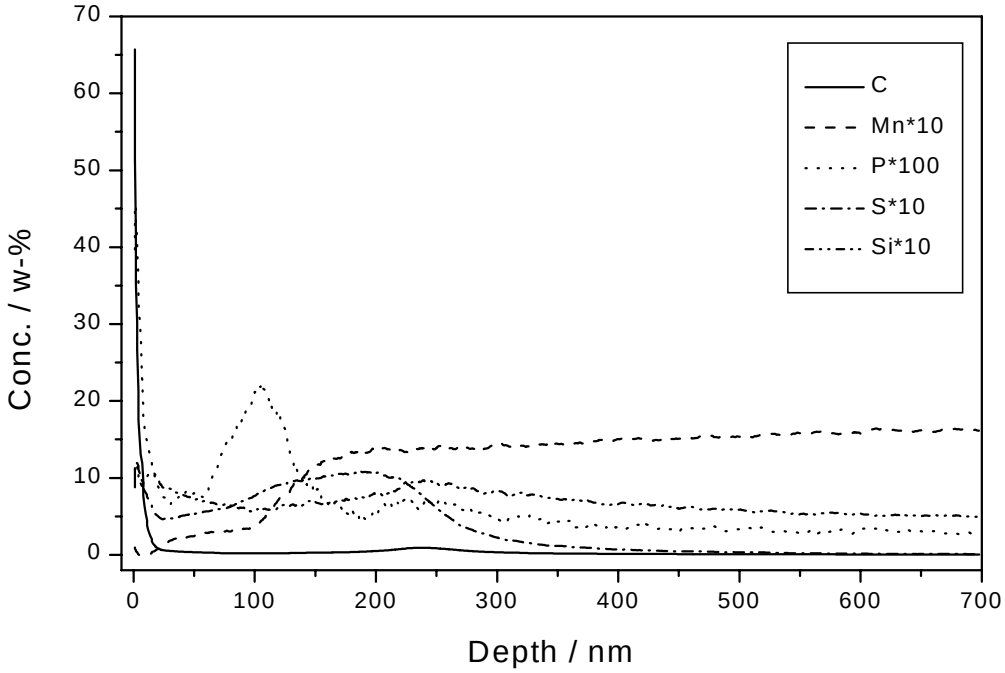

Appendix 7a: Ralloy 654MO 3 days in O_2

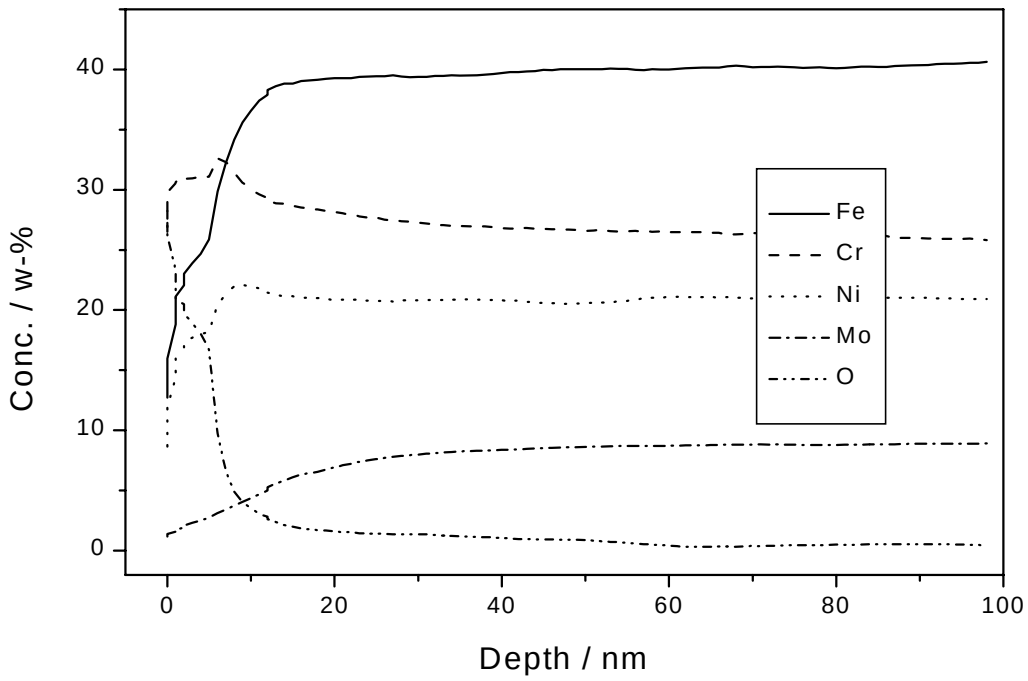

Appendix 7b: Ralloy 654MO 3 days in O_2

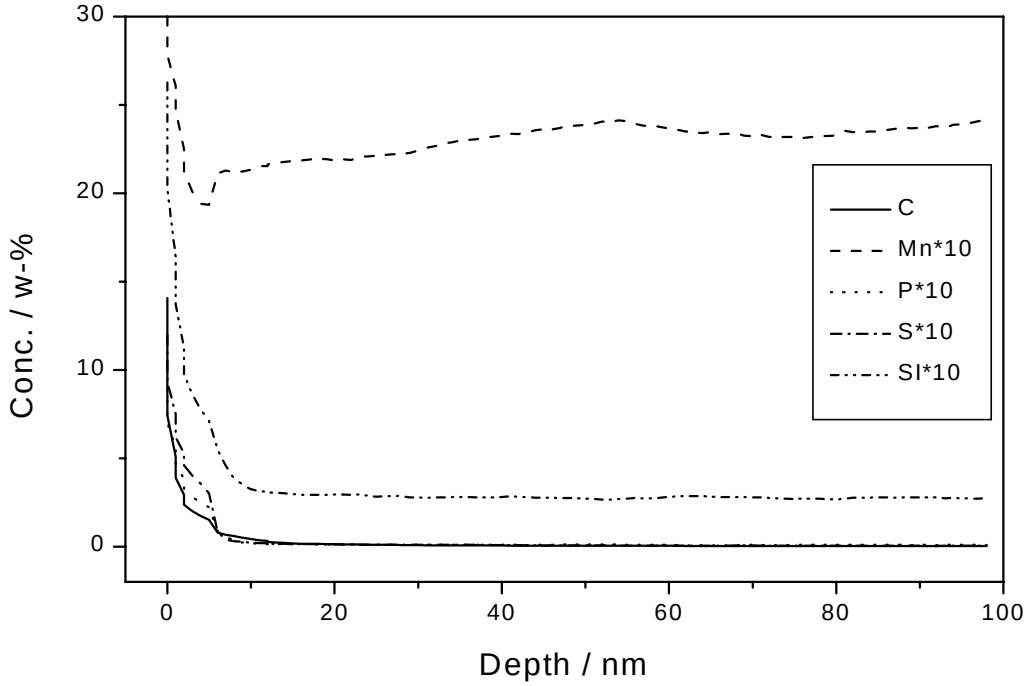

Appendix 8a: Ralloy 654MO 16 days in O_3

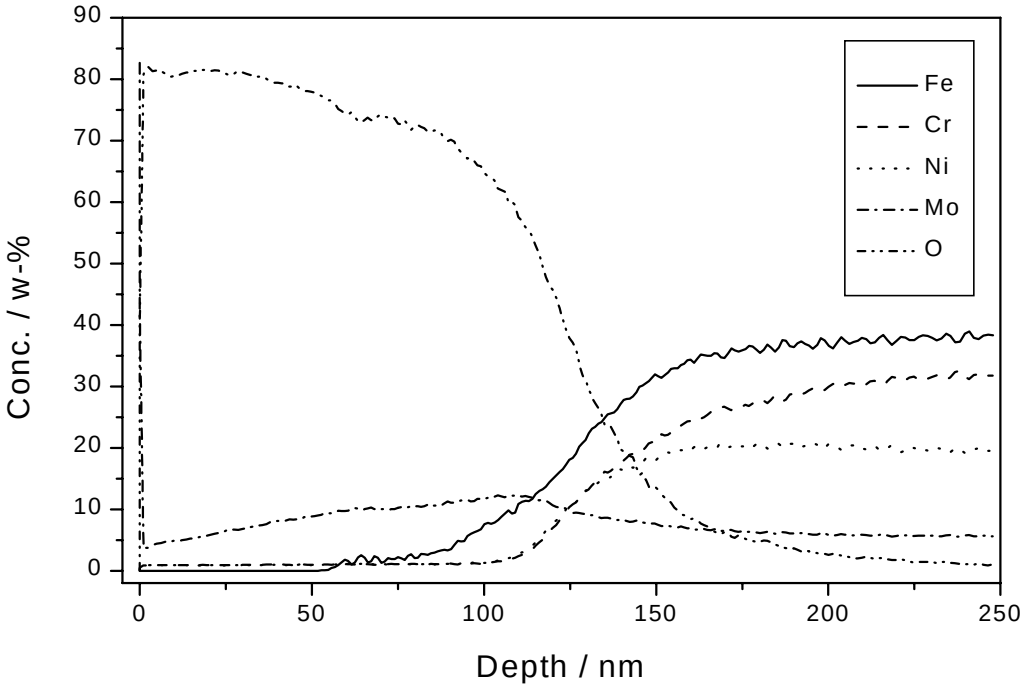

Appendix 8b: Ralloy 654MO 16 days in O_3